Department of Precision and Microsystems Engineering

3D Printable flexible electrochemical sensors with carbon-polymer composite electrodes

Yujing Zhang

Report no : 2025.014

Coach : Dr. J.G. Buijnsters
Professor : Dr. J.G. Buijnsters
Specialisation : Micro and Nano Engineering (MNE)

Type of report: Thesis

Date : 15 April 2025



MSc thesis in Mechanical Engineering

3D Printable flexible electrochemical sensors with carbon-polymer composite electrodes

Yujing Zhang

April 2025

A thesis submitted to the Delft University of Technology in partial fulfillment of the requirements for the degree of Master of Science in Mechanical Engineering

Contents

Abstract	5
Acknowledgements	6
1 Introduction	7
2 Literature Review	8
2.1 Electrochemical Sensors: Fundamentals and Applications	8
2.1.1 Basic Operating Principles of Electrochemical Sensors	8
2.1.2 Electrochemical Principles	
2.1.3 Electrochemical Methods	11
2.1.4 Applications	15
2.2 Flexible Electrochemical Sensors	16
2.2.1 Why flexible?	16
2.2.2 Materials of flexible sensors	18
2.2.3 Fabrication of flexible sensors	20
2.3 Electrode Design	21
2.3.1 Electrode shape	22
2.3.2 Electrode materials (WE, CE, RE)	22
2.3.3 Manufacturing methods	27
3 Research Proposal	
3.1 Knowledge gap	30
3.2 Research objective	30
3.3 Research questions	31
4 Materials and Methods	32
4.1 WE materials	32
4.1.1 TPU/CNT/BDD filament	32
4.1.2 TPU/CB filament	
4.2 3D Printing	
4.3 Characterization	34
5 Results and Discussion	38
5.1 TPU/CNT/BDD electrode: Fabrication and Characterization	38
5.1.1 Fabrication	
5.1.2 Electrical characterization	
5.2 TPU/CB electrode: Fabrication and Characterization	42
5.2.1 Fabrication	

	5.2.2 Mechanical characterization	.44
	5.2.3 Electrical characterization	.47
	5.2.4 Electrochemical characterization and surface treatment	.50
6 Conc	lusion and Outlook	.58
6.1	1 TPU/CNT/BDD printed electrode	.58
6.2	2 TPU/CB printed electrode	.58
6.3	Recommendations for future work	.58
Refere	nces	.60

Abstract

The advancement of sensor miniaturization and intelligence has led to the emergence of flexible sensors for human health monitoring and drug monitoring. Flexible electrochemical sensors are biocompatible and can be bent and stretched to a certain extent to achieve a good fit for human skin, for instance. Currently, nanomaterials are predominantly employed as electrode materials in such sensors. The combination of conductive metal ions and flexible polymers is believed to enhance the conductivity of the electrodes. Alternatively, boron-doped diamond (BDD), which possesses outstanding electrochemical characteristics and corrosion resistance, is a promising electrode material for integration into flexible electrochemical sensors. It has demonstrated significant market potential for sensitive rigid electrochemical sensors. A completely novel approach is to manufacture flexible BDD electrodes by using 3D printing technology. Conducting polymer-diamond composite material could be synthesized for electrode design by mixing BDD particles with a flexible polymer such as thermoplastic polyurethane (TPU).

TPU/carbon black (CB) conductive composites integrate polymer flexibility with CB-derived conductivity, enabling tunable electrochemical performance via filler ratio control and post-treatment (e.g., in DMSO). They have the advantages of processability, low cost and environmental adaptability, and provide high-performance electrode material solutions for flexible energy storage devices and smart sensors.

Fused deposition modeling (FDM), as a low-cost, high-precision 3D printing technology, has shown significant advantages in the manufacture of flexible sensors. FDM 3D printing leverages conductive polymer melts to fabricate flexible sensors with embedded electrodes. Process parameter optimization (nozzle temperature, infill density) combined with surface treatments enhances electrode sensitivity and stability, accelerating their adoption in wearable sensors and environmental monitoring systems.

This study explores the potential and possibility of TPU/CNT/BDD and TPU/CB materials being printed with FDM as electrodes. Firstly, the processing and difficulties of printing TPU/CNT/BDD filament using FDM were evaluated, and the surface shape of the printed sample was observed and analyzed. It was found that it was difficult to reproducibly print the as-prepared TPU/CNT/BDD filament, and the resistance after printing was much higher than that of the filament itself. Therefore, FDM printing of TPÛ/CB materials was studied subsequently. That printing process proved much simpler, and the repeatability and stability were good. The printed samples were tested for mechanical, electronic, and electrochemical properties. In terms of mechanical stretching, the electrodes printed on TPU substrates were well bonded with the TPU, and they did not get damaged by stretching and bending. The effect of filling direction of the TPU materials on the stressstrain response was explored. In terms of electrical properties, the electrode resistance after printing is higher than that before printing, but it still has good and stable conductivity, and the resistance of the printed sample can be effectively reduced through thermal cycling. In terms of electrochemistry, cyclic voltammetry was selected to explore the electrochemical performance of the electrode before and after surface treatment, and two classical redox probes, [Ru(NH₃)₆] ^{3+/2+} (RuHex) and [Fe(CN)₆] ^{3-/4-} (Ferrocyanide), were selected to test the TPU/CB samples soaked in DMSO for different durations. The results showed that DMSO treatment was an effective strategy to improve the electrochemical performance of FDM-printed TPU/CB electrodes, and the conductivity, redox activity and interfacial interaction ability of the electrodes could be significantly improved by optimizing the processing time. This modification method makes the electrode have broad application potential in the fields of electrochemical sensing, flexible electronic devices, supercapacitors, and wearable energy storage devices.

Acknowledgements

The completion of this project is inseparable from the guidance and support of many people. Therefore, I would like to take this opportunity to express my sincerest gratitude to those who have helped and encouraged me during my study journey at TU Delft, especially during my master's thesis. At the same time, I would like to express my sincere gratitude to TU Delft for providing me with the opportunity to deepen my academic research skills, and I am proud to be a part of this world-renowned institution of higher learning.

First of all, I would like to thank my supervisor, Dr. Ivan Buijnsters, Associate Professor, for his valuable advice, continuous support and careful guidance throughout my master's studies. His in-depth knowledge, extensive experience, and outstanding research enthusiasm in diamond materials and electrochemical sensors have greatly helped me in my project work and played a vital role in advancing my research. I am very honored to have the opportunity to participate in his research team and benefit from his professional insight and careful guidance. His open-mindedness, clarity of thought, and constructive feedback have helped me to continuously refine my research, which has made working with him an invaluable academic experience. His positive attitude and timely response were the most powerful boosters for me when I was uneasy about the experiment. I am very honored to have such an outstanding supervisor to guide my master's research.

I would also like to express my gratitude to the technical support staff at PME and Dr. Simona Baluchova who helped me on my experimental path. In particular, Spiridon, Patrick, Alex and Bradley have been my reliable pillars of support. Whenever I have a sudden problem, I can always get the quickest help from them. Especially Spiridon, he not only helped me solve a lot of unexpected situations during my printing experiments, but also gave me a lot of suggestions for operation, which inspired me a lot. Their support and a large number of suggestions made a significant contribution to the project.

Thanks to the presence of all graduate students, researchers, and PME staff, the small exchanges that took place in the lab were very helpful in adjusting the experimental approach. Thank you very much for your interest in my research topic!

Finally, I have to say a lot to my parents and best friend YiRan, whose love, trust and encouragement have always been the reason for my efforts. Without them, this project would not have been possible. Thank you.

1 Introduction

Miniaturization and intelligence have become popular development directions for electrochemical sensors. As a result, more and more sensors are being used in various scenarios in life beyond the lab. Among them, wearable health monitoring devices show great market potential. To better fit the human skin, flexible electrochemical sensors are required. Unlike traditional rigid sensors, flexible electrochemical sensors need to allow a certain number of bends and stretches while meeting the sensor's performance. Therefore, the processing and modification of electrode materials commonly used in conventional rigid body sensors to adapt to flexible substrates have become a new field that scientists focus on.

Boron-doped diamond (BDD), which is considered one of the best electrode materials due to its wide potential window, low background current, and excellent corrosion resistance, is a promising material for integration into flexible electrochemical sensors. Diamond is a form of pure carbon known for its hardness and chemical inertness. Pure diamond is insulating, but if other (dopant) elements (e.g., boron) are incorporated during the synthesis process, the conductivity of the material can be greatly increased.

Different printing methods can meet different electrode manufacturing requirements. For example, traditional inkjet printing can print flat patterns with high precision, screen printing can be suitable for the processing of high-volume products, and there is additive manufacturing technology that can process complex 3D shapes such as fused deposition modelling. At present, printing technology is also widely used in the field of sensors, and conductive nano-inks are fixed to the substrate by printing. The conductive nano-inks for the electrodes of flexible electrochemical sensors are frequently based on mixtures of conductive particles and polymers to form composite materials, which can not only meet the needs of high electrode conductivity but also the mechanical needs of flexible sensors.

The main objective of this master's thesis project is to develop a flexible electrochemical sensor with BDD-enriched electrodes fabricated based on printing technology, which is a novel research direction in the TU Delft team. The sensor's flexible substrate and various electrodes (working, counter, and reference) will be fabricated primarily by 3D printing technology, feasibly simplifying the process steps. In addition, the newly developed sensor will undergo electrochemical tests and mechanical property evaluations, such as bending and tensile tests, to evaluate its performance.

This report consists of six chapters, the first of which is the introduction. Chapter 2 covers the fundamentals and applications of flexible electrochemical sensors, while Chapter 3 presents the research proposal with main objective and research questions. Chapter 4 reviews the electrode design with particular focus on the materials selection and electrode manufacturing. Chapter 5 presents the results and discussion of the various printing experiments and material characterizations. Finally, the list of reviewed references is given in Chapter 6.

2 Literature Review

2.1 Electrochemical Sensors: Fundamentals and Applications

Sensors are now extensively incorporated into diverse areas of contemporary society, such as industrial manufacturing, space exploration, marine investigation, environmental protection, resource identification, medical diagnosis, biotechnology, and cultural heritage conservation. Sensors are complex devices that are widely used to detect and respond to electrical or optical signals. Sensors convert several physical variables, such as temperature, blood pressure, humidity, velocity, and others, into measurable electrical signals. A chemical sensor is an analytical instrument that transforms collected data into observable or quantifiable signals for the examination of chemicals [1]. Its significant market demand stems from its ability to deliver precise information regarding the chemical composition of its surrounding environment, whether in the form of a liquid or gas phase [2]. Chemical sensors encompass a variety of types, such as electrochemical sensors, magnetic sensors, optical sensors, mass sensors, and others [3]. An electrochemical sensor is a specialized chemical sensor capable of rapidly and continuously analyzing and monitoring hazardous compounds. Electrochemical sensors are extensively utilized in clinicopathological diagnostics, pharmacological analysis, and environmental monitoring because to their speed, sensitivity, simplicity, low cost, high reliability, and online detection capabilities [4-7].

2.1.1 Basic Operating Principles of Electrochemical Sensors

Electrochemical sensors are devices that transform the effect of the redox reaction on the surface of electrodes into electronically accessible signals that indicate changes in conductivity, current, and potential [8]. **Figure 2.1** depicts the configuration and functional mechanism of an electrochemical sensor [9]. The analyte initially diffuses to the surface of a so-called working electrode, where it undergoes a redox reaction (i.e., transfer of electron(s)), resulting in physical and chemical changes that generate an electrochemical signal. This signal is then converted into an isoelectric signal (such as current, voltage, or conductivity) by a signal conversion element. Finally, the electrochemical analyzer amplifies, converts, and outputs the collected electrical signal to accurately measure the concentration of the target analyte in the sample. The sensor can be categorized into current sensors, potentiometric sensors, and conductive sensors based on the electrical signal it detects [10].

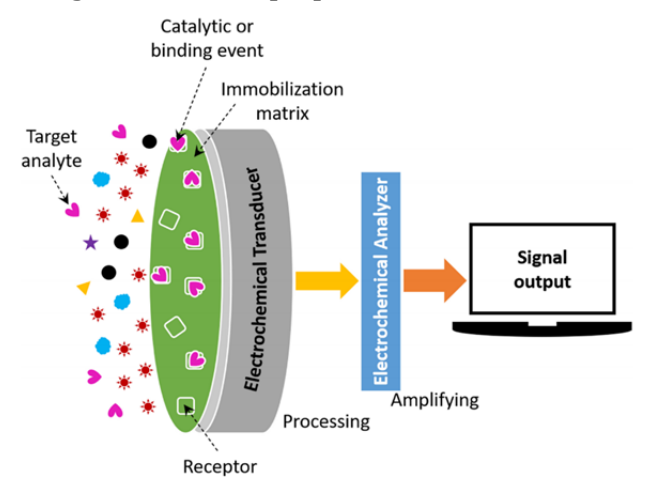


Figure 2.1: Structure and operating principle of an electrochemical (bio)sensor [9].

Electrochemical sensors can be categorized into two types: two-electrode systems (Figure.2a) and three-electrode systems (Figure.2b), depending on the number of electrodes used. Every electrochemical cell necessitates a minimum of two electrodes. The two-electrode system comprises a reference electrode (RE) and a working electrode (WE). The reference electrode regulates the potential of the working electrode by quantifying the voltage between the two electrodes. The inclusion of an auxiliary electrode (AE) or counter electrode (CE) in the three-electrode system serves the purpose of facilitating current flow. This is done to mitigate significant inaccuracies that may arise from potential variations in the reference electrode caused by the polarization current. Due to the constraints of the working electrode, the desired current is dependent on it, resulting in the working electrode being significantly smaller than the auxiliary electrode. However, in cases when the current produced by the system is extremely low and the resistance of the electrolyte is similarly very low, a two-electrode system is typically chosen. [11]

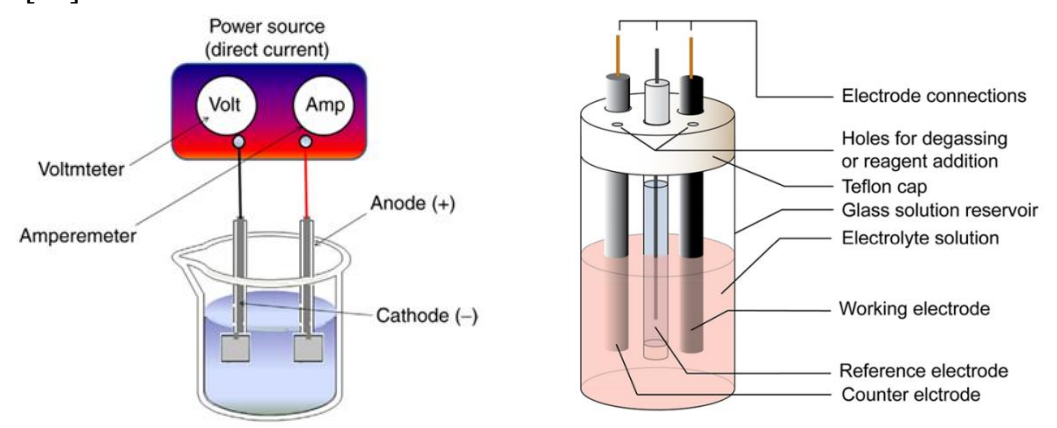


Figure 2.2: Schematic diagram of (a) two-electrode and (b) three-electrode systems [11].

In a three-electrode system, the counter electrode, working electrode, and power supply create a closed circuit to facilitate the desired electrochemical reaction and polarization state on the working electrode. Consequently, the present circuit measures the size of the electric current passing through the working electrode. The reference electrode is used to establish a potential loop with the working electrode and the potentiometer. Its main purpose is to regulate or measure the potential of the working electrode in relation to the reference electrode, thus ensuring a stable applied potential value.

One of the key factors to consider is the location of the target reaction, which occurs on the interface of the WE. Therefore, the WE which is the most crucial electrode, must possess the following characteristics: the electrochemical reaction being investigated remains unaffected by the electrode's own reaction and can be measured within a wide range of potential. The electrode must not undergo any reaction with the solvent or electrolyte components. The electrode area should not be excessively large, and the surface of the electrode should be even. The surface can be purified using straightforward methods, such as rinsing and electrochemical polarization. Typical "inactive" solid electrodes include glassy carbon, platinum, gold, silver, lead, and conductive glass.

In the field of electrochemical research, materials with stable qualities, such as platinum or graphite, are commonly utilized as CE for their ability to conduct electricity in the current circuit. The CE should thus have a low resistance and be resistant to polarization. Additionally, the CE's surface area is typically required to be bigger than that of the working electrode. This is because, when the electrode area is big, the current density decreases at the same current, this leads to a modest overpotential and low polarization [12]. Conversely, if the working electrode has a very small area, the polarization current will have a negligible effect on the auxiliary electrode's polarization. As an outcome, the potential of the auxiliary electrode remains stable during the measurement. Therefore, the auxiliary electrode can be used as a reference for potential in the measurement loop,

essentially functioning as a reference electrode. This configuration is known as a twoelectrode system.

It is required that a reference electrode can sustain the potential loop and possesses a well-defined and steady electrode potential. The exchange current density of the electrode process is significantly high, resulting in minimal polarization or difficulty in polarizing the electrode. Since, the thermodynamic equilibrium potential may be rapidly formed. Simultaneously, it is necessary for the electrolyte in the RE to be non-reactive with the electrolyte or any associated chemicals in the electrolytic cell. Furthermore, the introduction of electrolyte ions from the RE does not have any impact on the process occurring at the working electrode. Commonly used reference electrodes in electrochemical systems are the Saturated Calomel Electrode (SCE), Standard Hydrogen Electrode (SHE), and Ag/AgCl electrode. [13]

2.1.2 Electrochemical Principles

Electrochemistry is a discipline of science that investigates the interconversion of electrical energy and chemical energy, as well as the interconversion of electrical energy and matter, along with the principles governing these processes. To elucidate the operational design principle of electrochemical sensors, it is imperative to comprehend the primary reactions that take place within these sensors and their fundamental principles. This understanding is crucial for comprehending the composition and material selection involved in the design of electrochemical sensors.

An electrochemical reaction is a fundamental process where the transfer of electrons occurs between two substances, resulting in the generation or flow of an electric current. Typically, the interface occurs between solid and liquid phases, such as between electrodes and solutions. The formation of electrical current is based on the exchange of negatively charged electrons. A substance can either gain one or more electrons to conduct a reduction reaction, or the substance can lose electrons and undergo an oxidation reaction. Electrolytes or ionic conductors are substances that undergo electrochemical processes by gaining and losing electrons. Free electrons are essential in this process and are plentiful in electron conductors, which are typically metals. Electrochemical reactions occur exclusively at the interface where the electron conductor and the ionic conductor come into contact, as the activity of free electrons is confined to a narrow range. **Figure 2.3** depicts a schematic of electron transport occurring at the contact between the electrode and the electrolyte [14]. When the electrode emits electrons, the electrolyte solution experiences a reduction reaction. Conversely, when the electrode takes in electrons, the electrolyte solution undergoes an oxidation reaction [15].

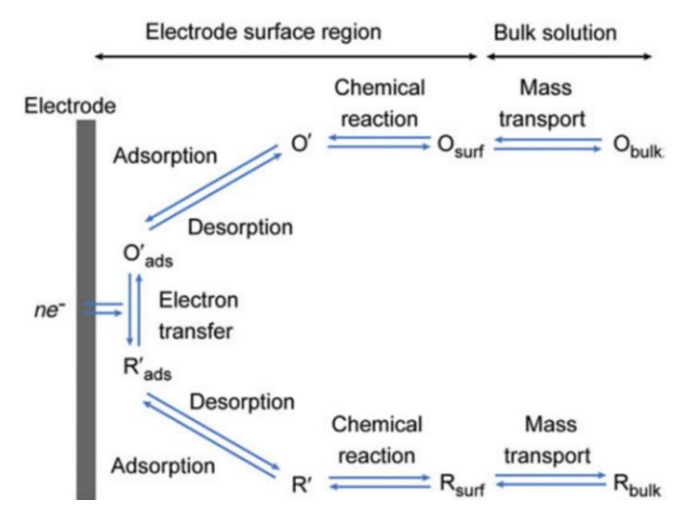


Figure 2.3: Schematic of inhomogeneous electron transfer occurring in the electrode surface [14].

Nevertheless, the production of the electrical current necessitates a fully integrated closed-loop system, rendering the electrodes incapable of existing independently. In other words, when one electrode experiences the loss of electrons and undergoes an oxidation reaction, the electrolyte solution is simultaneously reduced. Consequently, there must be another electrode that undergoes a reduction reaction, allowing the electrons to enter that electrode through the oxidation process of the electrolyte. This creates a fully closed-loop system. The processes mentioned above are classified as straightforward redox reactions. Other electrochemical reactions encompass reactions that generate gasses (such as gaseous hydrogen molecules) and reactions that precipitate and dissolve metals. [15]

2.1.3 Electrochemical Methods

The signal from an electrochemical sensor is typically derived from an electrical response such as current or potential due to an electrolytic, chemical, or biochemical reaction during the analysis of the analyte [16]. Electroanalytical methods are used to qualitatively or quantitatively analyze analytes by measuring electrical signals and determining their relationship to the analyte's relevant parameters (e.g., concentration). Electroanalytical sensing platforms offer a high sensitivity, short analysis time, low-cost, possibility for miniaturization, and portable solutions [17]. Consequently, electroanalysis is widely used in the medical field, environmental monitoring, industrial analysis, and has a good market prospect. In addition, the electrical analysis method can be divided into static (passive technology) and dynamic (active technology) using interface methods. In the static method, the electrochemical equilibrium on the electrode is not disturbed. A dynamic method involves an electron transfer between the electrode and the analyte, stimulated by an electric current and potential. This results in a redox reaction that breaks the electrochemical equilibrium and can be used in sensor analysis assays. **Figure 2.4** depicts the species branches for electrochemical analysis [18].

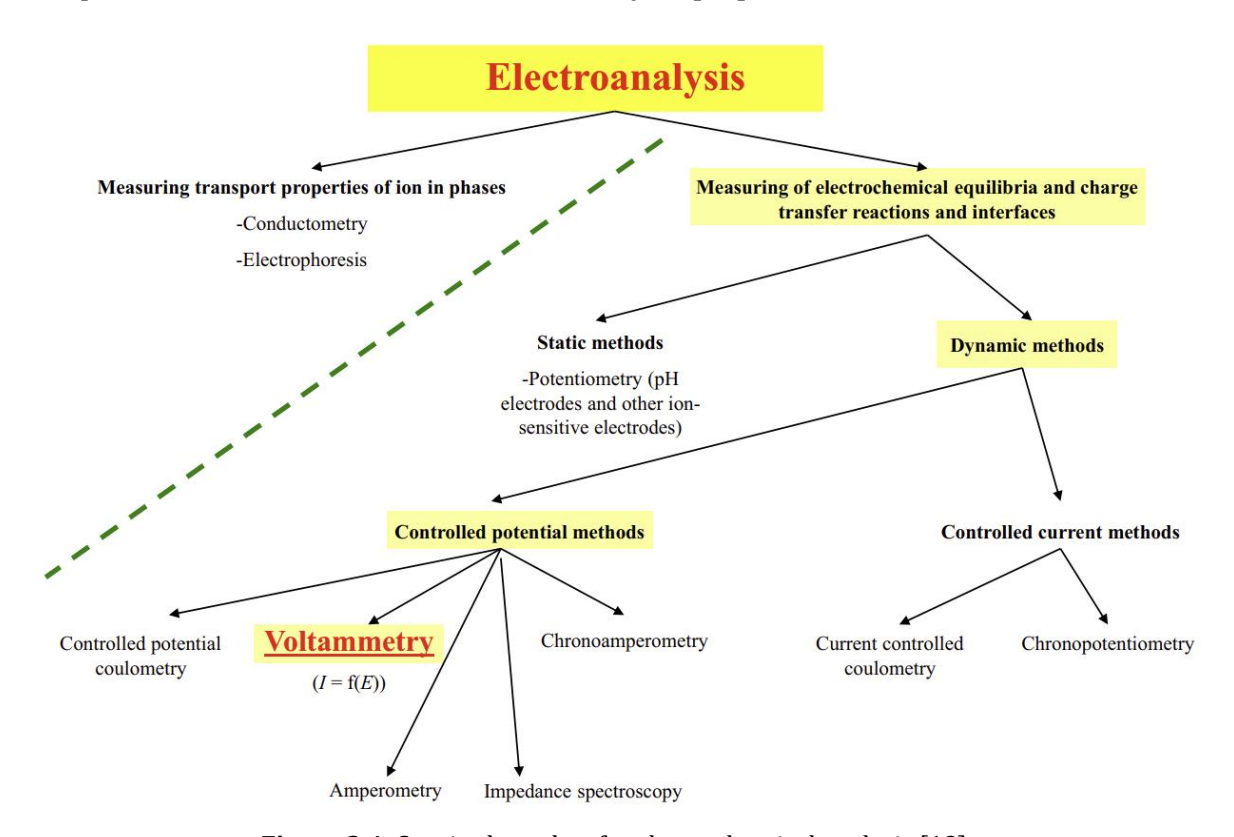


Figure 2.4: Species branches for electrochemical analysis [18].

Since electrical signals are generated from currents, resistances, and potentials in the system, **Table 2.1** classifies electrical analysis methods according to the type of electrical response they generate. Considering the common use in research and industry, the following sections focus on voltammetry and electrochemical impedance spectroscopy.

Table 2.1: Classification of electroanalytical methods [18]

Electrochemical Methods	Monitored Electrical Properties	Units	
Potentiometry	Potential difference (volts)	V	
Conductometry	Resistance (ohms)	Ω	
Amperometry and voltammetry	Current (amps) as a function of applied potential	I	
Coulometry (Q)	Current as a function of time (coulombs)	$C = I \cdot s$	
Capacitance (C)	Potential load (farads)	$F = C \cdot V^{-1}$	

2.1.3.1 Voltammetry

Voltammetry, as the name suggests, means measuring current as a function of voltage. By applying a potential (E) to the electrode, the analyte generates a current (I) on the electrode surface, and by measuring the resulting current, a graph between the current and the potential is obtained, which is called a volt-ampere diagram [19]. The applied potential can be varied, or the current over some time (t) can be controlled, and all volt-ampere techniques can be expressed as a function of current (I), potential (E), and time (t). Modern voltammetry is mostly used in three-electrode systems. Although voltammetry is not as crucial as chromatography and spectroscopy in industrial research [20], it has received extensive attention in research because of its good sensitivity, short analysis time, and the ability to measure multiple analytes simultaneously [21]. Voltammetry can be broadly divided into cyclic voltammetry, pulsed voltammetry, and stripping voltammetry, according to the different signals applied to the electrochemical cell. Cyclic voltammetry is selected as an example to introduce the analysis principle of voltammetry techniques.

As one of the most commonly used electrochemical analysis methods, cyclic voltammetry is widely used in the continuous inspection of redox reactions and the detection of products. In the cyclic voltammetry of a three-electrode system, an external voltage is applied to the system, i.e., a linear potential sweep is initiated, and a reverse point sweep is performed after reaching the highest potential point, accompanied by the measurement of the current between WE and CE throughout the process. Figure 2.5 illustrates a typical cyclic voltammetry scan. **Figure 2.5(a)** shows the change in applied external voltage over time, from which it can be seen that during the forward potential scanning, the reduced species in the solution is oxidized (i.e., loss of electron(s)) to the oxidized species, free electrons are generated, and the oxidation reaction occurs. When the direction of the scanning potential is changed to perform a reverse potential scan, the oxidized species in the solution is reduced (i.e., gain of electron(s)) to a reduced species, which consumes free electrons, and the reaction occurs in the opposite direction. Free electrons determine the current measured in a loop consisting of WE and CE. Figure 2.5(b) shows the key points are the peak-current and peak-potential of both anodic (I_{p, a} and E_{p,a}) and cathodic $(I_{p,c})$ and $E_{p,c}$ components. Kinetic and thermodynamic information, such as the rate of chemical processes for electron heterogeneity or homogeneous transfer, can be determined by measuring the above parameters as a function of the scan rate. [22]

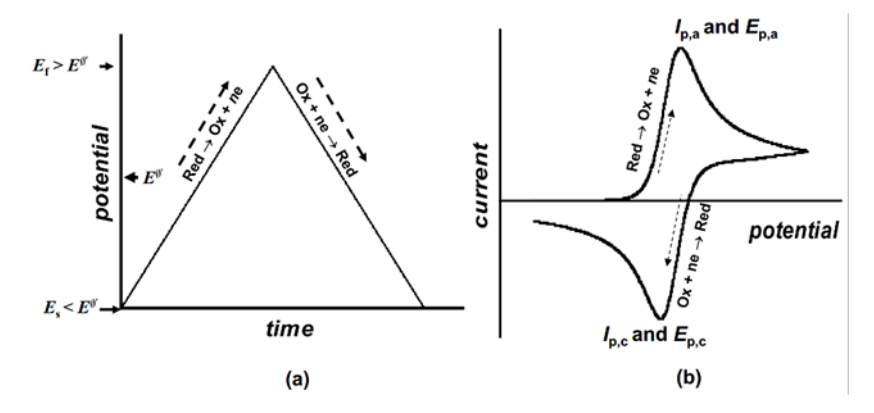


Figure 2.5: Typical potential changes (a) and the shape of I-E curves (b) in cyclic voltammetry [22].

From a microscopic point of view, when there is no applied voltage, the species in the electrolyte move randomly and irregularly (Brownian motion). As the potential increases, the working electrode acts as the anode region, and the cation emitted by the electrode diffuses into the solution. The oxidation reaction occurs at the interface between the working electrode and the electrolyte. **Figure 2.6** illustrates the formation of a double capacitance layer, which is a dense layer of ions that develops on the electrode's surface. The first area is referred to as the inner Helmholtz plane (IHP) and consists primarily of polar water molecules and specifically adsorbed anions. The second layer primarily consists of fully hydrated cations, referred to as the outer Helmholtz plane (OHP). The diffusion layer, which spans from the outer heliosphere (OHP) to a significant portion of the solution, is primarily composed of hydrated anions and cations. With the consumption of cations near the electrode, the cations in the electrolyte spontaneously diffuse to the electrode surface to replenish them, resulting in an increase in the ion concentration at the electrode-electrolyte interface, which is different from the concentration at the distal end of the electrode, forming a concentration gradient and leading to the formation of a diffusion layer [23]. As the diffusion layer gradually thickens, the resistance to the thickening of the diffusion layer is greater than the driving force of the chemical potential gradient, resulting in a decrease in the diffusion rate and a decrease in the current, resulting in concentration polarization, which is the reason for the current peak in **Figure 2.5(b)**. When the direction of the potential scanning is changed, the working electrode is negatively charged, and the cations in the solution move in the direction of it.

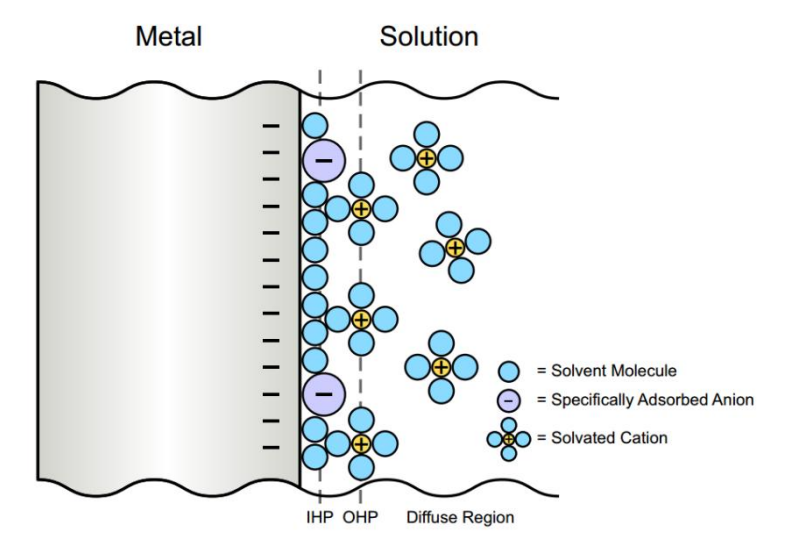


Figure 2.6: Schematic diagram of the electrical double layer, including IHP, OHP, and the diffuse layer in the Stern model [23].

The cause of ion diffusion is the chemical potential gradient. With the diffusion phenomenon, the diffusion impedance also appears, i.e., the occurrence of oxidation and reduction peaks in the cyclic voltammetry curve. The Randles-Sevcik equation (eq. 2.1) shows how to solve the diffusion coefficient using these peak data [24]:

$$i_p = 0.4463nFAC \left(\frac{nFvD}{RT}\right)^{\frac{1}{2}} \tag{2.1}$$

 $\cdot i_p = \text{Current maximum (A)}$

 $\cdot n$ = Number of electrons transferred in the redox event (usually 1)

 $\cdot A = \text{Electrode area (cm}^2)$

 $\cdot F = \text{Faraday Constant (C mol}^{-1})$

 $\cdot D = \text{Diffusion coefficient } (\text{cm}^2/s)$

 $\cdot C = \text{Concentration (mol/cm}^3)$

v = scan rate (V/s)

 $\cdot R = \text{Gas constant } (\text{J K}^{-1} \text{ mol}^{-1})$

T = Temperature (K)

· The constant with a value of 2.69×10^5 has units of C mol⁻¹V^{-1/2}

The peak current depends not only on the concentration of active substances in the electrolyte and the diffusion characteristics but also on the potential scan rate. This is due to a change in the applied voltage, which results in a change in the concentration of the electrolyte. The concentration and diffusion velocity affect the concentration gradient, the concentration gradient near the electrode affects the amount of diffusion, and the current is limited by the diffusion of the substance to the electrode surface. So, a faster potentiometric sweep speed results in a higher concentration gradient and, thus, a higher peak current. In addition, the Randles–Sevcik equation can be used to determine whether an analyte is free to diffuse, as well as to calculate the diffusion coefficient. [24]

2.1.3.2 Electrochemical Impedance Spectroscopy

Electrochemical impedance spectroscopy (EIS) can be used for complex electrochemical systems to analyze the electrochemical processes that occur at the interface between the electrode and the analyte and can measure complex resistance and mass, charge, and diffusion processes. EIS measurements in electrochemical systems can be simulated as equivalent circuits that consist of common passive components (such as resistors, capacitors, and inductors) and other more complex (called distributed) components connected in different ways, so most electrochemical analyzers are equipped with software that simulates impedance data into the model circuit [25]. The reactions that occur in the electrochemical cell are represented by establishing equivalent circuits containing resistance, capacitance, and inductance, and the measured values of EIS are explained by electrical equivalent circuits (EEC), and then the EIS values are used to detect the properties of materials and the laws of electron transfer.

EIS is based on the introduction of perturbations in a state of electrochemical equilibrium, i.e., the application of a sinusoidal signal over a wide frequency range, and the monitoring of the system's current or voltage response to the applied perturbation, which is a method of identifying and determining parameters based on models built on the frequency response of the electrochemical system under study.

In the experiment, if the input signal, $E = E_0 \sin(\omega t)$, is applied to the sample to be measured, the output current. $I = I_0 \sin(\omega t + \varphi)$, is measured by a frequency response analyzer coupled to the electrochemical interface, where the angular frequency $\omega = 2\pi f$,

and the φ is the phase angular displacement. The impedance, $Z = R - jX_c$, where R is the real part of the resistance and impedance (Z'), j is equal to 1, X_c is the capacitive impedance, and $-jX_c$ is the imaginary part of the impedance (Z''). By changing the frequency of the alternating signal, the complex impedance represented by $Z(\omega)$ is obtained, and the modulus $Z_o = E_o/I_o$ and phase angle are calculated so as to determine the real and imaginary impedance values, as shown in **Figure 2.7(a)**. **Figure 2.7(b)**, on the other hand, shows a schematic diagram of the impedance analysis of an equivalent circuit with a capacitor and resistor in parallel. The real axis is composed of $Z = Z_o \cos(\omega)$ and Z' = R, and the imaginary axis is composed of $Z'' = Z_o \sin(\omega)$. From the resonance condition, $2\pi f_o RC = 1$, the resonant frequency f_o at the top of the semicircle can be calculated. [27]

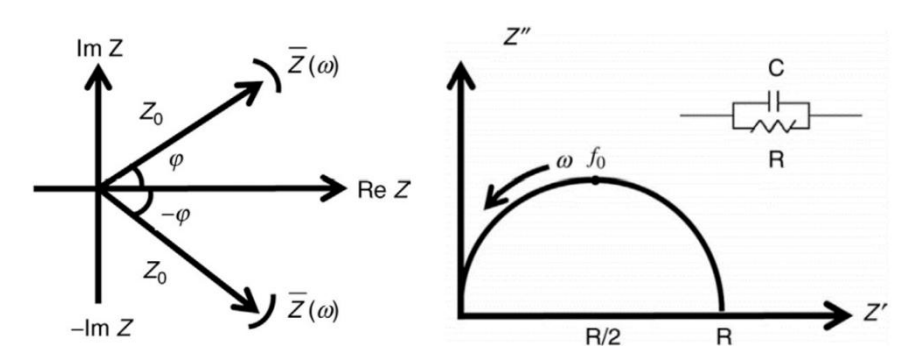


Figure 2.7: (a) Vector representation of the complex impedance Z; (b) Schematic illustration of the impedance analysis response of a parallel RC circuit [27].

Unlike time-domain-based voltammetry (e.g., cyclic voltammetry), EIS works in the frequency domain and simplifies complex electrochemical systems over a wide frequency range by deconvoluting them into individual processes with different time constants, making it easy to analyze processes that cannot be analyzed by voltammetry. Impedance spectroscopy is frequently employed for the analysis of thin coatings on electrodes due to its ability to differentiate between various conductivity mechanisms present in the material. This method of identifying and determining parameters based on models of the frequency response of electrochemical systems is frequently used in corrosion studies, thin film surface characterization, batteries, semiconductor electrodes, electrochemical sensors, and biosensors [28,29].

2.1.4 Applications

The use of electrochemical sensors for industrial oxygen monitoring in the 1950s could be considered the beginning of the application history of electrochemical sensors. With the continuous development of industry and the improvement of people's safety awareness, the monitoring of toxic gases and fluids in confined spaces led to a surge in market demand for monitoring equipment. Electrochemical sensors have attracted the attention of scientists because of their ability to monitor the concentration of specific substances in gases and liquids [30].

Clark, known as the "father of biosensors", proposed the concept of an oxygen sensor that separates the electrode from the electrolyte solution through an oxygen-permeable membrane, through which oxygen diffuses, and the diffused oxygen reaches the indicator electrode and is reduced [31]. In Clark oxygen sensors, the current generated is proportional to the oxygen concentration in the sample gas, but the current signal generated is unstable and requires constant recalibration.

Modern electrochemical sensors for gas monitoring are not only found in environmental monitoring and food quality monitoring but also in biomedical fields, as shown in **Figure 2.8** [32]. With their high selectivity, they can be employed in the biological field, e.g., for

the detection of specific biomolecules, to the medical field, where they can greatly contribute to drug development via the monitoring of drugs in clinical trials and the evaluation of drug efficacy in cancer treatment, for example.

At the same time, the combination of electrochemical sensors with other disciplines such as biology and nanotechnology has become a new popular trend. For example, advances in materials science have not only enriched the types of materials available for electrodes and substrates but also significantly improved the performance of electrochemical sensors. The development of nanoengineering has made it possible to integrate electrochemical sensors at the nanoscale [33], greatly facilitating the development of in vivo and portable medical devices. Advances in process manufacturing have greatly reduced the cost of manufacturing and maintenance and also made it possible to process nano-sized components and complex structures. The development of smartphones has made it possible to create miniaturized analytical systems outside of the laboratory, setting off a wave of technology for portable wearable devices.

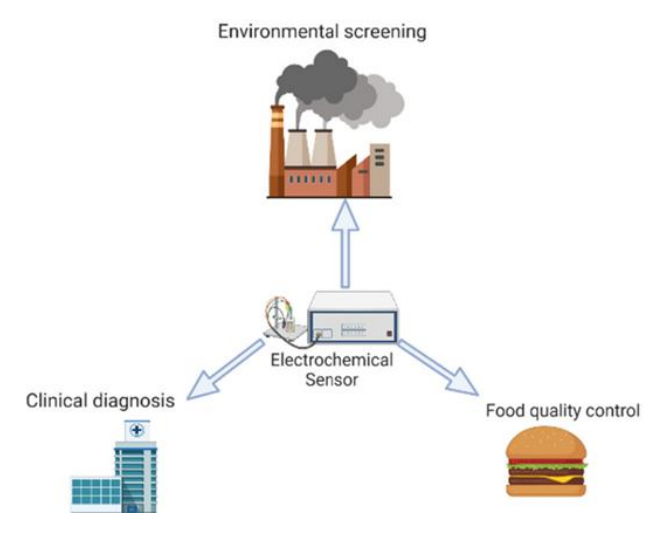


Figure 2.8: Schematic depiction of the application of electrochemical sensors in various fields [32].

2.2 Flexible Electrochemical Sensors

This section discusses the development of flexible electrochemical sensors, which are different from conventional rigid sensors. First, we will explain why flexible electrochemical sensors are of interest and how they differ from traditional non-flexible sensors. Next, we will introduce today's materials and processing methods commonly used in flexible electrochemical sensors. Finally, specific application examples of flexible electrochemical sensors will be given.

2.2.1 Why flexible?

Conventional electronic sensor components are mostly based on metal and semiconductor materials, and their flexibility and mechanical properties are limited, such as poor stretchability and bendability, which not only limits their application environment but also affects their sensitivity. Electrochemical sensors, which are widely used electronic devices, are also changing from being used only in the laboratory to being used in a variety of scenarios outside the laboratory (see Figure 2.8). Although traditional rigid electrochemical sensors are widely used, they are unsuitable for detecting human activity [34]. This is where flexible sensors come into being, which are made of inorganic and organic electronic materials in nanostructures combined with flexible substrates,

thus overcoming the weakness of the brittleness of rigid materials. [35]

Combining biomedical and mechatronic devices has received much attention. The development direction of modern electrochemical sensors is miniaturized, low-cost and high-sensitivity, which makes their application in the biomedical field possible. Flexible electrochemical sensors have great potential in monitoring human health physiological signals due to their good biocompatibility and flexible mechanical properties. On the one hand, flexible electrochemical sensors can detect target molecules outside the laboratory environment and analyze the interaction or specific binding between the target molecule and sensing probes such as enzymes, nucleic acids, or antibodies. On the other hand, selecting flexible substrates can overcome the effects of stretching and bending to a certain extent, making them suitable for bonding with human skin [36]. Flexible electrochemical sensors offer a wide range of possibilities for specific diagnosis and analysis while evoking good integration with the skin and can also be good candidates for wearable and continuous detection. Therefore, portable and wearable electrochemical sensors with high sensitivity, bendability, and stretchability have broad market prospects for detecting electrolyte solutions, drug analysis, and biomolecules [37].

Nowadays, most analytical methods rely primarily on laboratory analytical techniques, such as gas-liquid chromatography, which require expensive and cumbersome equipment, as well as relatively time-consuming and complex sample preparation processes (such as digestion or clean-up steps), complex equipment operations, trained personnel, and specific consumables, ultimately lengthening the detection process [38]. Miniaturized analytical systems have the particular advantages of portability and low cost and can be used for applications outside of the laboratory environment, overcoming the shortcomings of traditional analytical methods [39]. Wearable, flexible devices have recently become a major wave of technology, primarily for monitoring therapeutics and providing real-time health feedback. Wearable sensing devices are conveniently worn and allow for uninterrupted monitoring of the wearer's health without being invasive or obtrusive. Wearable and flexible chemical sensors can offer immediate physiological data by detecting the fluctuating levels of biomarkers in bodily fluids such interstitial fluid, perspiration, saliva, and tears. Figure 3.1 illustrates a flexible, glove-based electrochemical sensing device for external drug screening [40]. This smart glove sensor will address the urgent need for on-site, real-time drug screening rather than commercially available hypothetical colour testing or bulky, expensive portable spectroscopy tools. At present, portable sleeve sensors show a huge market potential.

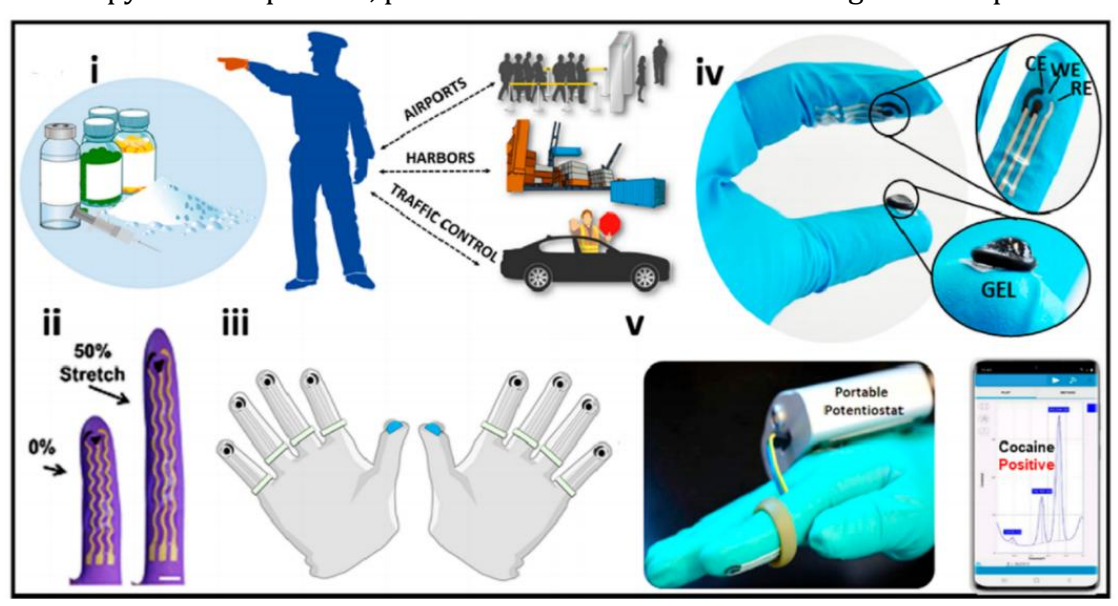


Figure 3.1: Applications of glove-based wearable sensors for drug detection. [40-44].

Flexible electrochemical sensors can also be applied to human health monitoring. For example, flexible electrochemical sensors can be applied directly to human skin (Figure **3.2(a)**)[41] or clothing (**Figure 3.2(b)**)[42] due to their excellent biocompatibility and flexible mechanical properties. Among them, many harmful heavy metal ions can cause renal insufficiency, bone disease, and lung injury [43]. Flexible electrochemical sensing devices can monitor trace metal ions in sweat. As shown in Figure 3.2(c), Kim et al. fabricated a flexible electrochemical sensor for noninvasive monitoring of trace metals (Zn) in human sweat [44]. The sensor electrodes are manufactured onto the tattoo paper via screen printing, guaranteeing that the temporary zinc tattoo is both flexible and capable of enduring repetitive mechanical stress deformations. Additionally, a clear and consistent zinc reaction is observed in human sweat. Flexible sensors have the capability to detect both ions and biomolecules. As shown in Figure 3.2(d), Yang et al. created a biosensor capable of identifying the presence of pathogenic E. coli O157:H7 DNA through hybridization. The researchers showed that a unique paper electrode has both high sensitivity and specificity towards the pathogenic strain of E. coli known as 0157:H7 [45]. Flexible electrochemical sensors have shown promising advancements in detecting physiological signals in human health, benefiting from the growing interest in healthcare and biomedicine in recent years. Future sensor development has seen a rise in their popularity as a trend. [46].

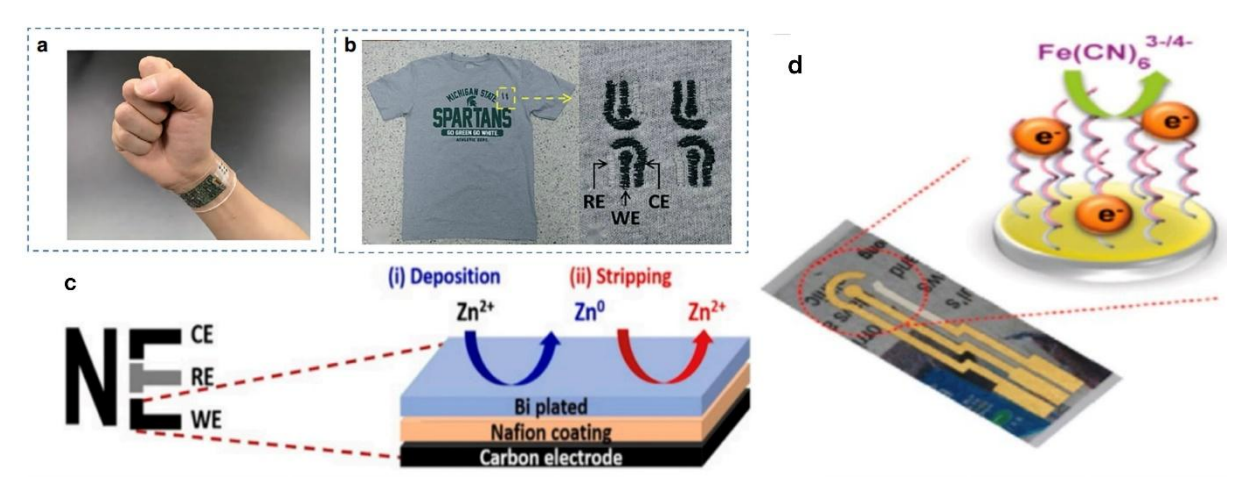


Figure 3.2: The following examples demonstrate different wearable sensing platforms: (a) a wearable sensing platform that uses PET as the substrate [41]; (b) an embroidered electrochemical sensor for biomolecular detection that is fabricated on a cotton t-shirt [42]; (c) a temporary tattoo sensor that utilizes a bismuth/Nafion working electrode for stripping-voltammetric analysis [44]; and (d) the P-paper electrode, which enables electrochemical detection of food-borne pathogens [45].

2.2.2 Materials of flexible sensors

Compared with traditional rigid semiconductor sensors, the key to selecting materials for flexible electrochemical sensors is that the flexibility and tensile properties of the materials under stress do not cause physical damage to the sensor and do not significantly affect the performance and sensitivity of the sensor. For this reason, flexible sensors are often made of a flexible substrate and specific electrode materials. Among them, the flexible substrate plays a supporting role, which must not only meet satisfactory flexibility and tensile properties but also maintain the ideal electrochemical and mechanical stability. Therefore, materials with relatively low Young's modulus are mainly selected for flexible substrates. Currently, plastics [47-49], paper [50-55], textiles [56-58], and polymers [59,60] are four common flexible substrate material classes. However, the use of plastics is widely limited due to their poor adhesion. Paper has the advantages of low cost, easy preparation, good biocompatibility, hydrophilicity, etc., and is an ideal substrate. The softness and foldability of paper are conducive to reducing the size of the device and

enriching the structural functions of the device, and the paper-based device can be relatively easy to process microfluidic channels [61]. Textile-based flexible substrates can be applied to everyday clothing and are more suitable for use in flexible electrochemical sensors that come into contact with human skin due to their breathability, flexibility, durability and lightweight.

Unlike the flexible substrates described above, the polymer substrates have the advantages of high flexibility, lightweight, high availability, and low price. Traditional flexible polymer substrates are polyethene terephthalate (PET) [62], polydimethylsiloxane (PDMS) [63-65], polyurethane (PU) [66], and polymethyl methacrylate (PMMA) [67], whereas polydimethylsiloxane (PDMS) has been the preferred choice in many studies. Compared with other flexible substrates, it has the advantages of easy availability, stable chemical properties, high transparency, and good thermal stability. However, polymer substrates are less breathable and elastic than textiles and have a lower degree of compatibility with the skin.

In electrode manufacturing, compared with traditional rigid electrodes, we need to consider the stability of the electrochemical properties and mechanical properties of the electrode in the tensile or bent state. Among them, flexible conductive nanomaterials are widely used in the electrode design of flexible electrochemical sensors. For the construction of flexible electrode materials, it can be considered to combine conductive nanomaterials with elastomer materials, such as dispersing conductive nanomaterials into elastomeric materials or coating and depositing them on the surface of elastomer materials. Below, we divide nanomaterials into 0D, 1D, 2D and hybrid nanomaterials [69].

OD nanomaterials mainly include metal nanoparticles (such as gold, platinum, silver, and copper), which usually have good stability and conductivity. The preparation of copper nanomaterials has attracted extensive attention due to their low price and non-toxicity advantages. Silver nanoparticles (AgNPs) have better electrochemical properties than copper nanoparticles and cost less than platinum or gold. Therefore, silver nanoparticles are commonly used in the preparation of conductive inks, and printed silver nanoparticles are often used on paper substrates for the preparation of electrodes. However, the mass production of silver-based flexible devices is considered difficult. [70]

1D one-dimensional nanomaterials, including gold nanowires (AuNWs), carbon nanotubes (CNTs), and silver nanowires (AgNWs), have inherent high aspect ratios, which reduce material consumption and improve tensile properties [71]. Compared with 0D metal nanoparticles, 1D metal networks are widely welcomed in the market due to their excellent electrical conductivity and mechanical flexibility. Carbon nanotubes (CNTs) are very desirable nanomaterials for creating flexible electrochemical sensors because they possess several advantageous properties, including high electrocatalytic activity, affordability, excellent conductivity, and strong chemical stability. However, it is a challenge to improve the electrochemical performance of flexible CNTs by improving their electrocatalytic activity and reducing the resistance of stretching on the separation of conductive networks. [72]

2D two-dimensional nanomaterials are a new type of nanomaterials with superior physical and chemical properties of two-dimensional layered structure. Their strong inplane chemical bonds and ultra-low thickness give them excellent mechanical strength and flexibility, providing good performance support and more possibilities for constructing flexible electrochemical biosensors [73]. Graphene is widely used in flexible electrochemical sensors due to its excellent physical and chemical properties and extraordinary mechanical strength. In order to reduce the impact of the electrode after multiple bending, microelectrode arrays can be prepared by adjusting the shape and size of graphene [74], and the conductivity and recognition area can also be increased by preparing a Molecularly imprinted polymers (MIP) layer on the surface of graphene [75].

Hybrid nanomaterials combine several nanomaterials to obtain better conductivity and

catalytic ability according to their synergistic effect to improve their electrochemical properties. For example, graphene can be directly combined with nanomaterials such as metal nanoparticles [76] and CNTs, and AgNWs can also be combined with other electrochemical nanomaterials such as metal NPs [77] to improve the electrochemical performance and good mechanical strain capacity of the electrode.

2.2.3 Fabrication of flexible sensors

To manufacture flexible electrochemical sensors, we need to consider the method of processing the electrode material and the method of processing the electrode material to the flexible substrate. Here are a few common methods used to process flexible electrochemical sensors:

♦ Sputtering

Sputtering technology is based on the physical phenomenon of forming a conductive layer and is applied to forming a thin metal conductive layer. Sputtering technology uses metal elements extracted from a metal target's surface to bombard the substrate's surface with plasma or gaseous high-energy particles, which can uniformly form a conductive metal layer on a non-conductive substrate [78]. Since the creation of conductive layers can be easily achieved, sputtering technology can also develop flexible electrochemical sensors with high conductivity by depositing novel metals on electrodes [79]. **Figure 3.3(a)** illustrates a susceptible, flexible electrochemical sensor for monitoring glucose levels in body fluids, in which indium oxide (In_2O_3) is sputtered and deposited on a PET substrate [80]. However, when developing flexible three-electrode sensors using sputtering technology, the use of this method is limited due to its random deposition characteristics over the entire area of the deposited substrate.

♦ Electrodeposition and chemical vapor deposition CVD

The deposition techniques applied to prepare electrochemical electrodes mainly include electrodeposition and chemical vapour deposition (CVD). Electrodeposition is a processing electrode technique that uses a metal ion solution and simple electrochemical techniques to form a highly conductive layer on the surface of a conductive or semiconductor substrate. Kim et al. fabricated a flexible ultrasensitive glucose biosensor using electrodeposition, in which platinum nanoparticles were electrodeposited on a flexible graphene-modified PI substrate [81]. CVD, as one of the standard methods for coating conductive films on the substrate surface, converts the conductive material into a volatile precursor, and the precursor gas is passed through the substrate surface that is heated to a specific temperature, and a chemical reaction occurs to produce solid deposition on the substrate [82]. The key to CVD is to control the substrate temperature, which in turn affects the occurrence of different reactions.

♦ Direct-writing

Direct writing is a simple, fast, and low-cost way to fabricate conductive films on solid substrates by applying conductive ink directly to the surface of a substrate using a roller ballpoint pen [83]. Hu et al. fabricated adhesive silver-based inks on paper to fabricate highly conductive stretchable circuits. The ink is composed of silver nanoparticles and ketones as solvents and has good chemical stability, which can be directly used to write conductive layers of electronic circuits on different substrates [84]. Figure 3.3b(a) shows a general conductive ink under a suitable solvent, (b) shows the filler dot, and (c) shows the resistance of a synthetic ink measured using a multimeter. Direct-writing has the advantage of being portable and versatile in fabricating functional nano-inks [85].

♦ Lithography technology

Photolithography can directly impart conductivity in different areas of the flexible substrate to establish an exemplary geochemical system. Photolithography adds conductive inks to the mask by adding monodisperse colloids to the mask and drying it. After a period of time, monodisperse colloids are removed from their surfaces to obtain patterns on which conductive materials form [85]. Therefore, lithography is well suited for fabricating precision conductive electrodes on flexible substrates with precise control of the electrode pattern. **Figure 3.3(c)** illustrates a flexible electrochemical interleukin-10 biosensor based on a three-electrode system that is fully integrated on a flexible PI substrate by photolithography and can simultaneously detect changes in ion, temperature, and pH [86]. At present, high-precision lithography is one of the most commonly used tools for the development of flexible electrochemical sensing platforms with multiple detection targets and multi-functional integration, but complex processes, cumbersome operations, and expensive instruments still limit it.

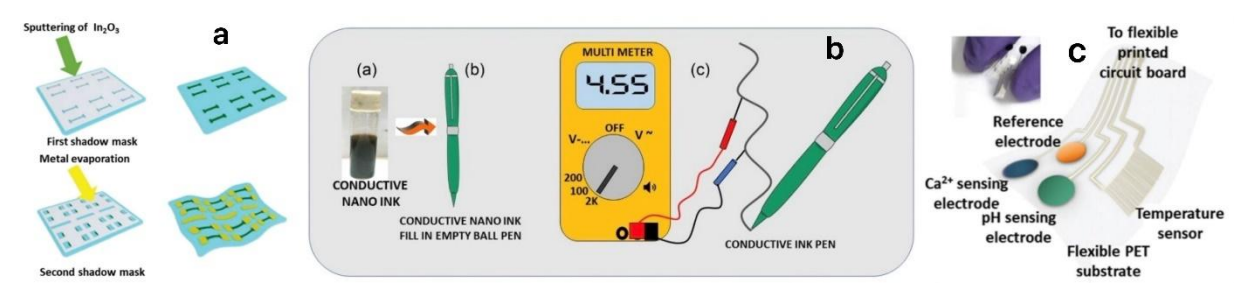


Figure 3.3: Applications of different process methods: (a) Sputtering [80]; (b) Direct-writing [84]; (c) Lithography [86].

♦ Printing

In recent years, printing technology has become increasingly popular in various fields by being accessible enough to be widely implemented. Printing technology creates complex structures on any substrate precisely and controllably by spraying any material that can be present in the solution. First of all, inkjet printing is a more traditional and popular method for manufacturing conductive materials because it is simple to operate, has high accuracy in direct computer control, and is suitable for a variety of substrates. However, the formulation of conductive nano-inks for inkjet printing on different substrates is very challenging, and ink defects can cause the printer nozzle to clog. Secondly, screen printing is also a simple, versatile and low-cost technology that is widely used in the manufacture of sensors. The process begins with the use of a screen mask consisting of a web of fibres and a template attached to the screen. The ink is applied and pressed on the screen template mask, and the ink passes through the part of the mesh that is not covered by the template to the surface of the substrate, thus forming a specific printing pattern. Screen printing is very suitable for mass production in manufacturing sensors due to its low cost and ease of operation [87]. In addition, 3D printing technology has become the trend of future printing technology development, with its unique ability to create specific threedimensional structures, providing a flexible, efficient, and customizable method for manufacturing flexible sensors. In the next section, we will take a closer look at the application of printing technology for processing flexible electrochemical sensors. [88]

2.3 Electrode Design

A flexible electrochemical sensor consists of a flexible substrate and three electrodes. Different from traditional rigid sensors, the electrode shape also needs to be considered in the design to ensure the mechanical properties of flexible sensors. In order to design and fabricate a flexible electrochemical sensor, it is necessary to select the electrode and substrate materials and consider the influence of different processing methods and

processing sequences on the finished product. The above shows that polymers are commonly used as flexible substrate materials, while electrode materials are more selective. Next, we will introduce some materials that have the potential to be used as flexible electrodes and how to process them.

2.3.1 Electrode shape

In order to obtain better mechanical properties of electrochemical sensors, Li et al. compared the mechanical properties of printed electrodes with different shapes by taking uniaxial tensile properties as an example [89]. In this experiment, three different periodic structures, namely S-shaped tortuous (SZ), triangular tortuous (TZ) and rectangular tortuous (RZ), were designed to study the molding effect of FDM process on flexible strain sensors and their strain-inducing properties. As shown in **Figure 4.1**, the different morphologies of these geometries improve the adaptability and performance of flexible TPU-based sensors in real-world applications. This study shows that the flexible sensor with the periodic structure of SZ has higher sensitivity than the TZ or RZ configuration, and at the same time has better flexibility and stretchability, and is not easy to crack due to deformation. In contrast, TZ and RZ structures tend to form stress concentrations at right or sharp corners when stretched, leading to fracture and thus reducing conductivity and sensing performance. Therefore, SZ shaped electrodes are a better choice as flexible sensor electrode shapes.

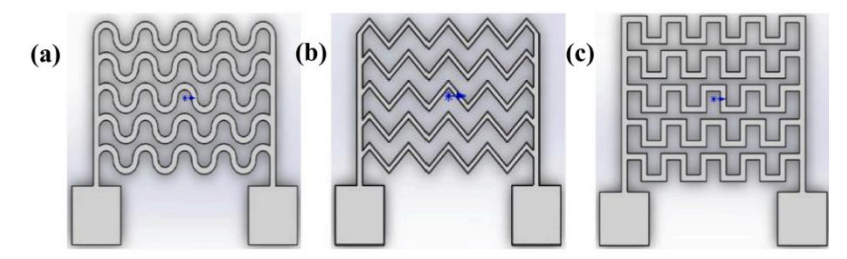


Figure 4.1: Schematic diagrams of the periodic configurations of SZ (a), TZ (b), and RZ (c) [89].

2.3.2 Electrode materials (WE, CE, RE)

2.3.2.1 Polymer (substrate)

According to chapter 3.2, we can see that the polymers commonly used in the processing of flexible electrochemical sensors are thermoplastic polyurethanes (TPU), polyethene terephthalate (PET), polydimethylsiloxane (PDMS) and polymethyl methacrylate (PMMA). These polymers can be used as flexible substrates for sensors and as flexible electrodes mixed with conductive materials. As flexible substrates, polymers are famous for their good plasticity, thermal stability, bending resistance, and excellent dielectric properties. Let us briefly examine each of the four commonly used polymers.

Thermoplastic polyurethanes (TPU) not only have most of the characteristics of rubber and ordinary plastics but also have excellent comprehensive physical and chemical properties. It is a new type of polymer environmental protection material between rubber and plastic, which has both the softness of rubber and the hardness of hard plastics. TPU overcomes many defects of Polyvinyl chloride (PVC) and polyurethane (PU) coatings and has made a breakthrough in applying waterproof and breathable fabrics. TPU is mainly divided into polyester type and polyether type, which has a wide range of hardness (60HA-85HD), high elastic modulus ($10\sim1000$ Mpa), high mechanical strength, good processing performance, oil resistance, wear resistance and good recycling. The normal operating temperature range of TPU is - $40\sim120^{\circ}$ C. However, TPU has average high-temperature resistance and is not resistant to polar solid solvents and strong acid and

alkali media. [89]

Polyethylene terephthalate (PET) is a thermoplastic polyester with excellent thermal, mechanical, chemical, electrically insulating and abrasion resistance. PET plastic has a high melting point, generally between 250-260°C. It has good thermal and dimensional stability and is able to maintain stable performance in high-temperature environments. At the same time, PET plastic has high tensile strength, bending strength and impact strength, as well as good wear resistance and fatigue resistance. PET plastic is a recyclable material. However, PET has poor hydrolysis resistance in high temperature, high pressure, acidic and alkaline environments, and is sensitive to some strong acids, strong alkalis and other chemicals. Although PET has a higher melting point, the heat deflection temperature is lower, generally between 80-90°C. In addition, PET plastic is difficult to process because it requires high temperatures and pressures during the moulding process. [90]

Polydimethylsiloxane (PDMS) is a common organosilicon compound consisting of multiple methylsilicon units linked by silicon-oxygen bonds. PDMS is widely used in many fields due to its excellent thermal stability, chemical inertness, dielectric properties, and excellent biocompatibility. The physical properties of PDMS determine its application in several fields. First, PDMS has extremely low surface tension and excellent wettability, exhibiting excellent fluidity and surface activity in liquids. Secondly, PDMS has a low refractive index, transparency, and lightfastness, making it suitable for preparing optical materials. In addition, PDMS also has good thermal conductivity and can be used in the preparation of thermally conductive materials. Currently, PDMS is one of the most commonly used materials for moulding microfluidic devices. [91]

Polymethyl methacrylate (PMMA) is a polymer compound with excellent optical properties (transmittance up to $90\%\sim92\%$), mechanical properties, electrical properties and chemical stability. In terms of mechanical properties, PMMA has high impact strength, good toughness, and wear resistance, and it can maintain stable performance in various environments. The melting point of PMMA is $130\sim140$ °C, and the glass transition temperature is about 105 °C. PMMA is mainly used in the medical field to make various artificial joints, teeth, orthopaedic implants, etc. Due to its high biocompatibility and abrasion resistance, PMMA products can provide patients with a comfortable use experience and a long service life. [92]

2.3.2.2 Diamond (WE)

Diamond properties

The diamond structure is shown in **Figure 4.2(a)** [93]. Diamond is a colourless octahedral crystal linked by carbon atoms with tetravalent bonds, making it the hardest substance known to exist naturally. Because the C-C bond in a diamond is very strong and the carbon atom is sp^3 hybridized, all the valence electrons are involved in the formation of covalent bonds; there are no free electrons, so the hardness of a diamond is very large, the melting point is 3500 °C, and the ignition point of diamond in air is $850 \sim 1000$ °C, and it is not conducive. It has high hardness and wear resistance, thermal conductivity, and good electrical insulation. It also has excellent light transmittance and corrosion resistance and is widely used in electronics. [93]

Another substance composed of pure carbon is graphite, which is a dark grey, metallic, opaque, fine, flake-like solid. Unlike diamond, graphite is soft due to the different structure of carbon atom arrangement. Its layered crystal structure with sp² hybridized carbon atoms is shown in **Figure 4.2(b)**. Every carbon atom is tightly bound to form a regular hexagon through strong interaction with the three carbon atoms around it. Because the distance between the middle layers of graphite is relatively large, and the interaction of carbon atoms is weak, it is easy to slide and crack in the direction parallel

to the layer, so graphite is very soft and slippery. The melting point of graphite is higher than that of diamond (3550°C).[94]

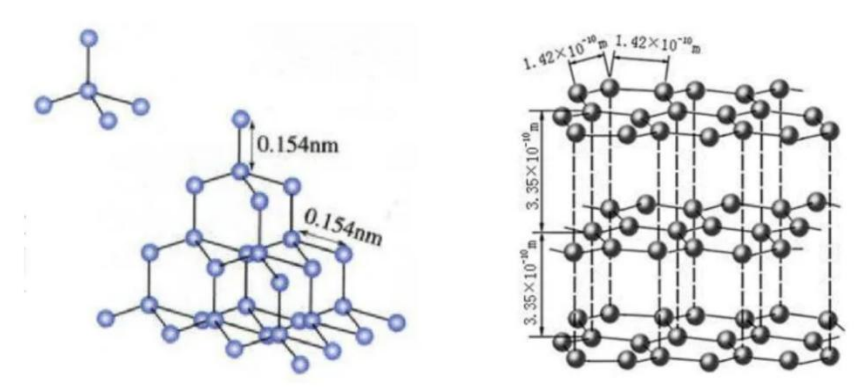


Figure 4.2: (a) Diamond crystal structure [93]; (b) Graphite crystal structure [94].

Synthetic diamond (CVD)

Two main methods are industrialized to synthesize diamonds: high-pressure, high-temperature (HPHT) and chemical vapor deposition (CVD). In the high-temperature and high-pressure method, the carbon source is placed at the central high temperature, a crystal seed is placed at the low temperature, and a temperature gradient generated in the axial direction is used to promote the diffusion of carbon atoms from high temperature to low temperature along the axial direction so that they "spontaneously" turn into diamonds in a high-pressure and high-temperature environment [96]. However, the size of the diamond single crystals synthesized by HPHT is relatively small, and the purity is often not ideal, making it difficult to prepare large-area and complex-shaped diamond films [97].

Chemical vapor deposition, on the other hand, decomposes hydrogen and hydrocarbon gases (such as methane) into hydrocarbon active groups at high temperatures and deposits diamonds on substrate materials under certain conditions. The chemical reactions that occur during the CVD process are shown in **Figure 4.3** [98]. This method is theoretically not limited in size, and the quality of the prepared diamonds is high. The CVD method generally adopts the homogeneous epitaxial method to prepare a single diamond crystal and polycrystalline diamond films are produced in the other cases. Commonly, ultrananocrystalline diamond (UNCD), nanocrystalline diamond (NCD), and microcrystalline diamond (MCD) films are distinguished based on the average diamond grain size. Suitable substrate materials for diamond deposition include, among others, diamond, silicon, silicon carbide, and metals like molybdenum, tantalum, and niobium [99].

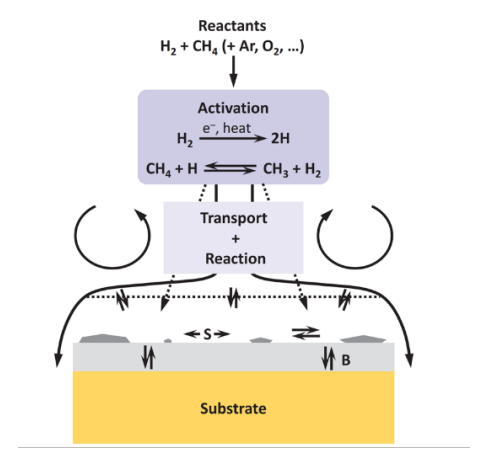
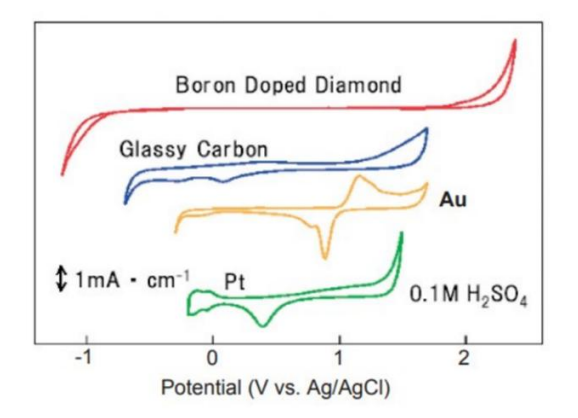


Figure 4.3: Schematic representation of the diamond CVD process [98].

BDD electrodes

Pure diamond has good electrical insulation, but if we dope a certain amount of boron when synthesizing diamond, the conductivity of the material can be significantly improved, and the bored-doped diamond electrode shows great application potential in the field of electrochemistry with its excellent physical and chemical properties. [100] The conductivity of intrinsic diamond is very low, the resistivity can reach $10^{12}\Omega \cdot \text{cm}$, the band gap is more than 5eV, and it is almost an insulator. However, after some boron is doped into the diamond, boron atoms can be doped into the diamond lattice, and holes can be formed, forming p-type semiconductors, and the resistivity drops to about 10^{-3} Ω ·cm, which meets the requirements for use as electrodes [101]. **Figure 4.4(a)** shows the cyclic voltammetry curve of the BDD electrode, which shows that the potential window of the BDD electrode is higher than that of the Pt electrode and the glassy carbon electrode, and the higher potential window allows the BDD electrode to oxidize almost any organic matter except fluoride. The hydrogen and oxygen evolution side reactions on the surface of the electrode are finally realized by the reaction intermediates that are weakly adsorbed on the surface through a multi-step electron transfer process. The essence of the BDD electrode is a diamond composed of sp³ hybrid carbon elements. The adsorption between the diamond and the reaction intermediate is very weak, which is the main reason for the wide potential window of the BDD electrode [102]. In addition, BDD electrodes have excellent physical and chemical stability, do not react chemically with electrolytes, and have excellent characteristics such as self-cleaning and low background current, making them have broad application prospects in sewage treatment, electrochemical synthesis, electrochemical analysis, energy conversion and other fields.

The electrical performance of BDD electrodes is affected by the following three factors in the manufacturing process: first, the boron doping level (boron/carbon ratio), as shown in **Figure 4.4(b)**, to a certain extent, with the increase of boron doping content, the resistance decreases, and the conductivity is better [103]. The second is the sp2 surface content; since the analyte must be adsorbed to the electrode surface for the redox reaction to occur, the pure sp³ carbon surface shows little catalytic activity, and the presence of sp2 on the electrode surface can enhance the electrocatalytic activity of the electrode. The second is surface termination; when processed into BDD, the end surface of BDD can be either oxygen (0) or hydrogen (H); these two surface characteristics are completely different; for example, the surface with the end of o is hydrophilic, while the surface with the end of h is hydrophobic. Since the synthesized BDDs are prepared by chemical vapor deposition (CVD), they are hydrogen-terminated. The hydrogen end, which has high electrochemical performance and high sensitivity, is often chosen as the initial surface for electrochemical sensor applications. However, as the number of uses increases and the contact time with air is longer, the hydrogen termination gradually changes to oxygen termination. [103]



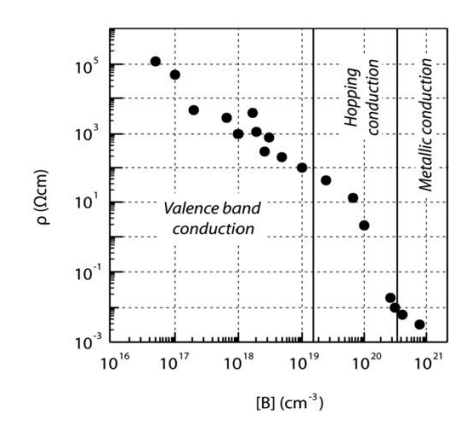


Figure 4.4: (a) BDD electrode potential window compared to other electrodes [102]; (b) Room-temperature resistivity as a function of boron doping concentration [103].

There are two primary types of BDD employed in the production of electrochemical sensing electrodes: BDD thin film and BDD nanoparticle. BDD films, known for their exceptional properties as electrode materials, may now be consistently produced on various substrates. Boron-doped diamond (BDD) films are commonly produced using chemical vapor deposition (CVD) and exhibit a certain level of electrical conductivity. When it comes to BDD NPs, utilizing NPs inks directly is the most convenient method for employing printing technology (such as screen printing) for large-scale processing. Liu et al. used a bottom-up technique to construct three-electrode sensors made of BDD [104]. The WE (Working Electrode) and CE (Counter Electrode) components of this sensor are produced by the inkjet printing technique, utilizing glycerin-based diamond ink containing 0.4% volume/weight of diamond nanoparticles. These components are printed onto a silicon-based substrate, which serves as a base for the BDD (Boron-Doped Diamond) generated through Chemical Vapor Deposition (CVD). Subsequently, CVD is carried out to achieve a uniform growth of a thin-film BDD electrode. Empirical investigations have demonstrated that the electrodes produced using this technique exhibit excellent performance, indicating that this technology has promise for the efficient creation of BDD electrodes of varying sizes. Stach et al. employed 3D printing to create flexible BDD electrode composite fiber materials with varying levels of boron doping, as depicted in **Figure 4.5** [105]. One of the methods involves heating BDD powder and mixing it with TPU and CNTs to form composite materials. These components are then precipitated and extruded into composite fibers using an FDM printer. In comparison to TPU/CNT materials, the inclusion of BDD in TPU/CNT/BDD materials will result in a decrease in the maximum tensile strength. However, the conductivity of the materials will see a significant improvement. However, the increased size of BDD particles compared to CNT particles may have an impact on porosity and roughness. This research demonstrates the potential of utilizing BDD electrodes in flexible applications using 3D printing technology, and shows that there is still room for improvement in the performance of flexible BDD electrodes fabricated of this experiment.

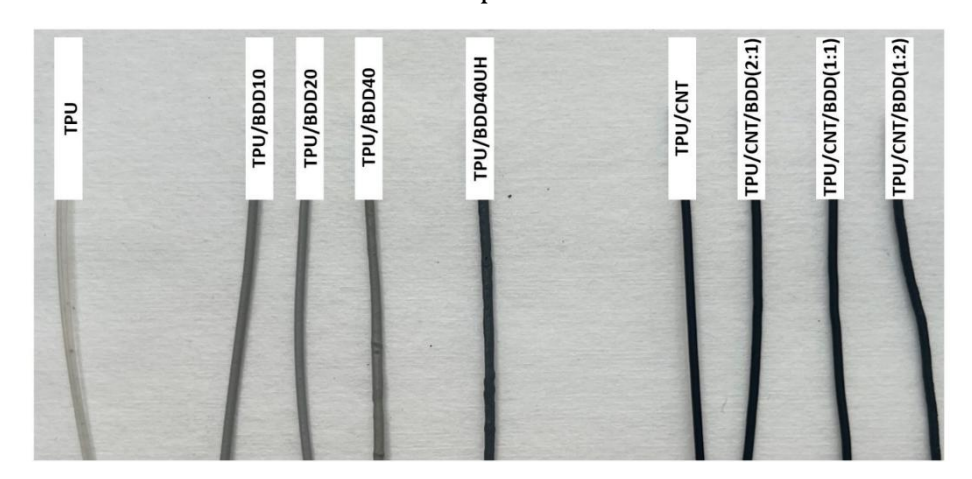


Figure 4.5: Comprehensive image of all manufactured FDM-based filament composites [105].

2.3.2.3 Graphene & CNTs (CE)

In addition to the diamond composed of carbon, which was just mentioned, many carbon-based electrodes are widely used in flexible electrodes. Carbon's valence state allows the existence of isomeric forms [106]. To further improve its conductivity as a transparent flexible electrode, two-dimensional (2D) graphene hybrid materials of one-dimensional (1D) carbon nanotubes (CNTs) have been discovered.

Carbon nanotubes (CNTs) are advanced one-dimensional nano flexible materials. They have the characteristics of high electrical conductivity, excellent electrochemical properties, excellent toughness, and tunable surface chemistry [107,108]. CNTs have a

tubular porous network structure that can be embedded with other materials and deposited externally. In the field of flexible electrodes, CNTs can be used as flexible backbones or active fillers to form highly conductive, self-supporting flexible electrodes that can be mixed with other polymers and conductive metal ions [109].

Graphene (G) is an emerging two-dimensional nanomaterial that is attractive for both traditional semiconductor applications and emerging applications for flexible electronic devices. Graphene has a desirable atomic thickness, high transparency, high conductivity and biocompatibility. The use of graphene has been reported primarily for the detection of small biologically relevant analytes. Graphene has attracted market interest due to its excellent elasticity and chemical stability at room temperature. In the biomedical field, it can show great potential for applications in portable, wearable, biocompatible, implantable, and flexible electrochemical sensing. [110]

2.3.2.4 Silver (RE)

Silver is a metallic material commonly used as a reference electrode in rigid-body electrochemical sensors. For flexible sensors, if silver is also used as a flexible reference electrode, two nano forms of silver can be considered according to different processing methods: 0D silver nanoparticles (AgNPs) and silver nanowires (AgNWs). For AgNPs, printing technology is mainly used to prepare the corresponding silver nano-inks [111]. AgNPs can also be mixed with other nanomaterials to obtain composites. For example, the hybridization of reduced graphene oxide with metal nanostructures (Ag NPs) has not only improved graphene's conductivity [112]. On the other hand, the presence of graphene improves the flexibility of the Ag NPs electrode. Developing composite materials enhances the electrochemical and mechanical properties of the electrode.

In addition, electrodes based on silver nanowires (AgNWs), a 1D material, have excellent mechanical flexibility, electrical and thermal conductivity, and optical transparency. First of all, AgNWs have good synthesis scalability and reproducibility. Therefore, they can be easily dispersed in solvents and are compatible with low-cost, large-area, and solution-based manufacturing processes. Second, the conductivity can be increased by reducing the resistance of individual nanowires or increasing nanowires' density within a specific range. However, the uniformity and stability of the AgNWs network still need to be improved, which is also the biggest challenge to the large-scale commercialization of AgNWs electrodes. [113]

2.3.3 Manufacturing methods

In chapter 3.3, we briefly summarize some of the processing methods for flexible sensors. Now, let us combine the equipment owned by the laboratory to introduce the processing method based on printing technology in more detail and depth. Whether traditional inkjet printing or 3D printing, it is a processing method with a high degree of automation controlled by computers. After the substrate and electrode are processed by printing, consider the connection between the substrate and the electrode, the influence of the substrate on the electrode performance, and whether pretreatment and post-treatment are required.

2.3.3.1 Inkjet printing

As the most commonly used 2D printing method, inkjet printing is non-contact, pressure-free, and plate-free. The computer-controlled inkjet printing press starts working by delivering instructions to the computer. Starting with the computer, you can set parameters such as Platen temperature, nozzle height and drop spacing. As shown in **Figure 4.6(a)** [114], the inkjet printing machine consists of a system controller, an inkjet

controller, a printhead, and a substrate driving mechanism. Under the control of the inkjet controller, the ink is sprayed from the nozzle of the printhead and printed on the substrate. According to the printing requirements, the driver conveys the substrate, and the system controller is responsible for the whole machine's operation.

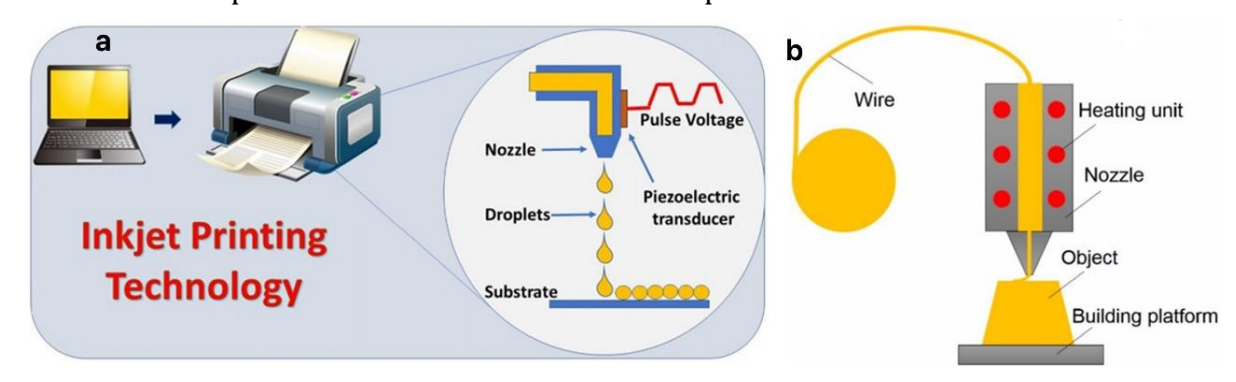


Figure 4.6: Schematic illustration of (a) inkjet printing [114] and (b) FDM process [117].

In electrochemical sensors, inkjet printers are often used with conductive inks. Conductive inks can be made from a mixture of conductive nanomaterials and polymers. For example, Nurul et al. used inkjet printing to manufacture flexible electrodes based on reduced graphene oxide/silver nanoparticles (RGO-AgNPs) [115]. They used water-based conductive inks for printing flexible electrodes on PET. Using a one-step synthesis method is simple and environmentally friendly and guarantees the conductivity of the printed nanoelectrodes.

2.3.3.2 3D printing

3D printing technology, also known as additive manufacturing, is a highly revolutionary technology developed in recent years, which has changed the traditional industrial manufacturing process, has a high degree of freedom in design, and can manufacture objects with highly complex structures, so it has excellent potential for development and application [116]. With the development of the biological field, new requirements are placed on the shape of electrochemical sensors. As the next generation of printing technology, 3D printing technology is highly automated; computers mainly control the processing process, and they can process products with complex shapes and structures. Because 3D printing technology is a kind of additive manufacturing, compared with subtractive manufacturing, the structural complexity of products can be significantly improved, so the manufacture of three-dimensional biological structures (such as artificial organs) can be considered, which has great application potential in bioengineering.

Fused deposition modelling (FDM) is a commonly used extrusion-based 3D printing technology. FDM is formed layer by layer by extruding molten thermoplastic filamentous material through a movable nozzle, as shown in **Figure 4.5(b)** [117]. The materials used in this technology are mainly insulating thermoplastic polymers. However, these materials are mainly used for structural purposes. Hence, fillers must be added to create new filaments with special functions (thermal conductivity, electrical conductivity, etc.), thus broadening the range of applications for FDM-molded devices. Due to its high thermal and electrical conductivity, graphite has become the focus of attention for modified filaments in FDM moulding technology. Researchers usually use ball milling, melt mixing, solvent mixing, etc., to mix the polymer substrate, graphite and other auxiliary materials evenly, and make the composite material into a uniform composite wire strip through an extruder, and then use a 3D printer to control the relevant parameters to print the layered model layer by layer. Among them, graphite can be used

as a reinforcing phase to greatly improve the mechanical, thermal, and electrical properties of FDM composites [118]. Adrian et al. used FDM to fabricate flexible electrodes that blend electroactive materials with molten thermoplastic polymers (e.g., polylactic acid, PLA) and successfully used them to fabricate electrochemical dopamine (DA) biosensors [119]. This method proposes an additive manufacturing method that does not require the preparation of conductive filaments for the rapid fabrication of low-cost electrochemical sensors in the field of biomedicine.

2.3.3.3 Electrode surface modification

For flexible substrates and electrodes that have been processed, we need to consider whether the electrodes are well adhesion with the substrate and whether the electrodes attached to the substrate still have good electrochemical properties. At this point, we consider some pre- or post-processing methods. For example, Marina et al. reported a new method to increase printability and adhesion to polymer flexible substrates to increase the adhesion of silver inks. As shown in **Figure 4.7**, the substrate was pretreated to apply novel thiols and silicones to the substrate, and then the electrodes were printed on the substrate [120]. This improves the adhesion between the silver ink and the flexible substrate while minimizing roughness effects.

Most of the time, conductive functional materials are printed on the surface of the substrate to exhibit poor conductivity. This is due to the presence of solvents and stable molecules between the particles, so the printed pattern is less conductive. [121] As a result, post-treatment of the surface is required, and commonly used post-treatment methods include mild annealing with curing, which can significantly affect the mechanical properties of composites. If you want to improve the conductivity of the electrode, consider sintering. During the sintering process, stabilizers and solvents are removed between the particles, maintaining a tight bond between the conductive particles to form conductive tracks [122]. After the electrode is printed onto a flexible substrate, sintering can be divided into thermal, electro, photonic, and microwave. Since the maximum working stability of flexible substrates is generally between 100 °C and 200 °C, to avoid the influence of temperature, one needs to choose a method that does not require high-temperature heating.

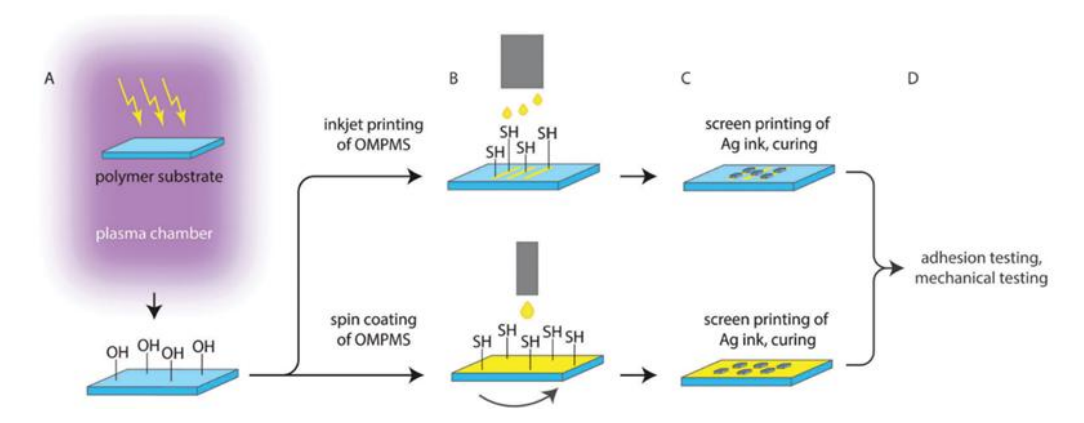


Figure 4.7: (A) and (B) Two-stage functionalization of polymer substrates, which involves plasma treatment followed by spin coating or inkjet printing of OMPMS; (C) Deposition of silver ink through screen printing; (D) Adhesion and mechanical testing of printed silver structures [120].

3 Research Proposal

The goal of this chapter is to outline the scope, knowledge gap, and research objective; of this M.Sc. thesis project. Initially, the research objective will be established in conjunction with the primary research question and its corresponding sub-questions.

3.1 Knowledge gap

Flexible electrochemical sensors are mostly utilized in human wearable health monitoring platforms. Graphene and carbon nanotubes are frequently employed as fillers in working electrode materials in flexible three-electrode electrochemical sensors. The primary processing techniques for these sensors involve photolithography and printing processes. However, diamond, another kind of carbon, exhibits excellent use in nonflexible electrochemical sensors. This electrode material, specifically boron-doped diamond, is known for its exceptional electrochemical performance and high sensitivity but it has not been utilized yet in the creation of flexible electrochemical sensors. Only recently, the first demonstration of the 3D-printing of BDD-CNT-TPU composite electrodes with good conductivity and electrochemical response by fused deposition modeling (FDM) was reported [105]. The objective of this study is to explore the possibilities of 3D printing and utilizing of these carbon-filler polymer composites as the working electrodes for the development of flexible electrochemical sensors.

3.2 Research objective

This project aims to explore the fabrication of BDD containing flexible sensors by inkjet printing and 3D printing technologies. The main goal is to develop a prototype three-electrode sensor for electrochemical application. The primary materials selected for the ultimate flexible sensor are TPU, BDD, and silver. TPU will be used as the flexible substrate for the sensor, while BDD will serve as the material for both the working electrode and counter electrode. Otherwise, CNTs or graphene can be used as counter electrode. Silver will be used as the reference electrode. The utilization of 3D printing and inkjet printing technology in sensor production enables the identification of the processing method, processing sequence, pre-treatment, and post-processing content. The performance of the flexible electrochemical sensor will be assessed by conducting a number of tests to evaluate its electromechanical and electrochemical properties.

The research objective of this project is to investigate the feasibility of utilizing diamond-based electrode materials for the manufacture of flexible electrochemical sensors. This study investigates the conversion of thin-film BDD electrodes, which are normally produced by chemical vapor deposition and exhibit excellent performance on non-flexible substrates, to newly developed flexible substrates via 3D printing of BDD particles within the polymer. The study examines the impact of flexible substrates and processing techniques on the performance of the electrodes. This not only expands the range of materials that can be used for flexible electrochemical sensors, but also allows for the fabrication of electrodes in a manner that promotes sustainable manufacturing.

3.3 Research questions

Main research question: How can inkjet printing and 3D printing technology be employed to manufacture flexible diamond-polymer composite electrochemical sensors?

Sub-question:

- How to choose the right constituent materials of the three electrodes and substrates?
- How to process each of the three electrodes, and in which order has their printing to be performed?
- What are the effects of the flexible polymer support on the adhesion and electromechanical response of as printed electrodes?
- Are BDD particles conductive enough for their use as (single) electrode filler?
- How to select appropriate pre-treatment and post-treatment techniques based on the processing approach, and what are their respective impacts on the structural integrity and conductivity of printed electrodes?

4 Materials and Methods

4.1 WE materials

4.1.1 TPU/CNT/BDD filament

The diamond-based filament for FDM printers is derived from the manufacturing done in a previous MSc thesis project [105]. In summary, The following is the production process of the TPU/CNT/BDD filament. The preparation of composite materials was first achieved by solution blending. TPU pellets (Netherlands 123-3d.nl) were dissolved in DMF (Dutch Sigma Aldrich) at a ratio of 1:10 (g/ml) and stirred magnetically at 60 °C for 2 hours. After it was completely dissolved, BDD powder (China UHD Ultrahard Tools Co., Ltd) was added and stirring was continued for 2 hours. Subsequently, the solution was treated at 45 kHz with an ultrasonic instrument (EMAG EMMI-60 HC type) at 100% power for 1 hour, and continuously stirred at room temperature for 12 hours with a magnetic stirrer turned to 500 rpm to ensure that the solution was homogeneous. Finally, the composite was molded by non-solvent-induced phase separation [121], the solution was precipitated in deionized water to obtain the composite precursor, and the residual solvent was removed by drying at 165°C for 2 hours. After drying, the composite was manually cut into 10-20 mm pellets, as shown in **Figure 4.1**. During the extrusion process, filaments were extruded at a temperature range of 195-215 °C at a speed of 3-5 rpm using a Felfil Evo single screw extruder (Felfil SRL, Italy). After cooling, the filament diameter is controlled between 1.55-1.70 mm. To improve compactness, the extrusion-cutting process was repeated several times until the material was free of significant porosity.



Figure 4.1: Schematic diagram of the FDM-based compound formulation process (picture taken from [105]).

4.1.2 TPU/CB filament

The conductive Filaflex TPU filament from RECREUS, Spain, was chosen as the consumable for the FDM printer. This composite filament material is composed of TPU and carbon black. With its good flexibility and conductivity, it is ideal for manufacturing electrodes for wearable sensors. It has a shore hardness of 92A, which makes it compatible with 90% of 3D printers on the market and eliminates the need for hardened nozzles to avoid damage to the printer. It is important to note that after using this filament, it is recommended to clean the nozzle with polyethylene terephthalate (PET) filament to remove any deposits that may remain in the nozzle.

4.2 3D Printing

The 3D printer used in this study is the PRUSA I3 MK3S+ FDM printer from PRUSA Research, Czech Republic. Firstly, the design of the 3D graphics of the electrodes was completed by using SolidWorks 2024 (Daussault Systemes SE, France) software, and exported to the STL file format. Secondly, Prusaslicer 2.8.0 (Prusa Research, Czech Republic) software was used to convert the STL format to G-code, and the printing parameters were set on the software, and the corresponding printing parameters for each filament are listed in **Table 4.1**.

Material	Nozzle	Print	Layer	Nozzle	Bed	Raster
	diameter	speed	thickness	temperature	temperature	angle
	(mm)	(mm/s)	(mm)	(°C)	(°C)	(°)
TPU/CNT/BDD	0.8	20	0.3	215-250	50	45
TPU/CB	0.8	20	0.3	245-250	50	45
Flexible TPU	0.8	35	0.3	210-240	50	45

Table 4.1: Process parameters for FDM fabrication with the three studied print materials.

It should be noted that due to the inclusion of diamond microparticles in the TPU/CNT/BDD printing material, the FDM printer was modified to accommodate the high abrasion of the diamond material. First, the original hot end was replaced with a version that can operate at higher temperatures (250 °C to 300 °C). In addition, a ruby nozzle that is widened to 0.8 mm was used to prevent clogging of diamond particles and to improve the wear resistance.

The process of printing electrodes onto substrates is shown in **Figure 4.2**. In the first step, the FDM printer was loaded with a flexible TPU filament (NinjaFlex, the Netherlands) to print the substrate, and a printing speed of 35 mm/s, a heated bed temperature of 50 °C, and a nozzle temperature of 210-240 °C were selected according to the technical table of the material. The substrate size is 30x45x0.3 mm³, and only one layer needs to be printed. The printer flow was set to 85% to reduce over-extrusion, reduce the material rebound effect, and make the nozzle extrusion pressure more stable, so as to improve the uniformity of TPU printing, and make the substrate surface more flat. It took about 1 minute to print the TPU substrate. **Figure 4.2(a)** illustrates the process of printing the TPU substrate.

In the second step, after the substrate printing was completed, the substrate material was unloaded and the working electrode material (TPU/CNT/BDD or TPU/CB) was loaded, as shown in **Figure 4.2(b)**. Since the required heating bed temperature for all three materials remained constant at 50 $^{\circ}$ C, only the nozzle temperature changed. Due to the strong viscosity of TPU material, the first layer can be firmly adhered to the hot bed under

the right printing and hot bed temperature. The flexibility of TPU makes it easier to fit the hot bed after extrusion, unlike rigid materials such as PLA that are easy to suspend. Therefore, in the process of replacing consumables and printing electrodes, only one layer of flexible TPU substrate can be well fixed on the hot bed without displacement.

In the third step, after replacing the consumables, the printing of the working electrode onto the substrate was done as shown in **Figure 4.2(c)**. When changing to the printing electrode filament, it was found necessary to let the nozzle extrude the filament several times before starting printing to ensure that the remaining flexible TPU in the nozzle was completely extruded, so as to ensure the purity of the printing electrode material to the greatest extent. When printing electrode materials, a lower printing speed of 20 mm/s was selected, a heating bed temperature of 50 °C, and a nozzle temperature of 244-250 °C according to the technical table of the material. It should be noted that since the electrode was printed directly onto the TPU substrate with a thickness of 0.3 mm, it was necessary to add a z-offset of 0.3 mm in the z-axis when setting in Prusaslicer 2.5.0. After all the printing was completed, because the TPU still had internal stress at high temperatures, it was necessary to wait for the heat bed to drop to room temperature, and then use a spatula to carefully peel the sample off the heat bed to prevent premature peeling and causing uneven shrinkage and deformation of the material.

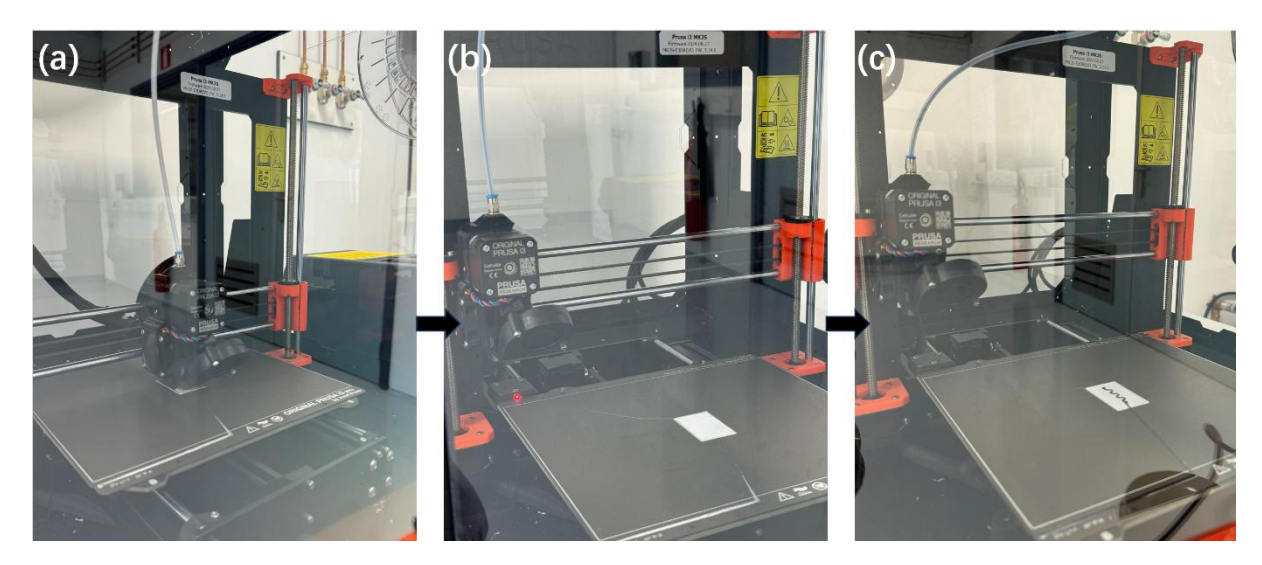


Figure 4.2: Flow diagram of the 3D printing of the electrode onto the TPU substrate: (a) printing of TPU substrate, (b) replacement of filament material, and (c) the working electrode (black) printed on the TPU substrate (white) still foixed to the heat bed.

4.3 Characterization

Scanning electron microscopy (SEM)

SEM was used to characterize the cross-section and topview of the 3D printed electrode on the substrate. SEM images were taken using a JEOL scanning electron microscope (JEOL-JSM6010LA), with options to operate at accelerating voltages of 5 and 10 kV. Since TPU is a flexible polymer material, in order to observe the cross-section of the internal microstructure, it was necessary to soak the sample in liquid nitrogen and freeze it. This way, it because brittle and then fractured, forming a natural cross-section, so as to avoid the impact of mechanical cutting. In addition, SEM was used to make a direct comparison of printed electrodes before and after chemical treatment. The microscopic morphology of the printed electrode as well as the distribution and interfacial bonding of CB particles in TPU before and after treatment were observed.

Raman spectroscopy

Raman microscopy was used to determine the bonding structure of the TPU matrix and the CB (carbon black) filler in the print electrode. Raman spectra were collected at room temperature using a Horiba Labram HR Micro-Spectrometer equipped with an x,y,z movement stage. A Cobolt Fandango 50 argon-ion laser operating at 532 nm wavelength and 50 mW was used as the excitation source. Raman spectra were analyzed using Origin Pro 2023 software. In this experiment, it was necessary to pay attention to the laser intensity and select a low laser power (0.5-2 mW) to prevent the thermal degradation of the TPU. The molecular composition of the electrode material can be confirmed by mapping the peaks of the obtained spectral pattern to the Raman characteristic peaks of the TPU and CB materials. The conductivity of CB was assessed by evaluating its key Raman peaks, namely the D-band (1350 cm⁻¹) and G-band (1580 cm⁻¹).

Keyence Digital Microscope

The shape and cross-section of the printed electrodes on the substrate were analyzed using the VHX-6000 bonded digital microscope to evaluate the difference between the printed size set by the FDM printer and the actual size obtained. Cross-sectional vs. topview images were taken using an X20 objective lens. The surface of the printed electrode before and after chemical treatment was also observed.

Mechanical properties

Uniaxial tensile testing with a Zwick&Roell tensile testing machines was performed to identify the mechanical properties of different 3D printed composites, to evaluate the mechanical properties of the substrate in different printing directions, and to evaluate the mechanical properties of the sensor sample containing the printed electrodes and substrates. A constant pull rate of 20 mm/min was selected. According to the standard ASTM D638 V-type, the sample thickness was selected to be 1.2 mm, and the geometry of the composite sample was printed as shown in **Figure 4.3(a)**. All samples tested were uniformly sized using this standard. For different substrate printing directions, the angles between the substrate and the stretching direction were 0°, 30°, 45°, 60°, and 90°, respectively, as shown in **Figure 4.3(b)**.

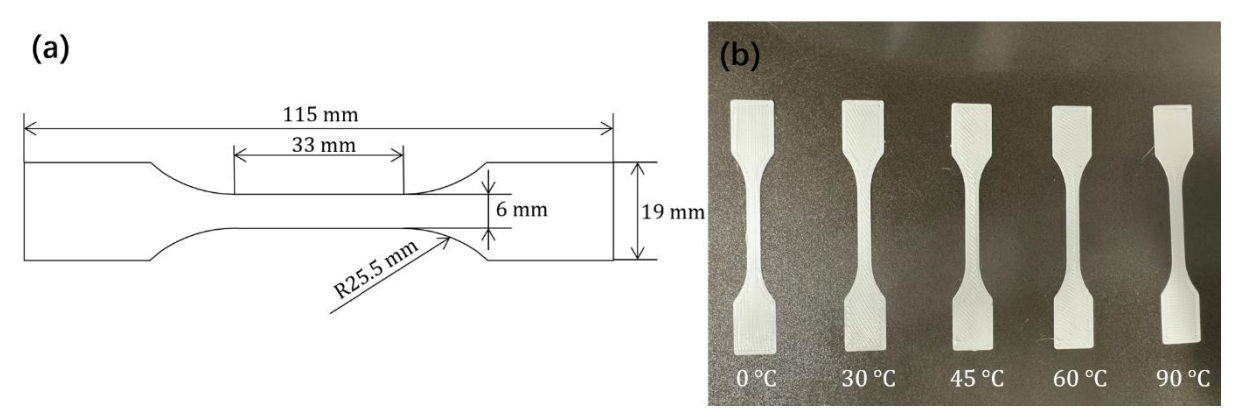


Figure 4.3: (a) Schematic drawing with dimensions of tensile test samples. (b) TPU samples printed in different filling directions for tensile testing.

Electrical properties

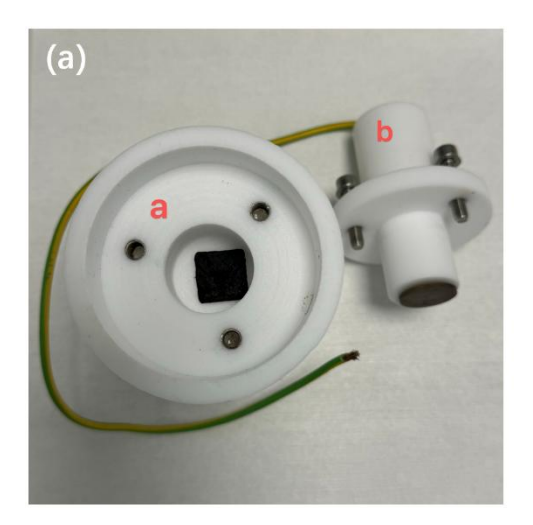
The electrical properties of 3D printed composites and the resistance of printed electrodes as a function of temperature were investigated using a digital multimeter (Voltcraft CV820-1) equipped with two probes. First, the probe was manually positioned at a fixed distance between the printed electrode sample and the unprinted filament, and the obtained resistance was converted to volume resistivity using **Equation 4.1**:

$$\rho = R \cdot (A/L) \tag{4.1}$$

where ρ is the volume resistivity, R is the resistance, A is the cross-sectional area, and L is the distance between the lengths of the conductive path. Silver contacts were applied to both ends of the printed electrode fixation on the substrate to mitigate the measurement error of uniform metal connections. Then, the same contact point location was selected, and five replicates of the five printed samples were performed to evaluate whether the samples were reproducible. Finally, a sample was selected, not peeled off from the hot bed after printing, and the probe position of the multimeter fixed while, waiting for it to cool to room temperature. Then, the temperature was raised from 20 °C to 100 °C, the value of the multimeter recorded every 10 °C. The process of continuously heating to 100 °C and then cooling down to room temperature was repeated five times, and the influence of the heating cycle on the resistance of the printing electrode was evaluated.

Electrochemical properties

Cyclic voltammetry (CV) was the main choice for electrochemical measurements, performed using an Autolab PGSTAT 128N controlled by NOVA 2.1 software (Metrohm, Netherlands) to evaluate the electrochemical properties of the printed bulk electrodes. Firstly, a three-electrode system was constructed, with 3D printed composite electrodes used as the working electrode (WE), silver-silver chloride (RE-1BP from ALS co.) As the reference electrode (RE), and 25 cm 99.9 % platinum wire (catalog No. 50HX15 purchased from redox.me, Sweden) as the counter electrode (CE). The working electrode was placed at the bottom of the cell (part a) shown in **Figure 4.4(a)**, and the cell component b was fixed with it through three screws, and the position of the working electrode was ensured to be fixed at the same time. The overall experimental setup is shown in **Figure 4.4(b)**. The cell was fixed and the electrolyte was introduced into it, ensuring that all electrodes were immersed in the measurement solution, and all experiments were performed under laboratory conditions (20 °C).



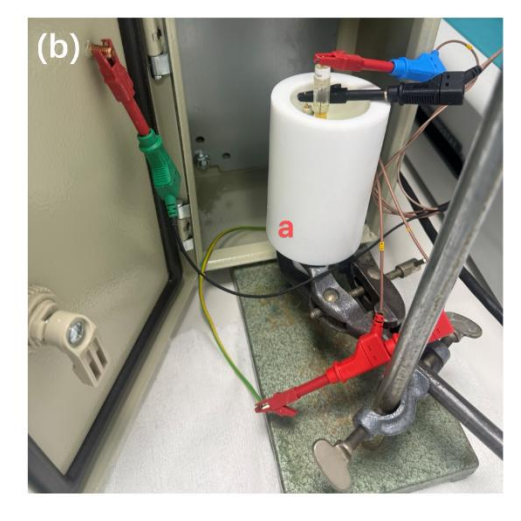


Figure 4.4: Image of (a) electrode holder parts and (b) CV experimental setup.

In addition, 0.5M KNO₃, 1mM [Fe(CN)₆]^{3-/4-} (ferrocyanide) in 0.5M KNO₃ and 1 mM [Ru(NH₃)₆]^{3+/2+} (RuHex) in 0.5M KNO₃ were selected as electrolytes, and the scanning voltage range was set between -1 V and +1 V, and the accuracy was verified by five CV scans. The following equation (**Equation 4.2**) was used to estimate the double-layer capacitance (C_{dl}) value:

$$C_{dl} = \Delta I_{AV} / A_{geom} v \tag{4.2}$$

where ΔI_{AV} is the average background current difference between forward (anode) and reverse (cathode) scans at a potential of 0 V, A_{geom} represents the geometric surface area (1 cm²), and V is the scan rate (0.1 V/s).

In the RuHex scan rate study, the effective electrode surface area (A_{eff}) was determined using the Randles-Sevcik equation (**Equation 4.3**):

$$i_p = 2.69 \cdot 10^5 n^{3/2} A_{eff} D^{1/2} C_0 v^{1/2}$$
(4.3)

where n is the number of exchanged electrons, D is the diffusion coefficient of the redox probe, v is the scan rate, C_0 is the concentration, and i_p is the peak current.

In addition, $1 \text{mM} [\text{Ru}(\text{NH}_3)_6]^{3+/2+}$ in 0.5 M KNO₃ was selected for the scan rate study, and different scan rates (10, 25, 50, 75, 100, 200, and 250 mV/s) were selected for five scans per scan to verify its accuracy.

5 Results and Discussion

5.1 TPU/CNT/BDD electrode: Fabrication and Characterization

5.1.1 Fabrication

5.1.1.1 Electrode shape design

Unlike conventional rigid sensors, flexible sensors are expected to have different mechanical properties. Among them, the appropriate printing electrode shape can be selected according to the target requirements. For wearable flexible electrochemical sensors, we expect better tensile performance. According to Section 2.3.1, the shape of the printed electrode needs to be chosen to exhibit better performance when stretched. Due to its smooth curve design, a semi-circular arc structure effectively avoids the stress concentration at right or sharp corners, making the stress distribution more uniform, thereby reducing the risk of local failure and crack propagation. During the tensile process, the structure can be gradually unfolded and easily returned to its original shape after the external force is released, improving its deformation ability and durability. In addition, the semi-circular arc structure has a certain energy buffering effect when stressed, absorbs part of the external load through deformation, and reduces the direct transmission to the material, thereby reducing the structural damage. At the same time, the structure can maintain stable force performance under tensile and bending conditions at different angles, avoiding failure caused by stress concentrations in specific directions [123]. The design of the electrode shape is shown in **Figure 5.1**. Combined with the diameter of the FDM printer nozzle used, a semicircular arc with a printing electrode width of 0.8 mm (i.e., the diameter of the printer nozzle) was selected and a printing radius of 2 mm, and conductive terminals at both ends.

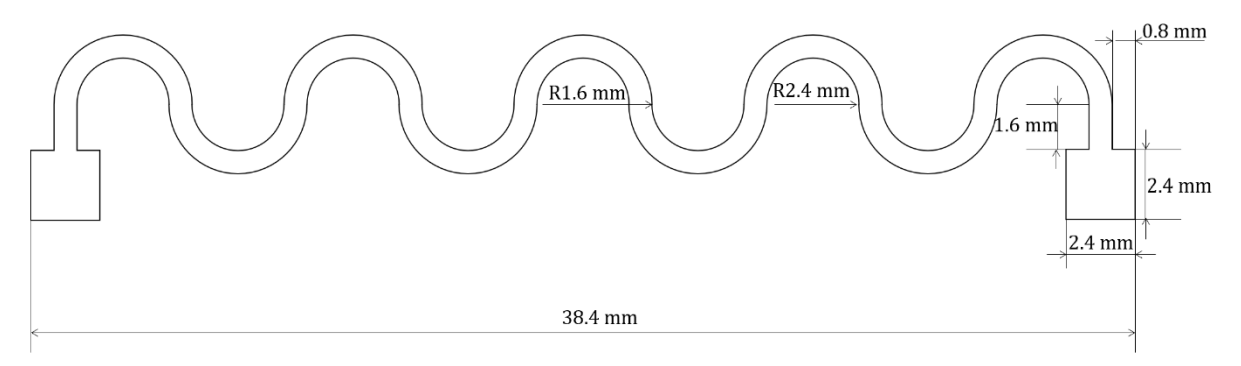
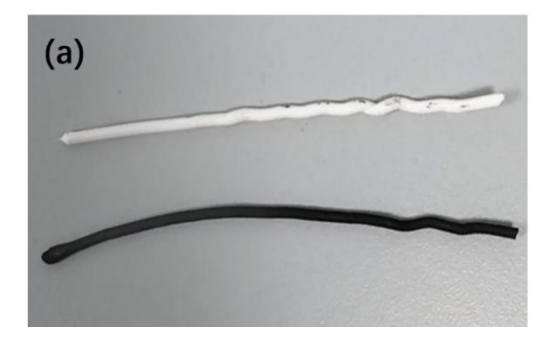


Figure 5.1: Schematic drawing with dimensions of S-shaped tortuous electrode design.

5.1.1.2 Printing of TPU/CNT/BDD electrode

During the printing process, the flexible filament was found to produce different results. Unlike rigid consumables, flexible materials can be stretched or compressed when the wire is fed through the extruder. First, this seemed to have caused the material to bend and buckle within the feed channel, making it difficult to extrude smoothly from the nozzle opening [124]. When the material blocks the nozzle, the print will be forced to abort and the filament will need to be reloaded. **Figure 5.2(a)** shows an optical image of buckled consumables after unloading in the feed lane. Second, the tensile deformation

that may have occurred to the flexible material in the extruder led to unstable wire feeding, and too little or too much material was extruded in some areas, as shown in **Figure 5.2(b)** of an unevenly printed electrode [125].



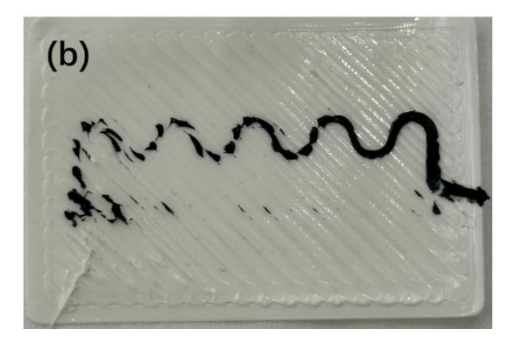


Figure 5.2: Images of (a) buckled TPU and TPU/CNT/BDD filaments and (b) unevenly printed electrode due to filament blocking in the printer.

For the TPU/CNT/BDD filament used in this experiment, the TPU matrix is a flexible material during the extrusion process, which may collapse, tensile deform, or warp at high temperatures [126], resulting in uneven wire feeding. CNT and BDD particles can cause uneven material feeds that affect extrusion flow. Considering the situation inside the nozzle, TPU has high viscosity and elasticity, which is easy to accumulate on the inner wall of the nozzle during long-term extrusion, and CNT and BDD particles may be deposited in the nozzle. As a result, the nozzle with a diameter of 0.8 mm gradually decreases as the number of prints increases. Also, the diamond particles in particular may damage the nozzle [127], further aggravating the nozzle blockage. In order to minimize the impact of the above conditions on printing, a new ruby nozzle (0.8 mm) was chosen to reduce diamond wear and reduce the problem of particle accumulation in the nozzle. Also, slightly altered printing settings were chosen for a series of new prints. The printing speed was reduced (20 mm/s) to lessen the problem of feed instability. A higher printing temperature (240 °C) was selected within a certain range to ensure that the filler material was fully melted to avoid particles from accumulating in the nozzle. A thermal bed temperature of 50 °C was maintained to ensure good interlayer adhesion and to avoid rapid cooling of the material that can affect adhesion [128].

5.1.1.3 Successful samples analysis

By adjusting to the above parameters, two successful printed samples were obtained as shown in **Figure 5.3 (a)** and **(b)**. The printer parameter settings were the same for the two samples, but the width of the printed electrodes was significantly different from the picture observation. This is due to the fact that sample A was printed with a newly replaced ruby nozzle, which was not yet worn out or clogged. Sample b was obtained by printing with the ruby nozzle after several print jobs using TPU/CNT/BDD filament. There is obviously residual material inside the nozzle, resulting in less extruded material from the nozzle and a thinner printing electrode width in the case of sample B.

Observation of sample B shows that the uniformity of the printed electrode is poor, and there are even discontinuities. In this experiment, the reproducibility of the printed samples was poor and the sample quality was unstable. In the printing process, the flexible composite fiber was very easy to be wound in the feeding channel due to the rough surface, and it needed to be repeated several times to load and unload the filament before it could be successfully extruded. In addition, in the load and unload cycles, PLA rigid consumables were needed to dredge the nozzle, and if the flexible filament was used continuously, the internal blockage of the nozzle got exacerbated, resulting in a more difficult foundation. This is the reason why there were only two successful samples in this

experiment.

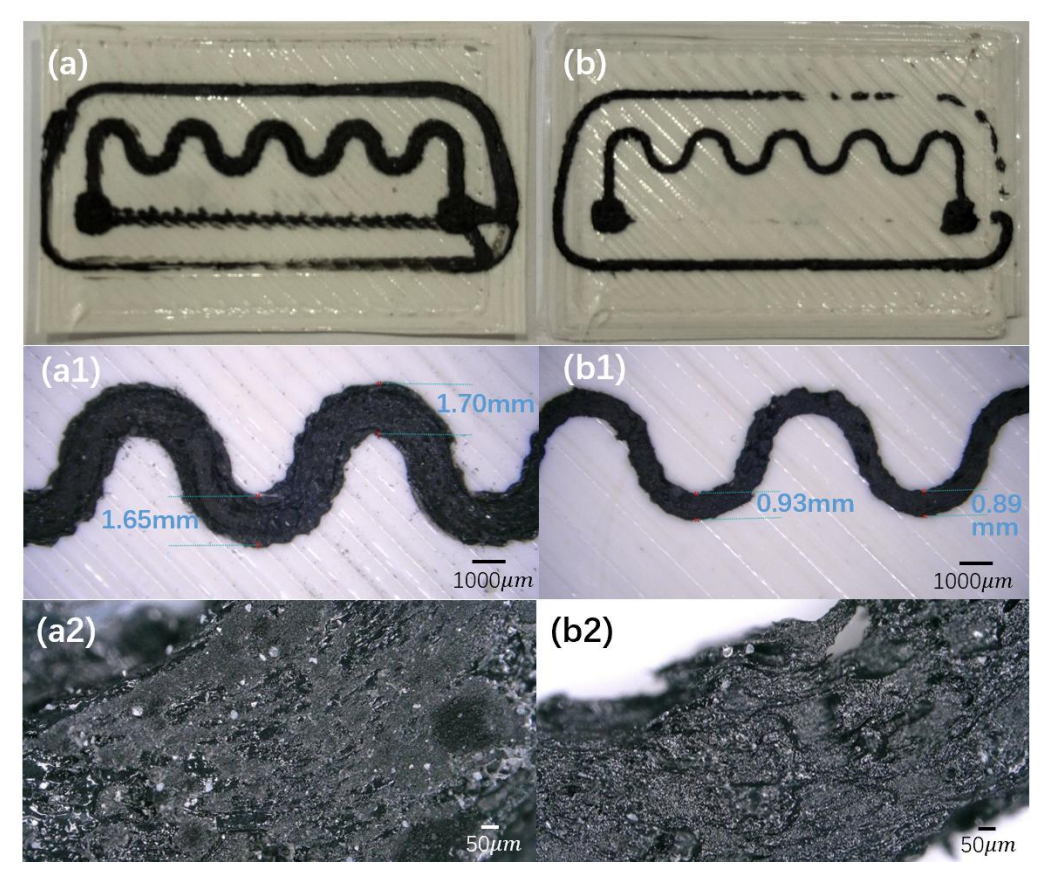


Figure 5.3: (a) and (b) Optical images of successfully printed electrode-on-TPU samples A and B; (a1)-(b1) and (a2)- (b2) are images of samples A and B magnified at 20x and 200x, respectively.

Observing the surface of the electrode at 200 times magnification, it was found that there were obvious rough areas on the surface of the electrode, and white particles accompanied by local agglomeration of BDD particles. This indicates that the CNT or BDD is unevenly dispersed, which may affect the conductivity of the electrode. Microscopic holes and cracks can be seen on the surface, which may be due to CNT/BDD particles that affected the molten state and reduced the fluidity of the material. However, the surface of the printed electrode is partially smooth and partly rough, and the smooth area is covered by more TPU, mainly because the TPU has strong melt fluidity and is easy to fill surface defects [129]. There are many BDD/CNT particles in the rough areas, which may lead to the enrichment of the filler in such local areas due to uneven mixing of materials, and BDD particles affect the fluidity of TPU, so that the material cannot be spread evenly [130].

5.1.2 Electrical characterization

Since the TPU/CNT/BDD filament used in the experiment had been produced about 1.5 years ago, and TPU is a hygroscopic material, moisture can cause bubbles or holes during the printing process, and CNTs may interact with water molecules and change the electron transport path, which will affect the integrity of the conductive network [131]. Therefore, considering that the TPU/CNT/BDD filament may be moist, which will affect the conductivity, an oven was sued to dry the samples at 80 °C for 1.5h before printing.

CNTs may interact with water molecules, altering electron transport paths and increasing electrical resistance. The two ends of the printed electrode were selected as the resistance test points, and the resistance of electrodes A and B was measured to be 44.25 Ω and

35.75 Ω respectively. The volume resistivity of the TPU/CNT/BDD filament is 92 Ω -cm, and the theoretical resistivity of the printed electrode should be 13.53 Ω . There may be several reasons why the actual resistance is greater than the theoretical resistance value: First, due to the problem of printer hardware and printing times, the actual volume of the printing electrode is different from the theoretical volume, and the volume of the printing electrode extruded by the actual nozzle is not consistent each time, which affects the measurement of resistance. Secondly, in terms of structure, micropores may have formed during the printing process, resulting in porosity and delamination inside the printed material, which affects the continuity of the conductive path. In addition, CNTs and BDDs in composites may be unevenly distributed during the printing process, carbon nanotubes are prone to agglomeration [132], and harder BDD particles may aggregate in the nozzle, resulting in poor conductivity in some areas and affecting the integrity of the overall conductive path. Finally, the design of the printed electrode with a wavy structure led to a relatively long current path and possible local stress concentrations, which may have led to microcracks and affected conductivity [133].

From the above discussed irreproducible printing with the self-formulated TPU/CNT/BDD filament material, it was decided to redirect the research towards the printing of electrodes using the commercial TPU/CB filament.

5.2 TPU/CB electrode: Fabrication and Characterization

5.2.1 Fabrication

5.2.1.1 Printing of TPU/CB electrode

Using the purchased TPU/CB filament as the electrode consumable for printing, the same electrode shape described in Section 5.1.1.1 was selected, and the obtained sample C is shown in **Figure 5.4**. Shown is a 3D-printed electrode based on a TPU/CB composite with a wavy structure with large conductive contacts at both ends. The electrode is printed on a white TPU substrate. The overall molding is better, and the electrode and the substrate bond is better. Also, the width of the printed electrode is more uniform, although there is still a certain variation, but within a reasonable range (i.e., < 13 %).

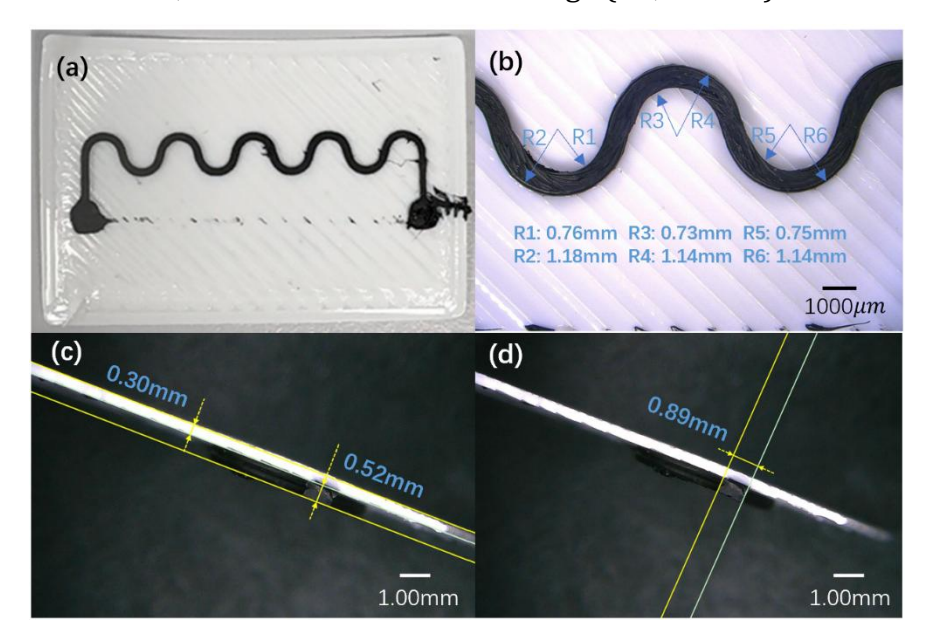


Figure 5.4: (a) Image of printed TPU/CB electrode on TPU substrate; (b)(c)(d) images of the printed sample C at 20x magnification, including the measurement dimensions of top-view (b) and cross-section (c,d).

SEM was used to perform cross-sectional structural analysis of the printed electrode. As can be observed in **Figure 5.5**, the printed electrode is the result of two-layer printing, and the material fusion between the two layers is good, and no obvious boundary is observed. The cross-section of the printed electrode was magnified 900 times, and the inside of the material showed a relatively uniform matrix structure, and the overall cross-section showed a certain interlayer texture, and no obvious holes were observed. The overall printing process went smooth and was easy to repeat. Following, the printed samples were tested and evaluated on the mechanical, electrical and electrochemical properties.

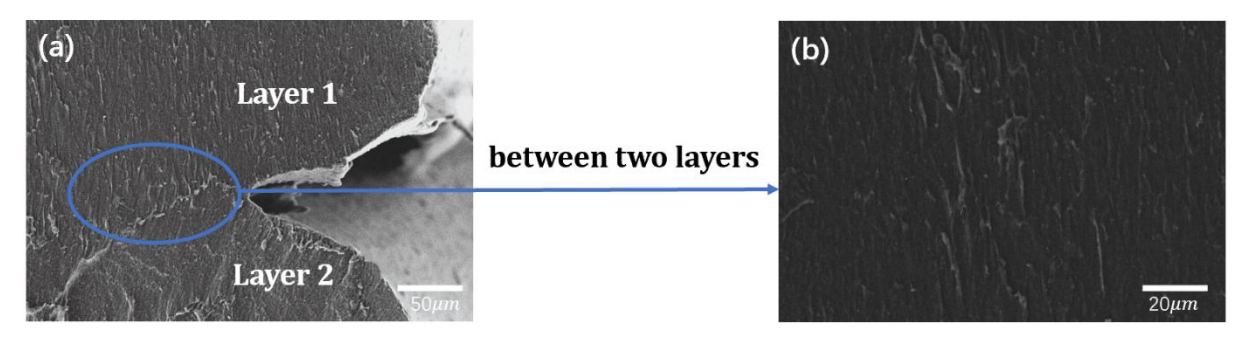


Figure 5.5: SEM images of the cross-sections magnified x400 (a) and x900 (b).

5.2.2.1 TPU/CB filament electrode composition

Raman spectroscopy was used to evaluate the composition of the TPU/CB printed electrodes. Blue curve in Figure 5.6 shows the Raman spectrum of an electrode printed with the FDM printer using TPU/CB filament. From left to right, three key characteristic peaks can be observed. The first characteristic peak is the disorder band (D-band) around 1350 cm⁻¹ which is one of the two main Raman peaks of carbon black, associated with amorphous carbon, an irregular structure, or defects. The second characteristic peak, the graphitic band (G-band) around 1580 cm⁻¹, another major Raman peak of carbon black, representing graphitized carbon (sp² carbon-carbon bond), indicating the degree of crystallization of CB. The presence of both peaks illustrates the presence of CB in the TPU matrix, which in turn participates in the formation of conductive networks [134]. The intensity ratio of the D/G peak (ID/IG) is about 0.96, which is less than 1, indicating that the CB has a high degree of graphitization, which is conducive to the formation of a conductive network of TPU/CB composites. The third characteristic peak is the C-H bond peak of TPU at 2900 cm⁻¹, indicating that the molecular structure of TPU remains intact and CB does not cause significant matrix degradation [135]. In summary, the printed TPU/CB electrode material has a certain disordered carbon (D-band) and graphitized carbon (G-band) structure. The conductivity of CB was evaluated by calculating the D/G peak ratio. The TPU structure in the material has not been severely damaged or excessively affected by the CB filler.

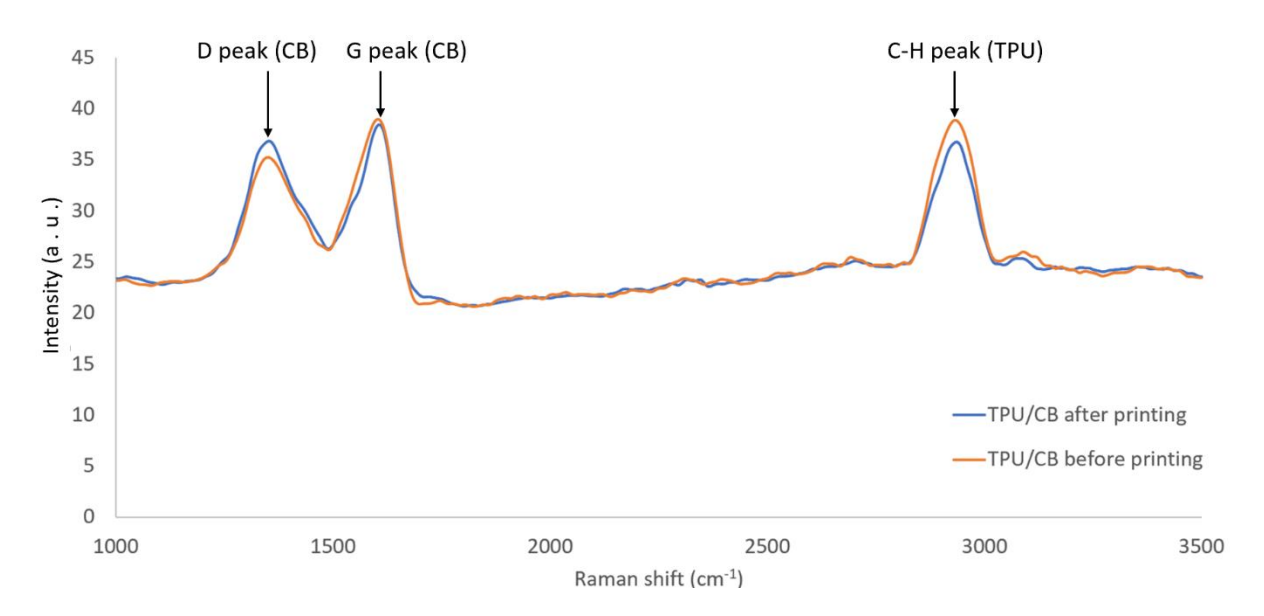


Figure 5.6: Raman spectra of a TPU/CB printed sample and TPU/CB filament without printing.

In addition, **Figure 5.6** compares the Raman curves of flexible TPU/CB materials before and after FDM printing. Samples with slightly different peaks before and after printing indicate a slight change in the structure of the material during the printing process. The D-band is stronger and the D/G ratio (ID/IG) is slightly higher than before printing, indicating that heat exposure may trigger local agglomeration or increased defects, increasing disorder. At the same time, the intensity of the C-H stretching vibration peak of TPU decreases slightly, considering that the polymer segments have undergone some rearrangement or weak degradation at high temperatures. Taken together, the filament sample before printing has a lower D/G ratio, a sharper and more symmetrical C-H vibration peak, and a lower background noise, reflecting a more complete and orderly material structure. This comparison shows that FDM thermal processing has a certain effect on both the carbon black conductive network and the TPU skeleton structure, and then the actual impact on the electrode performance is further evaluated in combination with resistance or heat treatment optimization.

5.2.2 Mechanical characterization

Firstly, considering the single-layer printed TPU as the substrate, the tensile properties of the substrate at different filling angles were studied. In Figure 5.7, the tensile stressstrain curves of TPU samples with different filling angles and a TPU/CB sample with a filling angle of 45° are shown. The filling angles were all based on the tensile direction, and different samples were printed at 0°, 30°, 45°, 60° and 90°, respectively, from the tensile direction (axial). Comparing the TPU samples with different filling angles, it was found that the tensile strength of 90° (the filling direction was perpendicular to the tensile direction) was the highest. In a single-layer infill structure, a 90° fill means that all infill lines are perpendicular to the tensile direction. In this way, the tensile force acts on the overall deformation of the monolayer structure without directly breaking the individual filling lines. The deformation of the material is mainly contributed by the bending and compression of the filler wire, rather than tensile failure, and therefore has a high strength [136]. Due to the flexibility of TPU, a 90° fill can absorb large tensile stress without immediate failure. The second best performance was with the 45° fill. During the stretching process, the force on each fill line can be broken down into tensile force in the direction along the line and shear force perpendicular to the line direction. The shear effect can reduce the stress concentration, avoid the failure of a single filler line, and enhance the structural strength [137]. Moreover, 45° filling is the best angle for shearing effect, which can readjust the shape to a certain extent and adapt to the change of tensile direction during the tensile process. The 0° case (filling direction parallel to the tensile direction) is the weakest in tensile performance. This is because all the filling lines are parallel to the tensile direction, all the stress is concentrated in the filling line itself. TPU is a flexible material, so a single filling line is easy to fail after stretching to a certain extent. Once some areas are broken, the tensile load will be quickly transferred to other filling lines, and the overall bearing capacity will decrease rapidly. This is also consistent with the results of Bruère et al. (2023) on the mechanical performance of elastic TPU in different filling directions under FFF printing [138]. Finally, the performance of 30° and 60° filling is very similar to 0°, and the 30° angle is closer to 0°, which is prone to failure modes like 0° filling. The 60° angle data are closer to the 45° case, but the angle between the filling and stretching directions is greater, so the shear effect is not as pronounced as the 45° angle. Therefore, at 60° and 30° angles, the component of the force on the filling line is uneven, and there is a stress concentration that reduces the mechanical properties.

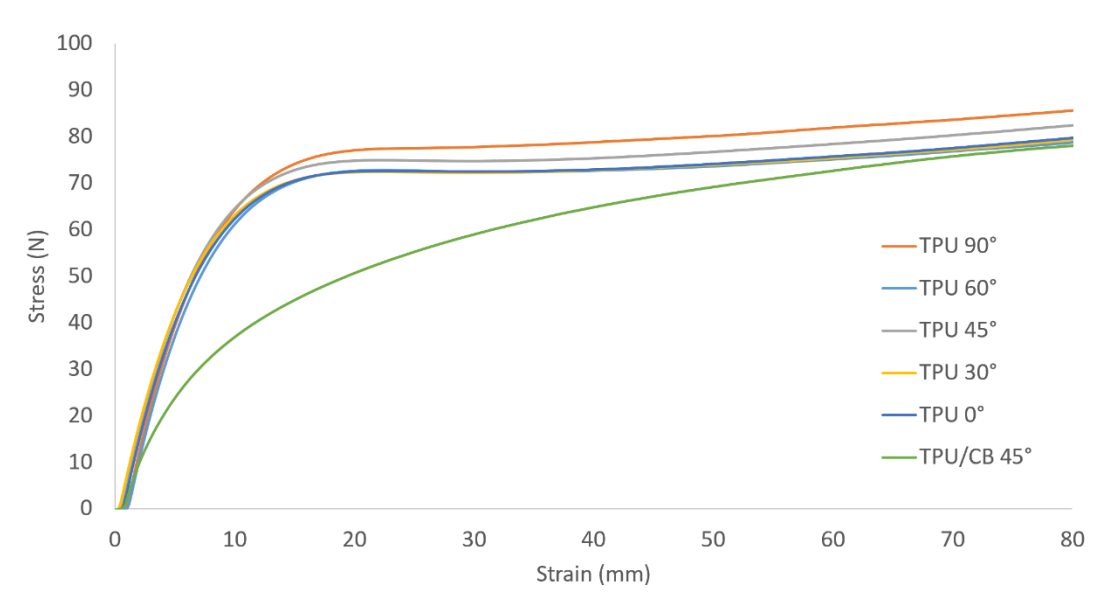


Figure 5.7: Stress-strain curves of TPU samples with different filling angles and 45° filled TPU/CB sample.

At the same time, TPU/CB samples of the same size (see **Figure 4.3**) were printed to analyze the tensile properties of TPU and TPU/CB at the same filling angle of 45°. The tensile properties of TPU/CB are lower than those of TPU, mainly due to the addition of carbon black particles in the composites. Although the carbon black filling enhances the stiffness, it sacrifices the ductility of the material and reduces the uniformity of the TPU material, making it easier for internal microcracks to form [139]. The experimental results are consistent with the mechanical performance of the TPU/CB tensile test by Zhao et al. [140]. **Table 5.1** shows an overview of all the Young's modulus calculated for the TPU samples in different filling directions and the 45° filled TPU/CB sample based on the elongation test. For the manufacture of flexible wearable sensors, materials with low Young's modulus (low rigidity) are more suitable [141]. The low Young's modulus has better flexibility and can better conform to the curved surface of the human body. High fit reduces measurement signal interference, and is more resistant to stretching and adapting to the dynamic movement of the human body. The materials used in this experiment all have low Young's modulus (<2 MPa) and perform well in above respect.

Table 5.1: Young's modulus of the samples calculated from tensile testing data.

Sample name	Young's modulus (MPa)	
TPU 90°	0.66	
TPU 60°	0.81	
TPU 45°	0.68	
TPU 30°	0.80	
TPU 0°	0.87	
TPU/CB 45°	1.97	

Next, considering the tensile properties of the electrode samples printed on the substrate, the TPU/CB filament was printed on a single layer of dog-bone shaped substrate in a semi-circular arc shape with 8 sinusoidal loops (i.e., double the number in the design shown in **Figure 5.1**. Five specimens were repeatedly printed and subjected to tensile tests

respectively, and the resulting stress-strain curves are shown in **Figure 5.8**. In the initial tensile stage (0-10 mm), the material undergoes elastic deformation, and the stress and strain are linearly related up to about 4 mm, which indicates that the mechanical properties of the TPU/CB filament are relatively stable under low strain. All the curves almost coincided, showing good repeatability. After that, the material enters the yield phase (10-30 mm), and the curve enters the nonlinear region, indicating that the material begins to enter the plastic deformation stage. Although there is a slight deviation in different experimental curves, the maximum force of about 20N is basically the same, indicating that the yield strength of the material is relatively constant. At the end of the 30 mm-stretch, the curve rises slowly, the material can still bear the load but the stiffness is weak, and the five curves show certain fluctuations at this stage, which may be caused by printing deviations and test deviations. When the tensile end point of 70 mm is near, the five curves tend to be consistent, indicating that the material still has good repeatability in the large deformation range.

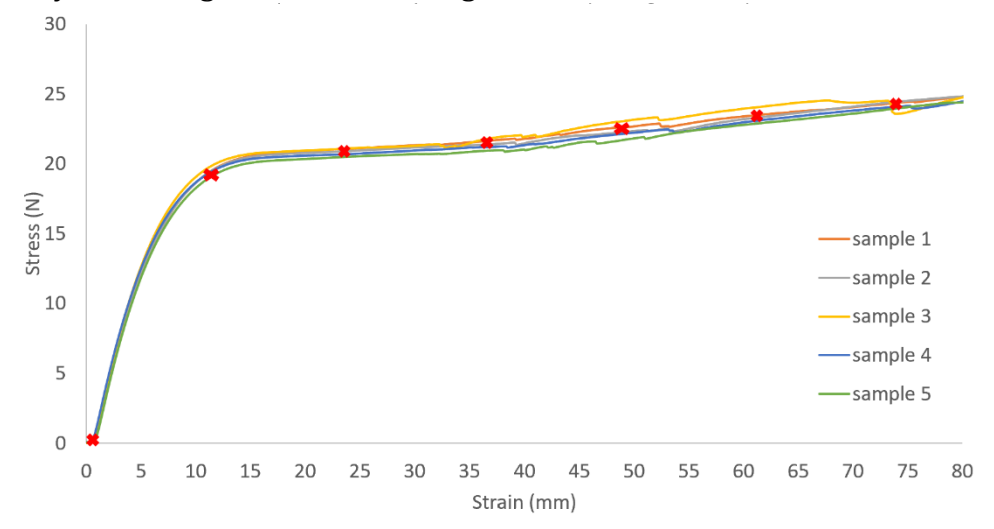


Figure 5.8: Stress-strain curves of five printed specimens with TPU/CB electrode on TPU.

Figure 5.9 visualizes the entire stretching process. Screenshots (a)-(g) are from the initial state, selected every 10 seconds, to the final printing electrode is pulled off (about 1 minute), and the corresponding stress-strain state of each screenshot is marked with a red "x" in the **Figure 5.8** curve. During the tensile test, after the strain of 30 mm, a creaking sound begins to appear, and the surface material gradually enters the damage stage, and the internal conductive network of the material begins to be destroyed, microcracks begin to germinate, or the interface begins to debond. This phenomenon was also observed by Wu et al. when they studied the tensile properties of the conductive networks of carbon-based fillers, including carbon black, in polymer matrices [142]. This may be due to the fact that as the material is stretched to a certain extent, the connection between the carbon black particles may gradually pull apart, causing a partial disruption or displacement of the conductive network, producing a sudden microstructural breakdown that makes a creaking sound. It may also be accompanied by local interfacial debonding, where insufficient adhesion between the carbon black and TPU leads to interfacial cracking, resulting in local microcracks or structural changes with audible creaks.

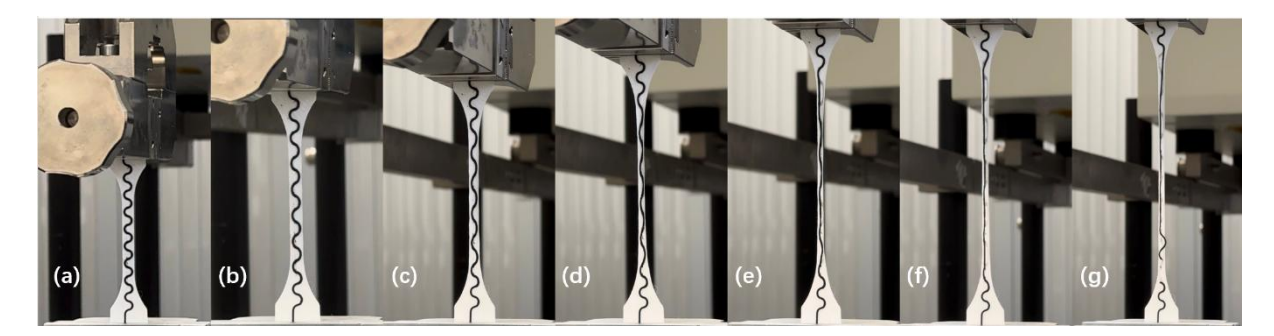


Figure 5.9: Visualization of sample tensile experiments (pictures were taken every ten seconds apart).

Exploring the complete tensile process, the stress-strain curve fluctuates at about 40 mm. i.e., screenshot (e), and the printed TPU/CB electrode gradually detaches from the substrate. Finally at about 73 mm, i.e., screenshot (g), the TPU/CB electrode breaks first, and the TPU substrate does not break. During the tensile test, the TPU/CB detached from the matrix first, which was related to the interfacial bonding strength. The binding between TPU and TPU/CB is mainly based on physical adsorption or intermolecular interactions (van der Waals forces, hydrogen bonding), and generally does not have strong chemical bonding [143]. Therefore, during the tensile process, due to the large difference in the elastic modulus between TPU/CB and the flexible TPU matrix, an obvious stress concentration will be formed at the interface when the tensile load is applied, which will cause interface debonding [144], resulting in the detachment of TPU/CB from the TPU substrate. When TPU/CB is detached from the support, the tensile load is more concentrated on TPU/CB, and after the addition of carbon black, TPU has lower flexibility and higher rigidity, making it more brittle and easier to fracture than pure TPU [145]. The TPU matrix can continue to stretch without breaking after TPU/CB fracture, because the TPU material itself has excellent flexibility, and most of the load during stretching is absorbed by interfacial debonding and TPU/CB fracture, and the remaining stress acting on the matrix is not enough to cause the pure TPU substrate to fracture [146]. In summary, in terms of mechanical tensile properties, the electrode performs well in the stress range of wearable application scenarios typically not exceeding strains of few dozens of %, and the printed electrode has good repeatability. If there is a need to work under large tensile stress conditions in the future, the selection of electrode material can be adjusted according to the needs and the interface bonding strength between the electrode and the substrate can be enhanced by secondary heat pressing or adding an intermediate transition or compatible layer.

5.2.3 Electrical characterization

First, the repeatability of the printed electrode in terms of resistance was evaluated. The samples in **Figure 5.5** were printed five times in duplicate and the resistance values were tested five times with a multimeter for five samples to perform repeatability and stability analysis. The repeated test results (**Figure 5.10**) showed that the samples prepared in this study showed excellent electrical consistency over five consecutive measurements. The experimental data of resistance repeatability show that the results of the five measurements of each sample are close to each other, the data distribution is concentrated, and the maximum deviation does not exceed $\pm 2\%$ of the initial measurement value, and no obvious anomalies or outliers are found, which proves that the test method has good reliability and high repeatability [147]. This result also shows that the human error and systematic error in the test process are effectively controlled.

In the stability evaluation, the analysis of variance found that there was no significant monotonic increasing or decreasing trend in the longitudinal measurement data of the sample, and the fluctuation range of the resistance value was strictly controlled within

±2% of the initial measured value. Small fluctuations can occur due to slight differences in the amount of electrode material extruded from each printer; There is a slight change in the contact position of the electrode probe for each measurement; Thermal drift in the intrinsic resistance of the material and the inherent accuracy error of the measurement device caused by changes in ambient temperature and humidity. In summary, the deviation of the resistance value of the five measurements is very small and the repeatability is good, indicating that the test system is reliable. There was no significant resistance drift in the five sample resistors, indicating that the printed electrodes had high reliability under repeated measurements.

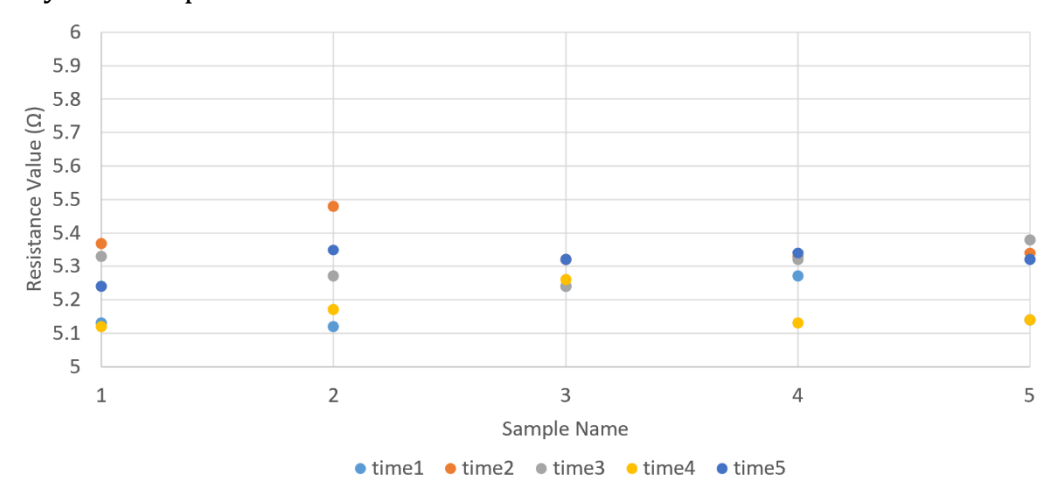


Figure 5.10: Scatter plot plotted by five resistance measurements of five replicated samples.

Next, the effect of printing on the resistance of the material is studied. **Equation 4.1** was used to calculate the volume resistance of the printing electrode and the TPU/CB filament before printing, which were $26.68~\Omega \cdot cm$ and $8.25~\Omega \cdot cm$, respectively, and the resistivity of the surface TPU/CB filament increased significantly after FDM printing. In general, the FDM process has a significant effect on the electrical resistance characteristics of TPU/CB composites, which usually results in a $2{\sim}10$ fold increase in the resistance value of the printed material compared with the original filament [148]. This phenomenon is mainly due to the following three mechanisms:

- Molten shear causes damage to conductive networks [149]. In the melt extrusion process, the high-viscosity TPU matrix undergoes nozzle shear flow, resulting in forced migration and local agglomeration of CB particles. This shear-induced redistribution of the filler cuts off the continuity of the original conductive path, creating a local insulating area. At the same time, the rapid cooling and curing inhibited the thermal movement and reorganization of CB particles, making it impossible to effectively reconstruct the damaged conductive network.
- The high-temperature thermal effect has a certain effect on the dispersion of fillers [150]. Although the heat energy input in the melting stage can promote the diffusion of CB particles, the viscoelastic constraints of the TPU matrix and the difference in CB surface energy lead to abnormal aggregation. However, the re-aggregation or reunion of CB particles affects the uniformity of the conductive network, and the resistance will increase significantly when the conductive path is uneven or the particles are severely aggregated.
- Interlayer bonding defects can cause an increase in volume resistance [151]. The layer-by-layer deposition of FDM leads to the existence of microscopic pores in the prints, and the CB particles at the interlayer interface are arranged in an orientation due to the limited Z-direction flow. This anisotropic distribution increases the tortuosity of the electron transport path [152], which is macroscopically manifested

as an increase in volume resistivity.

Then, a thermal cycling experiment was performed on the sample electrode. The printed sample was fixed on the hot bed, the position of the multimeter used for the measuring electrode was fixed, and the cycle heating to cooling was repeated five times to obtain the experimental results as shown in **Figure 5.11**. It is found that the resistance of TPU/CB composites shows a unique resistance evolution behavior during thermal cycling: the resistance of TPU/CB composites increases monotonically with the increase of temperature in the single heating stage, but in the continuous heating-cooling cycle, the resistance value at the same temperature point gradually decreases with the increase of the number of cycles (the resistance of the fifth cycle decreases by about 15%~30% compared with the first cycle). This phenomenon can be attributed to the dynamic coupling of the reconfiguration of the conductive network inside the material and the thermodynamic response of the matrix. Firstly, as a flexible polymer matrix, TPU gradually releases internal stress during thermal cycling, which will promote the rearrangement and tightness of carbon black particles to form a more stable conductive network. Secondly, multiple thermal cycles may improve the interfacial contact between carbon black particles, increase the effective conductive path, and reduce the resistance. In addition, the microscopic irreversible structural changes caused by the shape memory effect may occur when TPU is repeatedly heated, which makes the carbon black network tend to be dense and stable. At the same time, the residual stress of the TPU matrix is gradually released during repeated heating and cooling, which further stabilizes the conductive path, so that the resistance gradually decreases with the increase of the number of cycles [153]. This has a positive effect on the stability and conductivity of the material. With the heating cycle, the resistance value of the material tends to be stable, indicating that the carbon black network structure tends to be stable, which may be beneficial to improve the reliability of sensors or flexible electronic devices. As the resistance of thermally cycled materials decreases, the conductivity increases, which provides a potential optimization direction for increasing the conductivity of flexible electrochemical sensors. On the other hand, however, the long-term stability of the material needs to be further verified, and if the cycling resistance continues to decrease, it may affect the long-term measurement consistency of the sensor. In addition, the irreversible changes that may occur in the material may affect the repeatability and the stability of the sensor during long-term use.

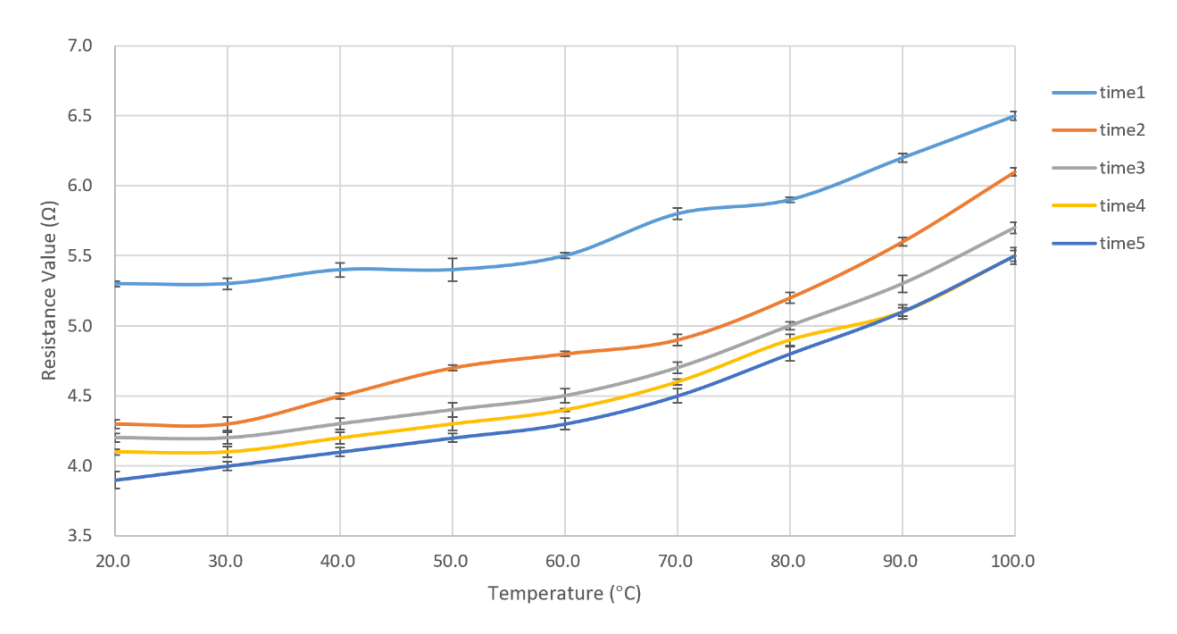


Figure 5.11: Line graph of sample resistance under five repeated thermal cycles.

5.2.4 Electrochemical characterization and surface treatment

In the case of good mechanical and electrical properties, this section evaluates the potential of TPU/CB printed electrodes as electrochemical sensor electrodes. The following experiments were performed using a single electrode sample of the same size printed by the TPU/CB filament by FDM.

Electrode surface treatment

Post-processing is often required for electrodes printed with FDM [154]. Due to the inherent problems in the FDM printing process, it will not only affect the conductivity of the material, but also affect the electrochemical activity of the material. Chapter 5.2.3 examines the effect of FDM printing on the conductivity of materials, and this chapter will focus on the study of electrochemical activity. In extrusion melt using the fused deposition model, the TPU melt typically coats the carbon black particles inside, resulting in the formation of an insulating polymer layer on the surface, which affects electron transport on the electrode surface [155]. After the conductive CB particles are coated with TPU, the conductive particles on the surface of the electrode are not exposed enough, which reduces the effective contact area between the electrode and the external electrolyte or conductive probe, and significantly reduces the number of effective sites in the electrochemical reaction. In response to the above problems caused by FDM printing, the most common post-processing methods include chemical treatment [156], thermal treatment [157], mechanical treatment [158], and biological treatment [159]. For the TPU/CB electrode selected in this experiment, in order to remove the thin layer of TPU covered by the electrode surface, a polar solvent immersion electrode was selected to partially dissolve the thin layer of TPU on the surface [160] and expose the carbon black particles. Through appropriate heat treatment, the residual stress in the TPU matrix is released, and the recombination of carbon black particles is promoted to form a more uniform and stable conductive network. Combined with mechanical treatment and polishing, the thin layer of insulating polymer covered on the surface is directly removed, increasing the number of conductive paths and improving the electrode transmission ability from the outside world. Figure 5.12 illustrates the flow chart of electrode processing.



Figure 5.12: Optical images showing the various steps of the electrode surface treatment procedure.

In the first step, the TPU/CB printing electrode was soaked in dimethyl sulfoxide (DMSO) and soaked for 10, 20 and 30 minutes respectively for comparison. Firstly, DMSO has strong polarity and permeability, which can penetrate deep into the TPU and swell and soften the TPU through intermolecular polarity, promote the movement of polymer segments, and expose more carbon black particles. Secondly, the swelling of TPU promotes the rearrangement of carbon black particles to form a more stable and dense conductive network, which effectively increases the number of conductive contact points between carbon black particles. In addition, the TPU insulating layer formed on the surface of the electrode after FDM printing was also effectively swollen and thinned by

DMSO, which significantly increased the exposure of carbon black particles and the number of electrochemically active sites of the electrode. Compared with the traditional use of DMF solvents, DMSO has stronger polarity, better permeability, higher safety, and lower toxicity, which can achieve more efficient, environmentally friendly, and safe post-processing effects [160]. Observing **Figure 5.12(b)**, it can be seen that the polymer has been precipitated in the DMSO solution at this time, and the electrode surface is partially dissolved by clamping the electrode with tweezers, forming a slightly concave and convex surface. Subsequent ethanol rinsing quickly and effectively removes residual DMSO from the electrode surface and improves the cleanliness of the electrode and the surface exposure of carbon black particles. After ultrasonic treatment with pure water, the cavitation of ultrasonic produces a large number of microbubbles, which mechanically removes fine impurities, residual solvents, and unstable TPU overlays on the surface and inside, thereby further improving the exposure of the conductive filler and the uniformity of the conductive network.

In the second step, the chemically treated electrode is dried in an oven at 80°C for one hour to ensure that the residual water, ethanol and possible residual DMSO inside and outside the electrode are completely volatilized. After the swelling of the previous DMSO, the TPU rebounded and rearranged the segments during the drying process, reforming a strong intermolecular hydrogen bond network, which further brought the carbon black particles into close contact and made the conductive path more stable and dense [161]. After drying, the TPU layer on the surface of the electrode is further densified, exposing the carbon black particles more evenly, enhancing the effective contact area between the electrode and the electrolyte, and contributing to the improvement of electrochemical performance.

In the third step, the uneven electrode surface after drying is sanded with sandpaper (500 grit) for one minute, which can effectively remove or significantly thin the TPU surface insulation layer formed during printing, so that more carbon black particles are exposed to the surface, thereby significantly improving the conductive contact area and electrochemical active site on the electrode surface. In addition, the polishing treatment can also reduce the surface roughness of the electrode, and improve the consistency and stability of contact with the probe or electrolyte. At the same time, the mechanical action induces a small local pressure, which rearranges the carbon black particles and forms a denser conductive network, which is manifested as a significant reduction in electrode resistance and an improvement in electrochemical performance [162].

Further morphological and surface characterization of the electrodes before and after surface treatment was performed, and **Figure 5.13** is an image of the electrode surface before and after treatment using SEM. At 10 kV and 1800x magnification, the surface structure of the untreated electrode in Figure 5.12(a) is dense, and the carbon black particles are firmly coated by TPU polymer, and the particles are dispersed in the polymer matrix in an isolated state, lacking effective connections between them, and the conductive path is significantly limited. This structure results in a low overall conductivity and electrochemical activity of the material. In Figure 5.13(b), the surface of the electrode treated sample exhibits a clear porous network-like structure, with a large number of carbon black particles exposed and forming a continuous and dense conductive network. The TPU polymer layer originally covered on the carbon black particles is significantly removed or thinned, and the effective contact area between the particles is significantly increased, which promotes the conduction of electrons and ions, and effectively enhances the conductivity and electrochemical activity of the electrode. In conclusion, the electrode after surface treatment has a more open microstructure, and the carbon black particles are fully exposed to form a stable and continuous conductive network, which explains the significant increase in the electrochemical activity of the electrode in the subsequent CV curve test.

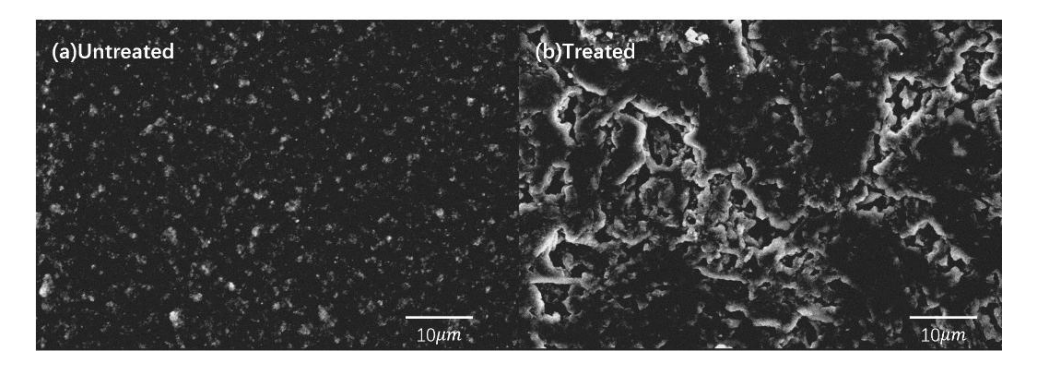


Figure 5.13: SEM images of the electrode surface (a) before and (b) after treatment.

Electron microscopy was used to observe the printed electrode samples before and after electrode surface treatment at magnification of 20 and 200x, respectively, as shown in **Figure 5.14**. Macroscopically, it was found that the surface of the untreated electrode (**Figure 5.14(a**)) was rough, showing obvious stripes and furrow-like structures, which are the characteristic textures formed by melt extrusion during FDM printing. In addition, a large amount of TPU polymer covers the surface, the carbon black particles are less exposed, and the conductive filler is coated with an insulating layer, which reduces the conductivity and electrochemical activity. However, the overall surface structure of the electrode after electrode treatment (Figure 5.14(b)) is significantly smoother, the original printing texture is almost completely lost, and the TPU overlay on the surface is significantly reduced or removed. The carbon black particles are fully exposed to the surface of the electrode, forming a denser and more continuous conductive network structure, which greatly improves the conductivity and electrochemical activity of the electrode. In summary, the electrode structure after surface treatment is more uniform and dense, and the exposure of conductive fillers is greatly increased, which is more suitable as a high-performance electrode material in the field of flexible sensors.

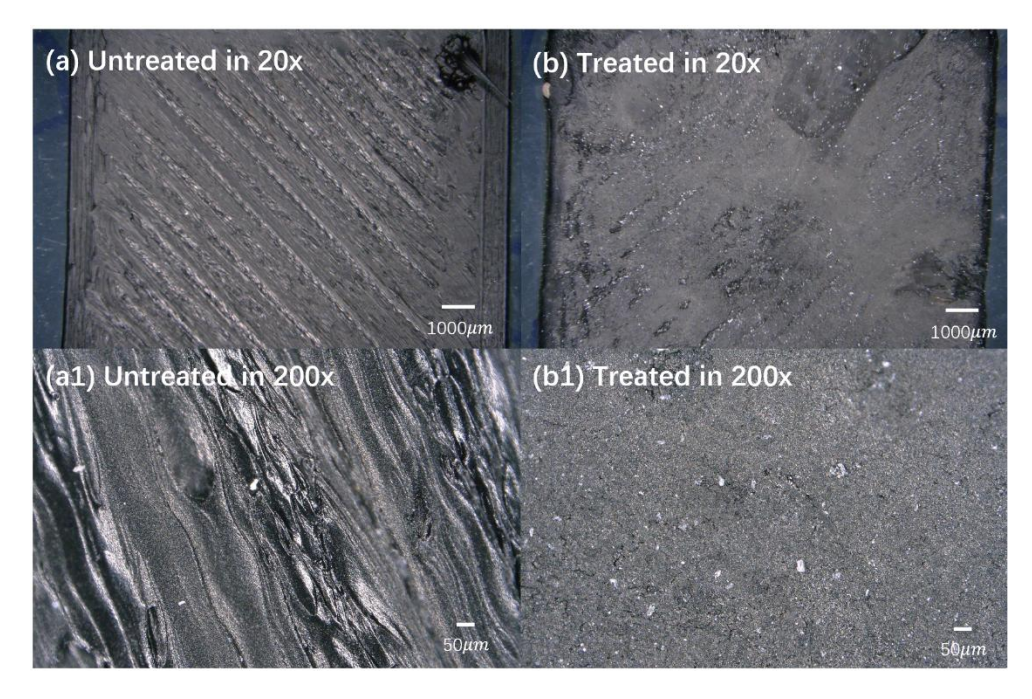


Figure 5.14: SEM images of the untreated and treated printed electrode samples magnified by 20x (a),(b) and 200x (a1),(b1), respectively.

Characterization in supporting electrolyte

The untreated electrodes and the electrodes soaked for 10, 20, and 30 minutes were characterized in a 0.5M KNO_3 auxiliary electrolyte, and the cyclic voltammetry response is shown in **Figure 5.15**. KNO₃ was chosen as the electrolyte mainly because KNO₃ is a stable neutral salt, the solution itself does not participate in redox reactions, has good conductivity and ion mobility ability, can effectively reduce the resistance of the solution, improve the charge transfer between the electrode and the solution, and is suitable for the objective evaluation of the electrochemical properties of the electrode material [163]. In addition, KNO₃ is non-corrosive to electrode materials, does not affect the structure of TPU/CB materials, and can be effectively compared with existing literature data as a commonly used standard electrolyte.

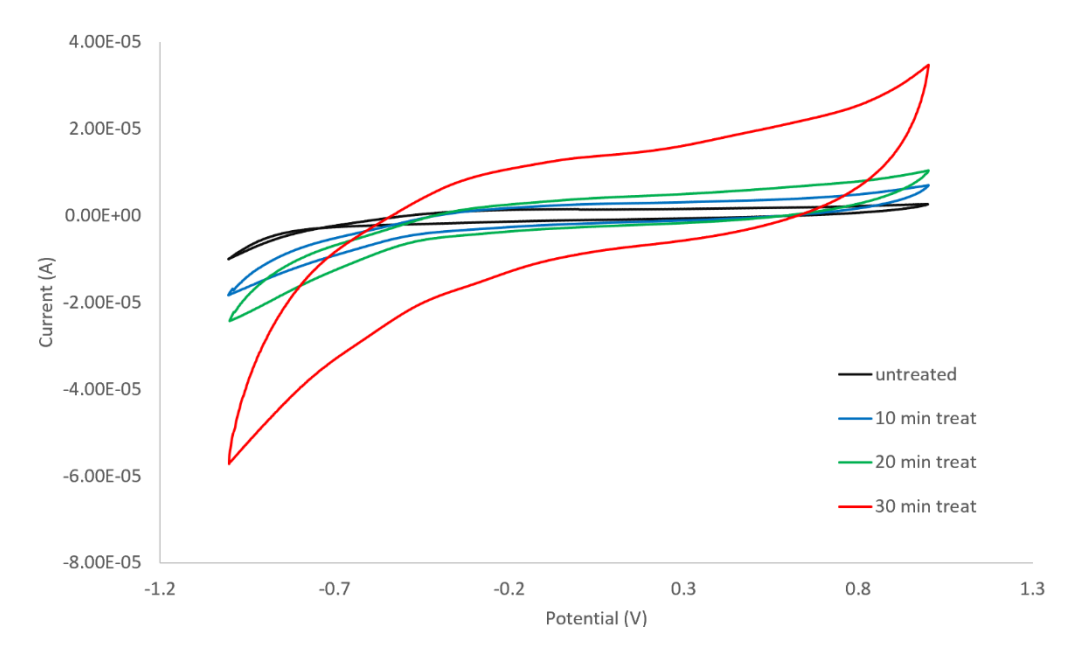


Figure 5.15: Cyclic voltammograms of 0.5M KNO₃, recorded on untreated and 10, 20, 30 min treated electrodes. (Scan rate: 0.1 V/s).

Observing the cyclic voltammetry curve in **Figure 5.15**, the curve area of the untreated electrode is small, the current response is low, and the obvious redox peak is lacking, indicating that the TPU insulation covering on the electrode surface is thick, and the carbon black particles are not exposed enough, which limits the electrochemical activity of the electrode. After 10, 20 and 30 minutes of DMSO treatment, the curve area gradually expands and the current response increases with the extension of the treatment time. This reflects that the surface insulation layer of DMSO is gradually removed, and the exposure of carbon black particles is gradually increased, which significantly increases the contact interface between the electrode and the ions, and significantly improves the conductivity and electrochemical reaction ability of the electrode. Among them, the electrode with 30 minutes of treatment had the best performance, showing the largest curve area and the strongest peak current response, which confirmed that the insulation layer on the electrode surface was significantly reduced, and the carbon black particles were fully exposed, thus effectively improving the overall electrochemical activity of the electrode.

Characterization with standard redox markers

To evaluate the electrochemical performance of the printed TPU/CB electrodes, two commonly used redox markers $[Ru(NH_3)_6]^{3+/2+}$ (RuHex) and $[Fe(CN)_6]^{3-/4-}$ (Ferrocyanide) [164] were selected. The electrochemical behavior of the untreated electrode and the

electrode samples soaked for 10, 20, and 30 minutes were investigated by cyclic voltammetry, as shown in Figure 5.16. In both redox markers, the electrochemical performance of the electrode was significantly improved with the extension of DMSO treatment time, which was manifested by a larger CV curve area and more obvious redox peaks. Among them, RuHex, as a positively charged probe, undergoes redox reactions on the electrode surface mainly through non-specific electrostatic adsorption and electron transfer, which is greatly affected by the charge density on the electrode surface [165]. Figure 5.16 (a) characterizes the RuHex system, where the untreated electrode (black curve) exhibits a low current response and the redox peak is not obvious, indicating that there is an insulating TPU covering on the electrode surface, which hinders electron transport and ion diffusion. With the increase of DMSO treatment time (10 minutes, 20 minutes, 30 minutes), the area of the CV curve gradually increased, and the redox peak became clearer, indicating that the conductivity and electrochemical activity of the electrode were significantly enhanced. The electrode treated in 30 minutes (red curve) showed the highest peak current and the largest curve area, indicating that the TPÚ insulation layer was basically removed, and more carbon black conductive particles were exposed, which improved the electron transport efficiency and the reactivity of the electrode-solution interface. The RuHex system is an externally diffusion-controlled redox probe, and the surface polarity of the electrode is increased after TPU treatment with DMSO dissolved electrode surface, which improves the adsorption capacity of RuHex, a positive ion probe, on the electrode surface, thereby enhancing the redox current. This indicates that the surface structure of the electrode has been optimized for higher charge transfer efficiency.

As a negatively charged probe, Ferrocyanide's redox process is mainly controlled by the diffusion process, and the ion exchange at the electrode-solution interface and the electrode surface state have a great influence on its reaction rate. However, it is sensitive to the hydrophilicity and conductive network exposure of the electrode surface, and is particularly suitable for studying the surface wettability and interface improvement of hydrophobic polymer-based electrodes (such as TPU/CB composites) after treatment [166]. **Figure 5.16(b)** characterizes the weak current response of the untreated electrode (black line) in the Ferrocyanide system, with fuzzy and inconspicuous redox peaks, indicating that the TPU overlay hinders the diffusion and interfacial electron transport of [Fe(CN)₆] ^{3-/4-} ions. With the DMSO treatment time from 10 minutes to 20 minutes, the redox current gradually increased, and the curve area and electrochemical peak gradually became clear, indicating that the insulation layer on the electrode surface was gradually removed, and the electrode activity was improved, but the improvement effect was lower than that of the RuHex system, indicating that the [Fe(CN)₆] ^{3-/4-} ions may be more sensitive to the electrode surface state or the diffusion is more limited. After 30 minutes of DMSO treatment, the current response was significantly improved, with obvious and clear redox peaks and a significant increase in the curve area, indicating that the longterm treatment greatly improved the conductive network and carbon black exposure on the electrode surface, and significantly improved the electrochemical response of the electrode to $[Fe(CN)_6]^{3-/4}$. Unlike the RuHex system, the Ferrocyanide system is a more surface-sensitive probe, and the redox process is mainly affected by the number and distribution of conductive sites on the surface. The peak current of the untreated electrode is small, indicating that the TPU overlay restricts the electron transfer process of ferricyanide on the electrode surface. As the DMSO processing time increases, the current of the redox peak gradually increases and the peak potential difference decreases, indicating that the conductivity and electron transport capacity of the electrode are improved. The electrodes (red curves) treated with DMSO for 30 minutes exhibited the best electrochemical activity, indicating that adequate exposure of carbon black particles on the surface improved electron exchange efficiency. In addition, DMSO treatment not only removes the insulation, but also makes the conductive network more uniform and dense, improves the electrode surface electron transport capacity, and makes the redox process more reversible.

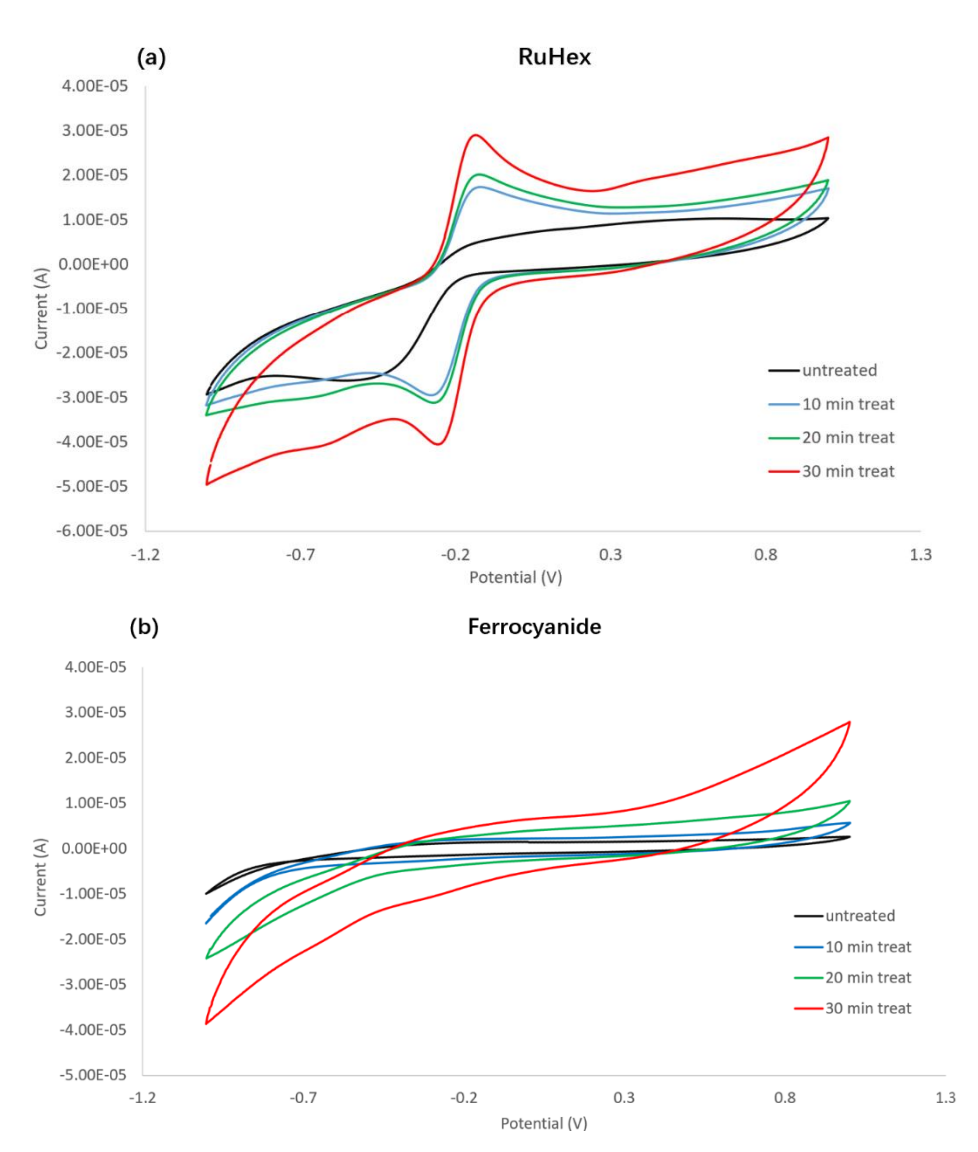


Figure 5.16: Cyclic voltammograms recorded in the solutions of 1mM RuHex in 0.5 M KNO₃ (a) and 1mM ferrocyanide in 0.5 M KNO₃ (b) on untreated and treated 10,20,30 electrodes. (Scan rate is 0.1 V/s).

Using **Equations 4.2** and **4.3**, the double-layer capacitance ($C_{\rm dl}$) value and the effective electrode surface area ($A_{\rm eff}$) of the treated electrode are calculated as shown in **Table 5.2**. In conclusion, the combined use of these two probes comprehensively evaluated the surface treatment effect of TPU/CB electrodes in terms of electrode surface conductivity, active site, charge transport efficiency, and electrode-solution interface characteristics.

Table 5.2: Calculated double layer capacitance (C_{dl}) and electrochemical active surface area (A_{eff}) for 10,20,30-min treated electrodes in 1mM RuHex in 0.5 M KNO₃ (-1 V – 1V).

Sample name	C_{dl} (μ F/cm ²)	A _{eff} (cm ²)
Treated electrode (10 min)	234.54	0.76
Treated electrode (20 min)	257.00	0.88
Treated electrode (30 min)	347.96	1.27

The electrochemical performance of the electrode improved significantly with the increase of DMSO treatment time, which was manifested by a simultaneous increase in electrochemical electric double capacitance and effective electrochemical surface area. The 30-minute treatment showed the best performance, with $C_{\rm dl}$ increasing from 234.54 $\mu F/cm^2$ to 347.96 $\mu F/cm^2$ and $A_{\rm eff}$ increasing from 0.76 cm^2 to 1.27 cm^2 , indicating increased electrode-electrolyte interface activity due to more conductive packing exposure. This indicates that DMSO treatment removes the insulation, optimizes the conductive network, and improves electron transport and ion exchange capabilities, making the electrode potentially valuable in applications such as electrochemical sensing, supercapacitors, and flexible electronics. However, in order to further optimize the process and ensure long-term stability, DMSO treatment parameters and electrode cycling performance still need to be studied.

Characterization with different scan rates

Cyclic voltammetry curves with different scan rates reveal the electrochemical response behavior of the electrode at different time scales. In **Figure 5.17**, the currents of the oxidation and reduction peaks increase as the scan rate increases (10 mV/s to 250 mV/s), which is consistent with the Randles-Sevcik equation, i.e., the peak current Ip is linearly related to the square root $v^{1/2}$ of the scan rate, indicating that the electrochemical process is mainly controlled by diffusion. In addition, the peak potential difference (ΔE_p) also increases with the scan rate, and theoretically the ΔE_p should be close to 59 mV for a reversible system, but the ΔE_p is often higher than this value in experiments due to the limited electron transfer kinetics and electrode polarization. At a lower scan rate (10-50 mV/s), the peak potentials of the oxidation and reduction peaks were relatively close, the change of ΔE_p was small, and the redox process was reversible. At higher scan rates (100 mV/s and above), the peak potential separation of the oxidation and reduction peaks was more obvious, and the ΔE_p increased significantly, indicating that the electron transfer process was dynamically controlled and the electron exchange rate was relatively slow.

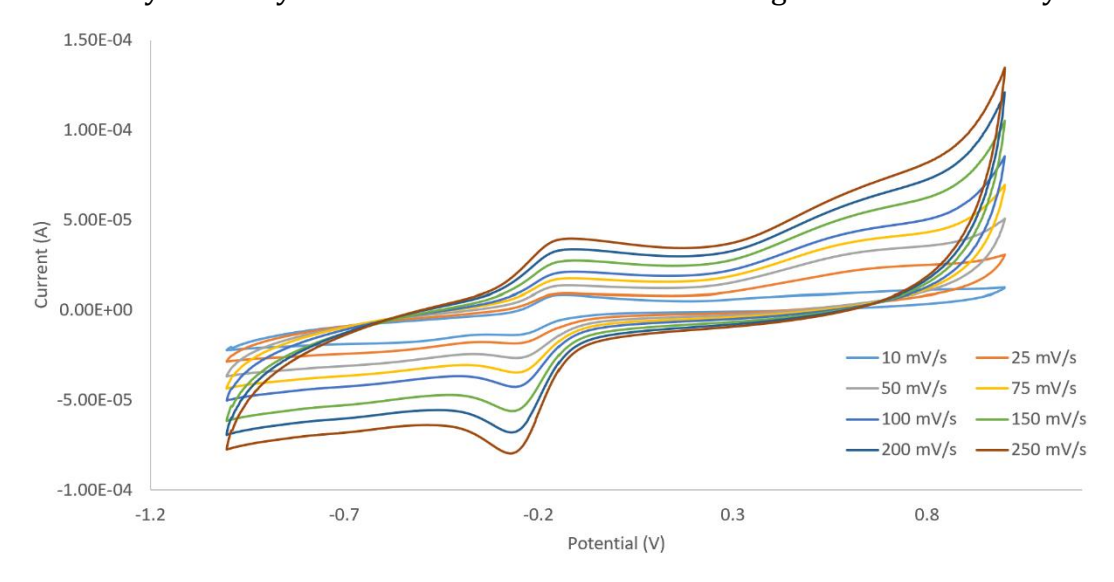


Figure 5.17: Multiple scan rate cyclic voltammograms in 1mM RuHex in 0.5 M KNO₃.

This trend is further confirmed by the change in the shape of the CV curve. At low scanning rate (10-50 mV/s), the CV curve was symmetrical and the redox peak was clear, indicating that the reaction was close to reversible. However, at high scan rates (100-250 mV/s), the curve is broadened, the resolution of oxidation and reduction peaks increases, and the current response is significantly enhanced, which may be related to electrode interface polarization and limited electron transport. In addition, the linear relationship between the peak current I_p and the square root $v^{1/2}$ of the scan rate was used to further

determine whether the reaction is controlled by diffusion, while the trend of ΔE_p was used to derive the electron transfer rate constant k_0 . **Figure 5.18** shows different ΔE_p at different scan rates. As can be seen from this figure, ΔE_p decreases at low scan rates (10–50 mV/s), indicating that the electron transfer process is reversible and the electrode reaction kinetics is good. In the medium and high scan rate range (75–250 mV/s), ΔE_p increases significantly, indicating that with the increase of scan rate, the shift between the oxidation peak and the reduction peak becomes larger, the charge transfer process is limited, and the electrochemical reversibility of the system decreases. This trend indicates that the material is affected by kinetics at high scan rates, resulting in poor charge transport or ion diffusion performance, and the reaction tends to be more quasi-reversible or irreversible. Overall, the electrode material exhibits good reversibility at low scan rate, while the kinetic process gradually becomes a limiting factor under high scan rate, indicating that electrode structure and electron exchange kinetics have an important influence on electrochemical performance.

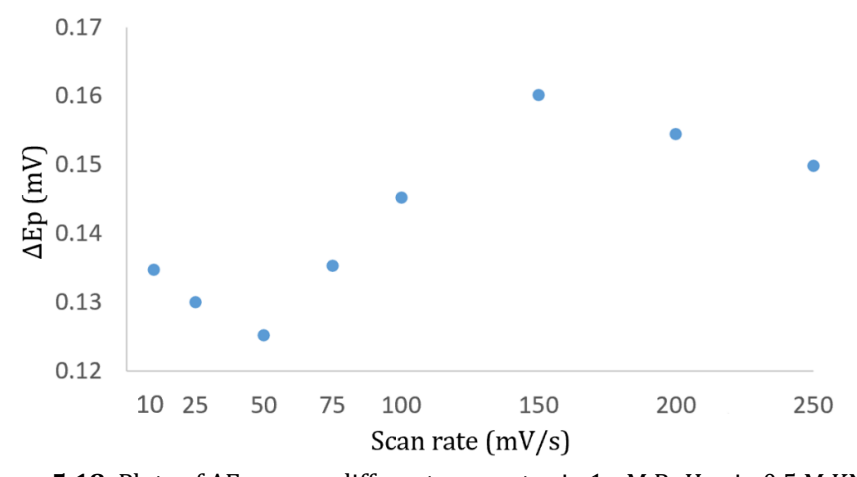


Figure 5.18: Plots of ΔE_P versus different scan rates in 1mM RuHex in 0.5 M KNO₃.

6 Conclusion and Outlook

This study discusses the application potential of FDM-printed TPU/CNT/BDD and TPU/CB materials for flexible electrochemical sensors, from fabrication to mechanical, electrical, and electrochemical performance evaluation. The main conclusions of the study are summarized as follows:

6.1 TPU/CNT/BDD printed electrode

- The flexible TPU substrate printed with FDM is well fixed to the heating bed.
- The BDD particles in the TPU/CNT/BDD filament and the rough surface of the filament itself lead to easy winding in the extruder and, consequently, the need for high nozzle temperatures.
- BDD particles may clog the printer nozzle, which will increase the difficulty of printing with the increase of printing times, and the size deviation of the printed sample is large.
- The resistance of TPU/CNT/BDD material increases significantly (by 230 %) after FDM printing (i.e., 44.25Ω).

6.2 TPU/CB printed electrode

- When printing the TPU/CB material directly onto a single-layer TPU substrate, the two are well combined, and the printed electrode will not be easily separated.
- When stretching and printing TPU samples with TPU/CB electrodes, the wavy electrodes will break away from the substrate first, but the tensile test data support good performance in the daily application range.
- The TPU/CB resistance after FDM printing has increased by about 3 times, but it still maintains good conductivity (i.e., 5.3Ω).
- If the printed TPU/CB electrode is heated and cooled cyclically, the electrode resistance is continuously reduced.
- The surface of TPU/CB electrode material is covered by TPU after printing, and the electrochemical performance is not good. When the TPU surface was (partially) dissolved with DMSO, the electrochemical performance gradually improved with the increase of treatment time.

6.3 Recommendations for future work

- Select an FMD printer with better and more accurate performance (for example, the Ultimaker S5 or Raise3D Pro3) and try to print TPU/CNT/BDD filament to reduce the impact of printer hardware on the printing effect.
- Repeat the heating and cooling process of the TPU/CB printed electrode for several times to test whether the resistance will continue to decrease or whether there is a minimum resistance value, and evaluate the long-term stability of the electrode.
- The cyclic voltammetry curves of the TPU/CB electrode after repeated heating and cooling need to be plotted, and the effects of thermal cycling on the conductive path

- and interfacial electron transfer of the electrode analyzed.
- Optimize the DMSO treatment process, explore the effects of different solvent systems (such as DMF and NMP) on TPU/CB electrodes, and study the regulation mechanism of treatment time, temperature and other parameters on the conductive network.
- Explore novel functionalization strategies, such as surfactant modification, plasma treatment, or nanocomposite enhancement, to further improve the electrode transport efficiency and ion diffusion capacity.
- In this project, due to time constraints, the RE manufacturing was not studied yet. Future work should be directed towards the printing of silver-based reference electrodes with particular focus on the mechanical adhesion to the flexible TPU substrate.
- Expand practical application scenarios, combine the needs of bioelectrochemistry, flexible wearable electronics and other fields, explore the feasibility of TPU/CB composite electrodes in biosensing, smart electronic skin, and flexible energy storage devices, and conduct systematic application testing and optimization.

References

- [1] Cheng, Shunfeng, Michael H. Azarian, and Michael G. Pecht. "Sensor systems for prognostics and health management." Sensors 10.6 (2010): 5774-5797.
- [2] Toniolo, Rosanna, et al. "Modified screen printed electrode suitable for electrochemical measurements in gas phase." Analytical chemistry 92.5 (2020): 3689-3696.
- [3] Shetti, Nagaraj P., et al. "Graphene-clay-based hybrid nanostructures for electrochemical sensors and biosensors." Graphene-based electrochemical sensors for biomolecules. Elsevier, 2019. 235-274.
- [4] Zijuan, H. E., et al. "Application progress of Ag/AgCl electrodes for electrochemical sensors." Precious Metals/Guijinshu 44 (2023).
- [5] Neethipathi, Deepan Kumar, et al. "MoS₂ Modified Screen Printed Carbon Electrode Based Flexible Electrochemical Sensor for Detection of Copper Ions in Water." IEEE Sensors Journal 23.8 (2023): 8146-8153.
- [6] Zhang, Li, et al. "A facile electrochemical sensor based on green synthesis of Cs/Ce-MOF for detection of tryptophan in human serum." Colloids and Surfaces A: Physicochemical and Engineering Aspects 648 (2022): 129225.
- [7] Bakker, Eric, and Martin Telting-Diaz. "Electrochemical sensors." Analytical chemistry 74.12 (2002): 2781-2800.
- [8] Hulanicki, Adam, Stanislav Glab, and F. O. L. K. E. Ingman. "Chemical sensors: definitions and classification." Pure and applied chemistry 63.9 (1991): 1247-1250.
- [9] Li, Zhanhong, et al. "A dual-function wearable electrochemical sensor for uric acid and glucose sensing in sweat." Biosensors 13.1 (2023): 105.
- [10] Bronzino, Joseph D. Biomedical engineering handbook 2. Vol. 2. Springer Science & Business Media, 2000.
- [11] Elgrishi, Noémie, et al. "A practical beginner's guide to cyclic voltammetry." Journal of chemical education 95.2 (2018): 197-206.
- [12] Dickinson, Edmund JF, and Andrew J. Wain. "The Butler-Volmer equation in electrochemical theory: Origins, value, and practical application." Journal of Electroanalytical Chemistry 872 (2020): 114145.
- [13] Walsh, Frank C., Luis F. Arenas, and Carlos Ponce de León. "Developments in electrode design: structure, decoration and applications of electrodes for electrochemical technology." Journal of Chemical Technology & Biotechnology 93.11 (2018): 3073-3090.
- [14] Islam, Md Nazmul, and Robert B. Channon. "Electrochemical sensors." Bioengineering innovative solutions for cancer. Academic Press, 2020. 47-71.
- [15] Saputra, Heru Agung. "Electrochemical sensors: basic principles, engineering, and state of the art." Monatshefte für Chemie-Chemical Monthly 154.10 (2023): 1083-1100.
- [16] Kissinger, P.T., Heineman, W.R., Achterberg, E.P.: Laboratory techniques in electroanalytical chemistry. TrAC Trends Anal. Chem. 15, 550 (1996).
- [17] Crapnell, Robert D., and Craig E. Banks. "Electroanalysis overview: Addressing the green credentials in the use of electroanalytical sensors." Green Carbon 1.1 (2023): 85-93.

- [18] Scholz, F. Voltammetric techniques of analysis: the essentials. ChemTexts 1, 17 (2015).
- [19] Zanello, P.: Inorganic Electrochemistry Theory, Practice and Application. Royal Society of Chemistry, UK (2003).
- [20] Majeed, S., Naqvi, S.T.R., ul Haq, M.N., Ashiq, M.N.: Electroanalytical techniques in biosciences: conductometry, coulometry, voltammetry, and electrochemical sensors. In: Analytical Techniques in Biosciences, pp. 157–178. INC (2022).
- [21] Skoog, Douglas A., F. James Holler, and Stanley R. Crouch. Instrumental analysis. Vol. 47. Belmont: Brooks/Cole, Cengage Learning, 2007.
- [22] Mirceski, V., Skrzypek, S. & Stojanov, L. Square-wave voltammetry. ChemTexts 4, 17 (2018).
- [23] Xu, Cong, et al. "In vivo electrochemical sensors for neurochemicals: recent update." ACS sensors 4.12 (2019): 3102-3118.
- [24] Paixão, Thiago RLC. "Measuring electrochemical surface area of nanomaterials versus the Randles-Ševčík equation." ChemElectroChem 7.16 (2020): 3414-3415.
- [25] Chang, Byoung-Yong, and Su-Moon Park. "Electrochemical impedance spectroscopy." Annual Review of Analytical Chemistry 3.1 (2010): 207-229.
- [26] Lazanas, Alexandros Ch, and Mamas I. Prodromidis. "Electrochemical impedance spectroscopy—a tutorial." ACS Measurement Science Au 3.3 (2023): 162-193.
- [27] Simões, Fabio Ruiz, and Miguel Gustavo Xavier. "Electrochemical sensors." Nanoscience and its Applications 1 (2017): 155-178.
- [28] Bigdeli, I.K., Yeganeh, M., Shoushtari, M.T., Zadeh, M.K.: Electrochemical impedance spectroscopy (EIS) for biosensing. In: Thomas, S., Nguyen, T.A., Ahmadi, M., Yasin, G., Farmani, A. (eds.) Nanosensors for Smart Manufacturing, pp. 533–554. Elsevier Inc. (2021)
- [29] Grassini, S.: Electrochemical impedance spectroscopy (EIS) for the in-situ analysis of metallic heritage artefacts. In: Dillmann, P., Watkinson, D., Angelini, E., Adriaens, A. (eds.) Corrosion and Conservation of Cultural Heritage Metallic Artefacts, pp. 347–367. Woodhead Publishing Limited, Cambridge, UK (Chapter 16) (2013)
- [30] Barhoum, Ahmed, et al. "Modern designs of electrochemical sensor platforms for environmental analyses: Principles, nanofabrication opportunities, and challenges." Trends in environmental analytical chemistry 38 (2023): e00199.
- [31] L. Neia, Milestones in the 50-year history of electrochemical oxygen sensor development, ECS Trans. 2 (25) (2007) 33–38.
- [32] Shetti, N.P.; Nayak, D.S.; Reddy, K.R.; Aminabhvi, T.M. Graphene–Clay-Based Hybrid Nanostructures for Electrochemical Sensors and Biosensors. In Graphene-Based Electrochemical Sensors for Biomolecules; Elsevier: Amsterdam, The Netherlands, 2019; pp. 235–274
- [33] Goud, K.Y., Satyanarayana, M., Hayat, A., Gobi, K.V., Marty, J.L.: Nanomaterial-based electrochemical sensors in pharmaceutical applications. In: Grumezescu, A.M. (ed.) Nanoparticles in Pharmacotherapy, pp. 195–216. William Andrew Publishing (2019)
- [34] Gao, Fupeng, et al. "Wearable and flexible electrochemical sensors for sweat analysis: a review." Microsystems & Nanoengineering 9.1 (2023): 1-21.
- [35] Lin, Tao, et al. "Flexible electrochemical sensors integrated with nanomaterials for in situ determination of small molecules in biological samples: a review." Analytica Chimica

- Acta 1207 (2022): 339461.
- [36] Gao, Fengxian, et al. "All-polymer free-standing electrodes for flexible electrochemical sensors." Sensors and Actuators B: Chemical 334 (2021): 129675.
- [37] Huarun, Liang, et al. "Flexible Electrochemical Sensors and Their Applications in Noninvasive Medical Detection." Acta Chimica Sinica 81.10 (2023): 1402.
- [38] Brownstein, Henry H., ed. The handbook of drugs and society. John Wiley & Sons, 2015.
- [39] Jane-Llopis, E. V. A., and Irina Matytsina. "Mental health and alcohol, drugs and tobacco: a review of the comorbidity between mental disorders and the use of alcohol, tobacco and illicit drugs." Drug and alcohol review 25.6 (2006): 515-536.
- [40] Teymourian, Hazhir, et al. "Wearable electrochemical sensors for the monitoring and screening of drugs." ACS sensors 5.9 (2020): 2679-2700.
- [41] Gao, W. et al. Fully integrated wearable sensor arrays for multiplexed in situ perspiration analysis. Nature 529, 509–514 (2016).
- [42] Liu, X. Y. & Lillehoj, P. B. Embroidered electrochemical sensors for biomolecular detection. Lab Chip 16, 2093–2098 (2016).
- [43] Engwa, G. Azeh, et al. "Mechanism and health effects of heavy metal toxicity in humans." Poisoning in the modern world-new tricks for an old dog 10 (2019): 70-90.
- [44] T. Guinovart, A.J. Bandodkar, J.R. Windmiller, F.J. Andrade, J. Wang, A potentiometric tattoo sensor for monitoring ammonium in sweat, Analyst 138 (22) (2013) 7031–7038.
- [45] M. Yang, S.W. Jeong, S.J. Chang, K.H. Kim, M. Jang, C.H. Kim, N.H. Bae, G. S. Sim, T. Kang, S.J. Lee, B.G. Choi, K.G. Lee, Flexible and disposable sensing platforms based on newspaper, ACS Appl. Mater. Interfaces 8 (51) (2016) 34978–34984.
- [46] Zhu, Chonghui, et al. "A dual-functional polyaniline film-based flexible electrochemical sensor for the detection of pH and lactate in sweat of the human body." Talanta 242 (2022): 123289.
- [47] H.Y.Y. Nyein, W. Gao, Z. Shahpar, S. Emaminejad, S. Challa, K. Chen, H. M. Fahad, L.-C. Tai, H. Ota, R.W. Davis, A. Javey, A wearable electrochemical platform for noninvasive simultaneous monitoring of Ca2+ and pH, ACS Nano 10 (7) (2016) 7216–7224.
- [48] H. Lee, C. Song, Y.S. Hong, M.S. Kim, H.R. Cho, T. Kang, K. Shin, S.H. Choi, T. Hyeon, D.-H. Kim, Wearable/disposable sweat-based glucose monitoring device with multistage transdermal drug delivery module, Sci. Adv. 3 (3) (2017), e1601314.
- [49] S. Emaminejad, W. Gao, E. Wu, Z.A. Davies, H.Y.Y. Nyein, S. Challa, S.P. Ryan, H. M. Fahad, K. Chen, Z. Shahpar, S. Talebi, C. Milla, A. Javey, R.W. Davis, Autonomous sweat extraction and analysis applied to cystic fibrosis and glucose monitoring using a fully integrated wearable platform, Proc. Natl. Acad. Sci. U. S. A 114 (18) (2017) 4625–4630.
- [50] G. Xiao, J. He, Y. Qiao, F. Wang, Q. Xia, X. Wang, L. Yu, Z. Lu, C.-M. Li, Facile and low-cost fabrication of a thread/paper-based wearable system for simultaneous detection of lactate and pH in human sweat, Adv. Fiber Mater. 2 (5) (2020) 265–278.
- [51] M. Parrilla, T. Guinovart, J. Ferre, P. Blondeau, F.J. Andrade, A wearable paperbased sweat sensor for human perspiration monitoring, Adv. Healthcare Mater. 8 (16) (2019), 1900342.
- [52] M.F. Hossain, J.S. Heo, J. Nelson, I. Kim, Paper-based flexible electrode using chemically-modified graphene and functionalized multiwalled carbon nanotube

- composites for electrophysiological signal sensing, Information 10 (10) (2019), 325.
- [53] Y. Li, R. He, Y. Niu, F. Li, Paper-based electrochemical biosensors for point-of-care testing of neurotransmitters, J. Anal. Test. 3 (1) (2019) 19–36.
- [54] Q. Lu, T. Su, Z. Shang, D. Jin, Y. Shu, Q. Xu, X. Hu, Flexible paper-based Ni-MOF composite/AuNPs/CNTs film electrode for HIV DNA detection, Biosens. Bioelectron. 184 (2021), 113229.
- [55] Wang, Cheng, et al. "Toward scalable fabrication of electrochemical paper sensor without surface functionalization." npj Flexible Electronics 6.1 (2022): 12.
- [56] M. Yang, S.W. Jeong, S.J. Chang, K.H. Kim, M. Jang, C.H. Kim, N.H. Bae, G. S. Sim, T. Kang, S.J. Lee, B.G. Choi, K.G. Lee, Flexible and disposable sensing platforms based on newspaper, ACS Appl. Mater. Interfaces 8 (51) (2016) 34978–34984.
- [57] W. Zeng, L. Shu, Q. Li, S. Chen, F. Wang, X.-M. Tao, Fiber-based wearable electronics: a review of materials, fabrication, devices, and applications, Adv. Mater. 26 (31) (2014) 5310–5336.
- [58] D.P. Rose, M.E. Ratterman, D.K. Griffin, L. Hou, N. Kelley-Loughnane, R.R. Naik, J.A. Hagen, I. Papautsky, J.C. Heikenfeld, Adhesive RFID sensor patch for monitoring of sweat electrolytes, IEEE Trans. Biomed. Eng. 62 (6) (2015) 1457–1465.
- [59] D.-K. Kang, M.M. Ali, K. Zhang, S.S. Huang, E. Peterson, M.A. Digman, E. Gratton, W. Zhao, Rapid detection of single bacteria in unprocessed blood using integrated comprehensive droplet digital detection, Nat. Commun. 5 (2014), 5427.
- [60] J.-K. Chen, G.-Y. Zhou, C.-J. Chang, C.-C. Cheng, Label-free detection of DNA hybridization using nanopillar arrays based optical biosensor, Sensor. Actuator. B Chem. 194 (2014) 10–18.
- [61] Li, Xu, et al. "Fabrication of paper-based microfluidic sensors by printing." Colloids and surfaces B: Biointerfaces 76.2 (2010): 564-570.
- [62] Gao, W. et al. Fully integrated wearable sensor arrays for multiplexed in situ perspiration analysis. Nature 529, 509–514 (2016).
- [63] Xu, G. et al. Battery-free and wireless epidermal electrochemical system with all-printed stretchable electrode array for multiplexed in situ sweat analysis. Adv. Mater. Technol. 4, 13 (2019).
- [64] Zeng, R. J. et al. CRISPR-Cas12a-driven MXene-PEDOT:PSS piezoresistive wireless biosensor. Nano Energy 82, 10 (2021).
- [65] Yu, Z. Z., Cai, G. N., Liu, X. L. & Tang, D. P. Pressure-based biosensor integrated with a flexible pressure sensor and an electrochromic device for visual detection. Anal. Chem. 93, 2916–2925 (2021).
- [66] Sempionatto, J. R. et al. Epidermal enzymatic biosensors for sweat vitamin C: toward personalized nutrition. ACS Sens. 5, 1804–1813 (2020).
- [67] Liu, J. et al. MXene-enabled electrochemical microfluidic biosensor: applications toward multicomponent continuous monitoring in whole blood. Adv.
- Funct. Mater. 29, 9 (2019).
- [68] Lv, S. Z., Lin, Z. Z., Zhang, K. Y., Lu, M. H. & Tang, D. P. Polyion oligonucleotide-decorated gold nanoparticles with tunable surface charge density for amplified signal output of potentiometric immunosensor. Anal. Chim. Acta 964, 67–73 (2017).
- [69] Yuan, Fan, et al. "Recent advances in inorganic functional nanomaterials based

- flexible electrochemical sensors." Talanta 244 (2022): 123419.
- [70] Rajan, Krishna, et al. "Silver nanoparticle ink technology: state of the art." Nanotechnology, science and applications (2016): 1-13.
- [71] S. Gong, W. Cheng, One-dimensional nanomaterials for soft electronics, Adv. Electron. Mater. 3 (3) (2017), 1600314.
- [72] Liu, Xian-Ming, et al. "Carbon nanotube (CNT)-based composites as electrode material for rechargeable Li-ion batteries: A review." Composites Science and Technology 72.2 (2012): 121-144.
- [73] R. Zhang, W. Chen, Recent advances in graphene-based nanomaterials for fabricating electrochemical hydrogen peroxide sensors, Biosens. Bioelectron. 89 (2017) 249–268.
- [74] A.M.H. Ng, Kenry, C.T. Lim, H.Y. Low, K.P. Loh, Highly sensitive reduced graphene oxide microelectrode array sensor, Biosens. Bioelectron. 65 (2015) 265–273.
- [75] W. Zheng, M. Zhao, W. Liu, S. Yu, L. Niu, G. Li, H. Li, W. Liu, Electrochemical sensor based on molecularly imprinted polymer/reduced graphene oxide composite for simultaneous determination of uric acid and tyrosine, J. Electroanal. Chem. 813 (2018) 75–82.
- [76] S. Dong, J. Xi, Y. Wu, H. Liu, C. Fu, H. Liu, F. Xiao, High loading MnO2 nanowires on graphene paper: facile electrochemical synthesis and use as flexible electrode for tracking hydrogen peroxide secretion in live cells, Anal. Chim. Acta 853 (2015) 200–206
- [77] Y.-L. Liu, Y. Qin, Z.-H. Jin, X.-B. Hu, M.-M. Chen, R. Liu, C. Amatore, W.- H. Huang, A stretchable electrochemical sensor for inducing and monitoring cell mechanotransduction in real time, Angew. Chem. Int. Ed. 56 (32) (2017) 9454–9458.
- [78] Baptista, Andresa, et al. "Sputtering physical vapour deposition (PVD) coatings: A critical review on process improvement and market trend demands." Coatings 8.11 (2018): 402.
- [79] Maiyelvaganan, K. Rudharachari, Shanmugasundaram Kamalakannan, and Muthuramalingam Prakash. "Adsorption of ionic liquids on carbonaceous surfaces: The effect of curvature on selective anion… π and cation… π interactions." Applied Surface Science 495 (2019): 143538.
- [80] Liu, Qingzhou, et al. "Highly sensitive and wearable In203 nanoribbon transistor biosensors with integrated on-chip gate for glucose monitoring in body fluids." ACS nano 12.2 (2018): 1170-1178.
- [81] H. Yoon, J. Nah, H. Kim, S. Ko, M. Sharifuzzaman, S. C.Barman, X. Xuan, J. Kim and J. Y. Park, Sens. Actuators, B,2020, 311, 127866.
- [82] H. Coskun, A.A. Aljabour, L. Uiberlacker, M. Strobel, S. Hild, C. Cobet, D. Farka, P. Stadler, N.S. Sariciftci, Chemical vapor deposition based synthesis of conductive polydopamine thin-films, Thin Solid Films 645 (2018) 320–325
- [83] L.Y. Xu, G.Y. Yang, H.Y. Jing, J. Wei, Y.D. Han, Ag-Graphene hybrid conductive ink for writing electronics, Nanotechnology 25 (2014) 055201.
- [84] Hondred, John A., Igor L. Medintz, and Jonathan C. Claussen. "Enhanced electrochemical biosensor and supercapacitor with 3D porous architectured graphene via salt impregnated inkjet maskless lithography." Nanoscale Horizons 4.3 (2019): 735-746.
- [85] H.W. Deckman, J.H. Dunsmuir, Natural lithography, Appl. Phys. Lett. 41 (1982) 377–379.

- [86] Qin, Dong, Younan Xia, and George M. Whitesides. "Soft lithography for micro-and nanoscale patterning." Nature protocols 5.3 (2010): 491.
- [87] X. Cao, H. Chen, X. Gu, B. Liu, W. Wang, Y. Cao, F. Wu, C. Zhou, Screening Printing, as a scalable and low-cost approach for rigid and flexible thin-film transistors using separated carbon nanotubes, ACS Nano 8 (2014) 12769–12776.
- [88] Li, Peng, Dongzhi Zhang, and Zhenling Wu. "Flexible MoS₂ sensor arrays for high performance label-free ion sensing." Sensors and Actuators A: Physical 286 (2019): 51-58.
- [89] Li, Bo, et al. "Strain sensing behavior of FDM 3D printed carbon black filled TPU with periodic configurations and flexible substrates." Journal of Manufacturing Processes 74 (2022): 283-295.
- [90] Ravindranath, K., and R. A. Mashelkar. "Polyethylene terephthalate—I. Chemistry, thermodynamics and transport properties." Chemical Engineering Science 41.9 (1986): 2197-2214.
- [91] Wolf, Marc P., Georgette B. Salieb-Beugelaar, and Patrick Hunziker. "PDMS with designer functionalities—Properties, modifications strategies, and applications." Progress in Polymer Science 83 (2018): 97-134.
- [92] Frazer, Robert Q., et al. "PMMA: an essential material in medicine and dentistry." Journal of long-term effects of medical implants 15.6 (2005).
- [93] Wort, Chris JH, and Richard S. Balmer. "Diamond as an electronic material." Materials today 11.1-2 (2008): 22-28.
- [94] Chung, D. D. L. "Review graphite." Journal of materials science 37 (2002): 1475-1489.
- [95] Pleskov, Yurii V. "Synthetic diamond in electrochemistry." Russian chemical reviews 68.5 (1999): 381-392.
- [96] Zhang, Jiabao, et al. "A review of diamond synthesis, modification technology, and cutting tool application in ultra-precision machining." Materials & Design (2023): 112577.
- [97] Jiang, Jiatong, et al. "A review and perspective on industry high-temperature heat pumps." Renewable and sustainable energy reviews 161 (2022): 112106.
- [98] D'Haenens-Johansson, Ulrika FS, James E. Butler, and Andrey N. Katrusha. "Synthesis of diamonds and their identification." Reviews in Mineralogy and Geochemistry 88.1 (2022): 689-753.
- [99] Butler, James E., et al. "Understanding the chemical vapor deposition of diamond: recent progress." Journal of Physics: Condensed Matter 21.36 (2009): 364201.
- [100] Luong, John HT, Keith B. Male, and Jeremy D. Glennon. "Boron-doped diamond electrode: synthesis, characterization, functionalization and analytical applications." Analyst 134.10 (2009): 1965-1979.
- [101] Cobb, Samuel J., Zoe J. Ayres, and Julie V. Macpherson. "Boron doped diamond: a designer electrode material for the twenty-first century." Annual review of analytical chemistry 11.1 (2018): 463-484.
- [102] Einaga, Yasuaki. "Development of electrochemical applications of boron-doped diamond electrodes." Bulletin of the Chemical Society of Japan 91.12 (2018): 1752-1762.
- [103] Macpherson, Julie V. "A practical guide to using boron doped diamond in electrochemical research." Physical Chemistry Chemical Physics 17.5 (2015): 2935-2949.
- [104] Liu, Zhichao, et al. "Inkjet printing-manufactured boron-doped diamond chip

- electrodes for electrochemical sensing purposes." ACS applied materials & interfaces 15.33 (2023): 39915-39925.
- [105] Baluchová, Simona, et al. "Advanced 3D-Printed Flexible Composite Electrodes of Diamond, Carbon Nanotubes, and Thermoplastic Polyurethane." ACS Applied Polymer Materials 6.23 (2024): 14638-14647.
- [106] Buckley, John D. "Carbon-carbon-an overview." American Ceramic Society Bulletin 67 (1988).
- [107] Popov, Valentin N. "Carbon nanotubes: properties and application." Materials Science and Engineering: R: Reports 43.3 (2004): 61-102.
- [108] Dai, Hongjie. "Carbon nanotubes: opportunities and challenges." Surface science 500.1-3 (2002): 218-241.
- [109] Zhao, Qiang, Zhenhai Gan, and Qiankun Zhuang. "Electrochemical sensors based on carbon nanotubes." Electroanalysis: An International Journal Devoted to Fundamental and Practical Aspects of Electroanalysis 14.23 (2002): 1609-1613.
- [110] Huang, Xiao, et al. "Graphene-based electrodes." Advanced Materials 24.45 (2012): 5979-6004.
- [111] Rajan, Krishna, et al. "Silver nanoparticle ink technology: state of the art." Nanotechnology, science and applications (2016): 1-13.
- [112] Liu, Huifang, et al. "Synthesis, characterization, and antibacterial properties of silver nanoparticles-graphene and graphene oxide composites." Biotechnology and bioprocess engineering 21 (2016): 1-18.
- [113] Zhu, Yuwen, et al. "Flexible transparent electrodes based on silver nanowires: material synthesis, fabrication, performance, and applications." Advanced Materials Technologies 4.10 (2019): 1900413.
- [114] Shrivas, Kamlesh, et al. "Advances in flexible electronics and electrochemical sensors using conducting nanomaterials: A review." Microchemical Journal 156 (2020): 104944.
- [115] Nayak, Laxmidhar, et al. "A review on inkjet printing of nanoparticle inks for flexible electronics." Journal of Materials Chemistry C 7.29 (2019): 8771-8795.
- [116] Shahrubudin, Nurhalida, Te Chuan Lee, and R. J. P. M. Ramlan. "An overview on 3D printing technology: Technological, materials, and applications." Procedia manufacturing 35 (2019): 1286-1296.
- [117] Liu, Changyong, et al. "3D printing technologies for flexible tactile sensors toward wearable electronics and electronic skin." Polymers 10.6 (2018): 629.
- [118] Karimi, Armin, Davood Rahmatabadi, and Mostafa Baghani. "Various FDM mechanisms used in the fabrication of continuous-fiber reinforced composites: a review." Polymers 16.6 (2024): 831.
- [119] E.M. Richter, D.P. Rocha, R.M. Cardoso, E.M. Keefe, C.W. Foster, R.A.A. Munoz, C.E. Banks, Complete additively manufactured (3D-printed) electrochemical sensing platform, Anal. Chem. 91 (2019) 12844e12851,
- [120] Kirikova, Marina N., et al. "Direct-write printing of reactive oligomeric alkoxysilanes as an affordable and highly efficient route for promoting local adhesion of silver inks on polymer substrates." Journal of Materials Chemistry C 4.11 (2016): 2211-2218.
- [121] Bastola, Anil, et al. "Formulation of functional materials for inkjet printing: A

- pathway towards fully 3D printed electronics." Materials Today Electronics (2023): 100058.
- [122] Exner, Hans E., and Eduard Arzt. "Sintering processes." Sintering Key Papers (1990): 157-184.
- [123] Rogers, John A., Takao Someya, and Yonggang Huang. "Materials and mechanics for stretchable electronics." science 327.5973 (2010): 1603-1607.
- [124] Larraza, Izaskun, et al. "Cellulose and graphene based polyurethane nanocomposites for fdm 3d printing: Filament properties and printability." Polymers 13.5 (2021): 839.
- [125] Quodbach, Julian, et al. "Quality of FDM 3D printed medicines for pediatrics: considerations for formulation development, filament extrusion, printing process and printer design." Therapeutic Innovation & Regulatory Science (2021): 1-19.
- [126] Haryńska, Agnieszka, et al. "Fabrication and characterization of flexible medical-grade TPU filament for fused deposition modeling 3DP technology." Polymers 10.12 (2018): 1304.
- [127] Kalsoom, Umme, Sidra Waheed, and Brett Paull. "Fabrication of humidity sensor using 3D printable polymer composite containing boron-doped diamonds and LiCl." ACS applied materials & interfaces 12.4 (2020): 4962-4969.
- [128] Harris, Conor G., et al. "Additive manufacturing with soft TPU-adhesion strength in multimaterial flexible joints." Frontiers in Mechanical Engineering 5 (2019): 37.
- [129] Trung, Tran Quang, and Nae-Eung Lee. "Flexible and stretchable physical sensor integrated platforms for wearable human-activity monitoringand personal healthcare." Advanced materials 28.22 (2016): 4338-4372.
- [130] Cieślik, Mateusz, et al. "Tailoring diamondised nanocarbon-loaded poly (lactic acid) composites for highly electroactive surfaces: extrusion and characterisation of filaments for improved 3D-printed surfaces." Microchimica Acta 190.9 (2023): 370.
- [131] Trung, Tran Quang, and Nae-Eung Lee. "Flexible and stretchable physical sensor integrated platforms for wearable human-activity monitoringand personal healthcare." Advanced materials 28.22 (2016): 4338-4372.
- [132] Gnanasekaran, Karthikeyan, et al. "3D printing of CNT-and graphene-based conductive polymer nanocomposites by fused deposition modeling." Applied materials today 9 (2017): 21-28.
- [133] Li, Shian, et al. "Wavy surface cathode gas flow channel effects on transport processes in a proton exchange membrane fuel cell." Journal of Electrochemical Energy Conversion and Storage 14.3 (2017): 031007.
- [134] Pawlyta, Miroslawa, Jean-Noël Rouzaud, and Stanislaw Duber. "Raman microspectroscopy characterization of carbon blacks: Spectral analysis and structural information." Carbon 84 (2015): 479-490.
- [135] Ferry, A. B. A. U. U., et al. "Raman, infra-red and dsc studies of lithium coordination in a thermoplastic polyurethane." Polymer 37.5 (1996): 737-744.
- [136] Verbeeten, Wilco MH, and Miriam Lorenzo-Bañuelos. "Material extrusion additive manufacturing of poly (lactic acid): influence of infill orientation angle." Additive Manufacturing 59 (2022): 103079.
- [137] Grest, Gary S. "Normal and shear forces between polymer brushes." Polymers in Confined Environments (1999): 149-183.

- [138] Bruère, V. M., et al. "The influence of printing parameters on the mechanical properties of 3D printed TPU-based elastomers." Progress in Additive Manufacturing 8.4 (2023): 693-701.
- [139] Zhao, Hui, et al. "Comprehensive characterization of 3D-printed TPU/carbon black composites: Morphological, thermal, and mechanical properties." Materials Today Communications 41 (2024): 111099.
- [140] Zhao, Hui, et al. "Comprehensive characterization of 3D-printed TPU/carbon black composites: Morphological, thermal, and mechanical properties." Materials Today Communications 41 (2024): 111099.
- [141] Chen, Rui, et al. "Highly stretchable and fatigue resistant hydrogels with low Young's modulus as transparent and flexible strain sensors." Journal of Materials Chemistry C 6.41 (2018): 11193-11201.
- [142] Wu, Shuying, et al. "Strain sensors with adjustable sensitivity by tailoring the microstructure of graphene aerogel/PDMS nanocomposites." ACS applied materials & interfaces 8.37 (2016): 24853-24861.
- [143] Wu, Guanzheng, et al. "Multi-stimuli responsive shape memory behavior of dual-switch TPU/CB/CNC hybrid nanocomposites as triggered by heat, water, ethanol, and pH." Chemical Engineering Journal 450 (2022): 138253.
- [144] Ghosh, Somnath, et al. "Interfacial debonding analysis in multiple fiber reinforced composites." Mechanics of materials 32.10 (2000): 561-591.
- [145] Atawa, Bienvenu, et al. "In-situ coupled mechanical/electrical investigations on conductive TPU/CB composites: Impact of thermo-mechanically induced structural reorganizations of soft and hard TPU domains on the coupled electro-mechanical properties." Polymer 256 (2022): 125147.
- [146] Mohsenzadeh, Rasool, et al. "Morphology-driven nanofiller size measurement integrated with micromechanical finite element analysis for quantifying interphase in polymer nanocomposites." ACS Applied Materials & Interfaces 16.30 (2024): 39927-39941.
- [147] Goh, Guo Liang, et al. "Potential of printed electrodes for electrochemical impedance spectroscopy (EIS): Toward membrane fouling detection." Advanced Electronic Materials 7.10 (2021): 2100043.
- [148] Dul, Sithiprumnea, Luca Fambri, and Alessandro Pegoretti. "Fused deposition modelling with ABS-graphene nanocomposites." Composites Part A: Applied Science and Manufacturing 85 (2016): 181-191.
- [149] Deng, Hua, et al. "Progress on the morphological control of conductive network in conductive polymer composites and the use as electroactive multifunctional materials." Progress in Polymer Science 39.4 (2014): 627-655.
- [150] Šupová, Monika, Gražyna Simha Martynková, and Karla Barabaszová. "Effect of nanofillers dispersion in polymer matrices: a review." Science of advanced materials 3.1 (2011): 1-25.
- [151] Chakraborty, Patatri, et al. "Unprecedented sensing of interlayer defects in three-dimensionally printed polymer by capacitance measurement." Smart Materials and Structures 27.11 (2018): 115012.
- [152] Chang, Peng, et al. "3D printed electrochemical energy storage devices." Journal of Materials Chemistry A 7.9 (2019): 4230-4258.
- [153] Zhang, Yinhang, et al. "Recent advanced thermal interfacial materials: a review of

- conducting mechanisms and parameters of carbon materials." Carbon 142 (2019): 445-460.
- [154] Ambrosi, Adriano, and Martin Pumera. "3D-printing technologies for electrochemical applications." Chemical society reviews 45.10 (2016): 2740-2755.
- [155] Hu, Chao. Hot melt extrusion of carbon fiber reinforced thermoplastic composites for injection molding and fused deposition modeling. Diss. The Australian National University (Australia), 2020.
- [156] Taberna, Pierre-Louis, Christele Portet, and Patrice Simon. "Electrode surface treatment and electrochemical impedance spectroscopy study on carbon/carbon supercapacitors." Applied Physics A 82 (2006): 639-646.
- [157] Fagan, Dan T., Ing Feng Hu, and Theodore Kuwana. "Vacuum heat-treatment for activation of glassy carbon electrodes." Analytical chemistry 57.14 (1985): 2759-2763.
- [158] Lee, Junqiao, Damien WM Arrigan, and Debbie S. Silvester. "Mechanical polishing as an improved surface treatment for platinum screen-printed electrodes." Sensing and biosensing research 9 (2016): 38-44.
- [159] Manzanares-Palenzuela, Carmen Lorena, et al. "Proteinase-sculptured 3D-printed graphene/polylactic acid electrodes as potential biosensing platforms: towards enzymatic modeling of 3D-printed structures." Nanoscale 11.25 (2019): 12124-12131.
- [160] Çay, Ahmet, E. Perrin Akçakoca Kumbasar, and Çiğdem Akduman. "Effects of solvent mixtures on the morphology of electrospun thermoplastic polyurethane nanofibres." Textile and Apparel 25.1 (2015): 38-46.
- [161] Treceño, Miriam Laiz. Synthesis and caracterization of fluorinated polimers. Diss. Universitat Autònoma de Barcelona, 2022.
- [162] Mu, Jierui, et al. "Application of electrochemical polishing in surface treatment of additively manufactured structures: A review." Progress in Materials Science 136 (2023): 101109.
- [163] Cammann, Karl. Working with ion-selective electrodes: chemical laboratory practice. Springer Science & Business Media, 2012.
- [164] Ho, Ja-an Annie, et al. "Development of an immunopredictor for the evaluation of the risk of cardiovascular diseases based on the level of soluble P-selectin." Methods 56.2 (2012): 223-229.
- [165] Radi, Abd-Elgawad. "Electrochemical Aptamer-Based Biosensors: Recent Advances and Perspectives." International journal of electrochemistry 2011.1 (2011): 863196.
- [166] Schnoor, Mary H., and Chad D. Vecitis. "Quantitative examination of aqueous ferrocyanide oxidation in a carbon nanotube electrochemical filter: effects of flow rate, ionic strength, and cathode material." The Journal of Physical Chemistry C 117.6 (2013): 2855-2867.
- [167] Fry, Albert J. Synthetic organic electrochemistry. John Wiley & Sons, 1989.
- [168] Fan, Xinzhuang, et al. "Reversible redox reaction on the oxygen-containing functional groups of an electrochemically modified graphite electrode for the pseudocapacitance." Journal of Materials Chemistry 21.46 (2011): 18753-18760.